PVD PROCESS MODELLING AND DEPOSITION INTO SUB-MICRON FEATURES

by

Stephen Daniels, B Eng

A thesis submitted in partial fulfilment
of the requirements for the degree of

Ph D

School of Electronic Engineering

Dublin City University

January 1999

Academic Supervisor Dr D C Cameron

DECLARATION

I hereby certify that this material, which I now submit for assessment on the programme of study leading to the award of Doctor of Philosophy is entirely my own work and has not been taken from the work of others save and to the extent that such work has been cited and acknowledged within the text of my work.

Signed: _____ Date: 07/02/99

Stephen Daniels

ACKNOWLEDGEMENTS

I would like to thank Dr David Cameron, my Academic Supervisor, for his unwavering support over the years It was an honour to work with a man so enthusiastic about his subject and so committed to his students

I drew strength and inspiration from my wife, Lisa, without whom I would never have been able to finish this work Countless evenings and weekends can never be replaced but the sacrifice will not be forgotten

Many people have assisted me along the way and to them I am deeply indebted In particular, I would like to thank Rob Wolters of Philips Research and Gerald Beyer of IMEC for their encouragement, suggestions and stimulating conversations

Among the many others to whom I would like to express my thanks include, Prashanthi Kola, Eric van de Riet, Michael Murphy, Davide Bassanani, Peter Curley and Mary Gray

The majority of this work was carried out part-time while working for Applied Materials I would like to thank my colleagues, in particular, Brendan Kenny, Fergus Clarke, Juergen Johnke and Frank Hochstenbach for their support

Last but by no means least, I would like to thank my parents for nurturing in me a desire to improve and educate myself

Stephen Daniels, December 1998

TABLE OF CONTENTS

Dublin City University

ABSTRACT

PVD PROCESS MODELLING AND DEPOSITION INTO SUB-MICRON FEATURES

by Stephen Daniels

Physical Vapour Deposition (PVD) is a thin film deposition technique used to deposit thin films for a wide variety of applications One key application area is the microchip fabrication process where PVD is used to deposit the various layers of metal which interconnect the devices on the microchip This study focuses on this application area and the emphasis is placed on using PVD deposited materials to coat and fill deep sub-micron vias and contacts Through a combination of modelling, simulation, and experiment it is shown that PVD will remain the technology of choice up to and beyond 0 25µm technology

Chapter 1 introduces both the PVD process and microchip fabrication The basic physics underlying PVD is studied and this discussion is extended to film growth kinetics, variations of the basic PVD process, and alternative / rival processes The microchip fabrication process is discussed and the role PVD plays in the larger picture is highlighted This is followed by a discussion on the direction the microchip fabrication industry is taking and what PVD must do to keep up

Chapter 2 looks at the PVD process in more detail After introducing some commercially available sputter simulation packages, the development of a model and 3-D sputter simulation package is detailed The sputter model / simulation is then used to investigate a number of key aspects of sputtering The reactive sputtering process is discussed as is the sputter etch process and film uniformity as a function of process and hardware configurations

Chapter 3 looks at the barriers, liners and wetting layers typically used as part of the metallisation scheme Emphasis is placed on achieving the required step coverage to achieve barrier integrity, reliable feature fill, and good yield The ionised metal PVD process is studied in detail and it is argued that this technique is probably the best available process for coating deep sub-micron features

Chapter 4 looks at the aluminium deposition process in detail in order to ascertain the best method of filling deep sub-micron high aspect ratio structures with aluminium Shrinking feature sizes means the low resistivity materials such as aluminium need to be used as the via and contact plug materials in order to maintain device optimum speed and performance A number of different via fill schemes are presented A remarkable bottom to top fill process is developed and explained with the help of a film growth simulation package

Chapter 5 follows on from chapter 4 and examines alternative fill processes using standard and collimated wetting layers Detailed simulations which include the effect of wetting and seed layers are performed and the influences of these underlayers on the fill mechanism discussed

Chapter 6 examines the ionised PVD processing detail Film profiles over sub-micron features are studied as a function of the material fluxes to the substrate

during deposition Material re-deposition at the bottom of features due to the effects of ion bombardment is studied both experimentally and theoretically It is found that re-deposition at the bottom of high aspect ratio features can be used to redistribute material to the lower sidewall, thus improving barrier integrity

Chapter 1 Introduction

1.1 Introduction

Physical Vapour Deposition (PVD) is a technique used to deposit high quality, ultra clean thin films which are used for a wide variety of applications. In this study the PVD process is studied mainly in the context of semiconductor fabrication. Other applications of PVD such as thin films for wear resistance etc. are also discussed.

For semiconductor fabrication applications the ability of PVD processes to deposit conformal thin films of various materials over small (micron range) high aspect ratio features is of critical importance. It is this ability of PVD processes to coat and fill small features which is the main topic discussed in this study.

In order for PVD technology to remain a useful process in the microelectronics industry, the technology has had to evolve to meet the requirements of modern day devices. In the 1970s devices typically had 10 micron geometries and 1000A gate oxides. In recent years many of the modern manufacturing facilities fabricated circuits with feature sizes of approximately 0.6 microns and gate oxide thickness of less than 120A. The most modern facilities currently fabricate devices with 0.35 micron geometries and research is ongoing on 0.25 and 0.18 micron technologies.

PVD processes are typically used in microelectronic manufacturing processes to deposit barriers and liners for subsequent materials and to deposit the interconnect metals. For a barrier / liner to be of good quality in a typical contact or via process, the film step coverage must be good enough to provide adequate barrier / liner thickness over the entire contact or via. As feature sizes shrink and aspect ratio's increase, it has become increasingly difficult to provide adequate barriers with the standard sputter deposition process. To overcome the limitations of the standard sputter process a number of extensions have been devised. One of these is called collimated or coherent sputtering[1]. Collimated sputtering involves placing a collimator between the target and the substrate. This collimator filters out atoms which have been sputtered from the target at oblique angles to the target surface, thus making the flux of atoms arriving at

the substrate more normal to the surface The most recent variation of the standard sputter process is known as ionised magnetron sputtering[2] This process involves placing an RF coil between the target and the substrate causing increased gas ionisation in this region Sputtered atoms passing through this discharge are more likely to undergo ionising collisions and so are likely to arrive at the substrate sheath in an ionised state The electric field in the sheath will accelerate the ions in the direction on the substrate, thus making the average impact angle more normal to the substrate surface

These and other extensions to the basic magnetron sputtering process are discussed in detail in subsequent chapters

In chapter 2 the various component processes of the PVD process are examined in detail A model of the PVD process is presented and the development of 2D and 3D simulation packages described

Chapter 3 examines in detail the basic sputtering process along with the collimated and ionised extensions in the context of reduced feature dimensions and increased aspect ratios Through both simulation and experiment the various PVD processes are compared and contrasted in terms of step coverage capabilities Conclusions are drawn on how well each process meets current technological requirements and how extendible each are into the future

As well as being used to deposit barriers and liners, PVD is also used to deposit the interconnect lines and to fill the vias between the various layers on a chip This involves filling sub-micron features such as vias and trenches with the interconnect material (typically aluminium) Chapters 4 and 5 examine in detail the filling of these sub-micron features with metal and through a combination of experiment and simulation the capabilities and limitations of existing techniques are examined

In chapter 6 an extension to the basic sputtering process, known as ionised PVD, is studied in detail

1 2 Thin Film Deposition Techniques

There exists many different deposition technologies for material formation on a substrate Thin film deposition methods refers to processes used for the formation of layers in the thickness range of a few nanometers to about 10 micrometers Thin films are normally prepared by condensation of atoms or molecules from the vapour phase Thin film deposition techniques are typically classified into one of three sub-classes

CHEMICAL VAPOUR DEPOSITION (CVD)
Solid films are formed on a substrate by the chemical reaction of vapour phase chemicals that contain the required constituents

LIQUID PHASE CHEMICAL FORMATION (LPCF)
This involves coating of a substrate with a liquid which dries to form a solid film

PHYSICAL VAPOUR DEPOSITION (PVD)
Species of the thin film are dislodged from a source to form a vapour which is transported across a reduced pressure region to the substrate where it condenses to form the thin film

CVD is a very important materials synthesis process for creating a wide variety of materials essential to advanced technology In the basic CVD process the reactant gases are introduced into a reaction chamber and are decomposed and reacted at a heated surface to form the thin film However, a host of variations of the basic process exist which use different techniques to provide the energy required to drive the various chemical reactions CVD processes are normally characterised by the reactor type used and the operating pressure regime CVD processes can operate at low pressure or at atmospheric pressure, depending on the film requirements and the material being deposited Atmospheric pressure CVD reactors (APCVD) are the oldest design and have the advantage of relatively simple design and a high deposition rate Low pressure CVD processes (LPCVD) typically provide better film uniformity and step coverage performance than APCVD systems LPCVD reactors operate in the 0 25 - 2T pressure regime, hence a vacuum pump is required LPCVD systems tend in general to have

lower deposition rates and higher operating temperatures than APCVD reactors Another sub-class of CVD exists known as Plasma Enhance CVD (PECVD) Rather than relying solely on thermal energy to initiate and sustain the chemical reactions, PECVD uses an rf-induced glow discharge to transfer energy into the reactant gases[3] PECVD allows deposition onto substrates without the high temperatures required by other CVD processes PECVD can also enhance deposition rates and create films with unique compositions and properties The relative advantages and disadvantages of the major CVD processes are summarised in table 1 1

Process	Advantages	Disadvantages
APCVD	Simple Design, High Deposition Rate Medium Substrate Temperature	Poor Step Coverage Dirty Process (Particles)
LPCVD	High Film Purity Good Step Coverage	High Substrate Temperature, Low Deposition Rates
PECVD	Low Substrate Temperature High Deposition Rate Good Step Coverage	Chemical Contamination

Table 1 1 *CVD Process Comparison*

The growth of thin films from liquid phases by chemical reactions is normally carried out using electrochemical processes such as anodization or electroplating or by chemical deposition processes such as reduction plating and electroless plating In the context of the present study the most interesting of these is electroplating as this technique has been proposed as an alternative to PVD and CVD for depositing copper in the most modern semiconductor metallisation processes[4] In electroplating a metallic coating is electro-deposited on the cathode of an electrolytic cell The standard electrolytic cell consists of an anode, a cathode and an electrolytic solution which contains the metal ions through which the electric current flows

This work is mostly concerned with PVD processes PVD can be divided into three major sub-classes evaporative technology, molecular beam epitaxy (MBE) and sputtering technology PVD denotes vacuum deposition processes where the thin film material is passed into a vapour transport phase by a physical mechanism i e evaporation, sublimation or ion bombardment

Thermal (or vacuum) evaporation is one of the oldest techniques used for depositing thin films and is still widely used for depositing metals and metal alloys[5] Basically, the evaporation process has three basic steps

a) A vapour is generated by boiling or subliming a source material
b) The vapour is transported from the source to the substrate
c) The vapour condenses on the substrate forming the thin film

A wide variety of techniques exist for creating the vapour, including

- Resistance heated filaments
- Electron beams
- Crucibles heated by conduction, radiation, or rf induction
- Arcs
- Lasers

The rate at which atoms pass into vacuum from a heated source is given by the Hertz-Knudsen equation

$$W = \frac{35 * 10^{22} \alpha P}{\sqrt{MT}}$$

where P is the vapour pressure in torr, T is the temperature in °K, M is the molecular weight in grams and α is the evaporation coefficient α is a function of the cleanliness of the evaporation surface[6] The vapour pressure is a function of the metal temperature

As the vapour needs to be transported from the source to the substrate, high vacuum is a critical requirement to ensure the vapour reaches the substrate without interference from other species which may react with the vapour

Molecular beam epitaxy is a multisource evaporation technology MBE has been applied primarily to the growth of single crystal films of compound semiconductors In this process thermal molecular beams of each of the constituents of the film to be deposited are directed to converge on a single crystal substrate under conditions suitable for epitaxial growth[7]

Sputtering is the third and perhaps most important PVD technology Metallisation of semiconductor devices constitutes one of the primary applications of this technology Sputtering involves physically removing the thin film species from a source (known as a target) by bombarding this source with atomic or molecular particles The basic and most widely used sputtering processes use ions from a gas discharge to bombard the target at a defined energy If this bombardment energy is large enough a fraction of the target atoms are dislodged and '*sputtered*' from the target surface The target is normally biased negatively and serves as the cathode for the discharge The cathode sheath which develops in front of the target serves to accelerate the discharge ions in the direction of the target surface

1 3 Basics of Sputtering

Figure 1 1 is a schematic of the basic sputtering process It shows ions from a plasma bombarding the surface of the cathode resulting in the ejection of target atoms and electrons Other phenomena that may occur when an ion impacts a surface include the emission x-rays, photons and the reflection of the incident ions The following is a list of possible events that may occur when and ion bombards a target surface

(A) ION MAY BE REFLECTED

If the bombarding ion does not have enough energy to imbed itself in the target it will be reflected The lower the mass of the incident ion relative to the target atoms the higher the probability of reflection[8] The energy of the reflected particle may be a significant fraction of its incident energy For a particle reflected by 180° the fraction of energy the reflected particle has is given by

$$\frac{E_R}{E_i} = \frac{M_i - M_t}{(M_i + M_t)^2}$$

where E_R is the energy after reflection, E_i is the initial energy, M_i is the mass of the incident ion and M_t is the mass of the target atoms

In most sputtering applications the majority of the particles bombarding the substrate are ions An ion approaching a clean conducting surface has a high probability of being neutralised prior to impact by an emitted electron[9] Therefore the reflected particle is unaffected by the electric and magnetic fields If $M_i < M$, the flux of energetic neutral particles bombarding the surface can be significant and need to be taken into account when designing a sputtering process

(B) ELECTRON MAY BE EJECTED (SECONDARY ELECTRON EMISSION)

When a particle strikes a surface one of the possible results is that an electron is ejected from the surface This phenomenon is known as secondary electron emission Secondary electron emission is observed for bombardment by ions, electrons, neutrals and photons Ejection of the electron proceeds by excitation of the electron into the kinetic energy continuum above the surface potential The necessary excitation energy comes from either the kinetic or potential energy of the incident particle[10] For typical sputtering processes used for depositing thin for the semiconductor industry secondary electron coefficients are in the range 0 05 to 0 1 A vast array of secondary electron emission coefficient data exists in the literature

(C) ION IMPLANTATION

A very important consideration is what is the ultimate fate of the inert gas ions The probability of the inert gas atom becoming entrapped in the target surface increases with ion energy above a threshold of about 100eV[11] It has been reported that the amount of gas trapped can influence the sputter yield but this is only the case at higher than normal target voltages[12]

(D) TARGET SURFACE STRUCTURAL REARRANGEMENT

The impact of a particle with a target surface may lead to structural rearrangements such as the introduction of interstitials or vacancies It may also introduce lattice defects such as stoichiometry modifications

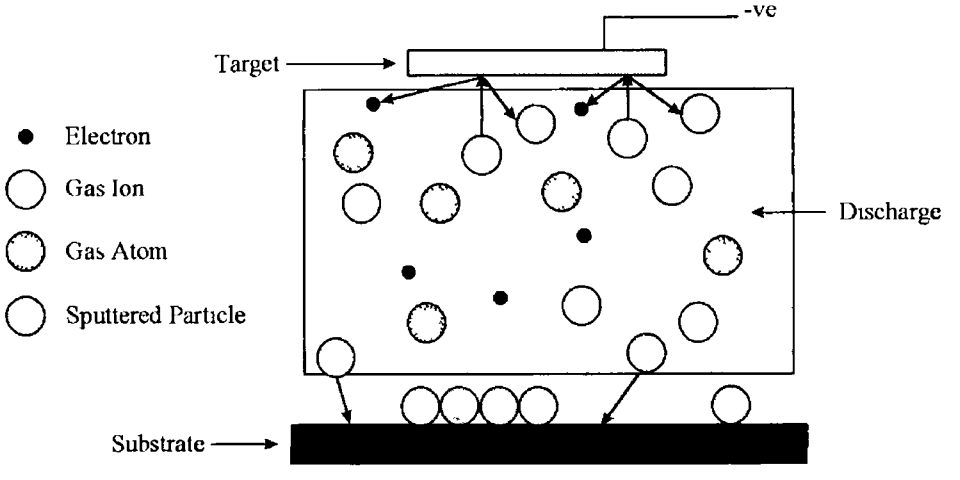

Figure 1 1 Schematic of the basic sputtering process

(E) ATOM EJECTION FROM A TARGET SURFACE (SPUTTERING)

The kinetic energy of the impinging ions largely dictates which of the above events is most likely to take place Of particular interest is the event which leads to the ejection of a target atom sputtering The main parameters which control the sputtering process include the kinetic energy of the incident ions, the bombardment angle of the incident ions, lattice structure and binding energy of lattice atoms

The most popular model used to describe the sputter deposition of a particle from a surface is a momentum transfer model known as the Billiard Ball model This model describes the sputtering process as a 3-D game of billiards played with atoms

In the energy regime relevant to sputter deposition (<1000eV), the interactions between the impinging ion and the target atoms (and target atoms with themselves) can be treated as a series of binary collisions This assumption can be made due to the fact that the interaction potentials in a target are sufficiently short range The series of

collisions generated due to the particle collision at the target surface is known as a collision cascade

Consider a binary collision between two particles of masses m_i and m_t Assume that m_t is stationary and that m_i collides with m_t with a velocity v_i at an angle θ to the line joining the particle centres

By conservation of linear momentum

$$m_i v_i \cos\theta = m_i u_i + m_t u_t$$

By conservation of energy

$$\frac{1}{2} m_i v_i^2 = \frac{1}{2} m_i (u_i^2 + v_i^2 \sin^2\theta) + \frac{1}{2} m_t u_t^2$$

Eliminating u_i yields

$$m_i v_i^2 \cos^2\theta = \frac{m_t}{m_t^2} (m_i v_i \cos\theta - m_t u_t)^2 + m_t u_t^2$$

The fractional energy transferred from m_i to m_t is given by

$$\frac{E_t}{E_i} = \frac{\frac{1}{2} m_t u_t^2}{\frac{1}{2} m_i v_i^2} = \frac{m_t}{m_i v_i^2} \left(\frac{2 m_i v_i}{m_t + m_i} \cos\theta\right)^2$$

so,

$$\frac{E_t}{E_i} = \frac{4 m_i m_t}{(m_i + m_t)^2} \cos^2\theta$$

The sputtering/ejection process is the result of a series of such collisions The sputtering yield S is defined as the number of particles (or molecules) ejected from the target per incident ion The sputtering yield therefore largely determines the process deposition rate The ejection of a sputtered atom due to a bombarding particle requires a series of such binary collisions such that the moment of the initial momentum is changed by more than 90° Sputtering is therefore a statistical process which is the result of a collision cascade which was initiated by the incident particle The physical mechanism of sputtering is believed to be the result of two mechanisms

a) Low Energy Knock On

This is a 'scooping' process where a surface atom passes underneath an adjacent atom See figure 1 2 for an illustration

b) Primary Knock-On

This is where a primary knock-on or reflected ion dislodges a surface atom by striking it on the underside See figure 1 2 for an illustration

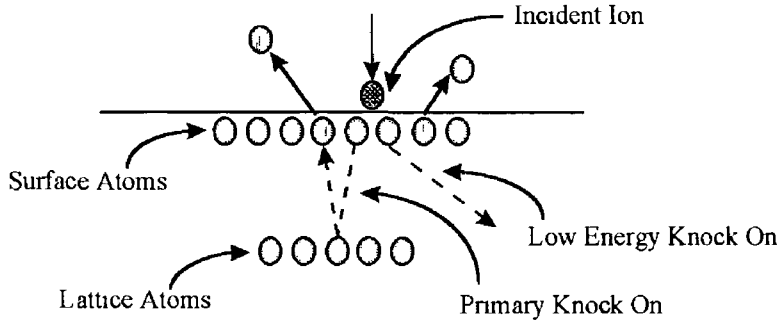

Figure 1 2 *Sputter Ejection Mechanism*

Physically the sputter rate is a function of the ion impact angle, the target material, mass of the ions, and ion energy No sputtering occurs until the ions reach some threshold energy E_T which is characteristic of the particular ion - target combination This energy is generally in the range of 20eV to 30eV[13]

According to Sigmund[14], the sputter yield is proportional to the energy deposited in a thin layer near the surface which is determined by the nuclear stopping power *s(E)* For relatively low energy bombardment (< 1000eV), the slowing expression for *s(E)* has been derived by Sigmund

$$s(E) = (m_i * m_t)/(m_i + m_t)^2 * E * constant$$

This is used to predict a formula for sputter yield *S*,

$$S = \frac{3a}{4\pi^2} \frac{4m_i m_t}{(m_i + m_t)^2} \frac{E}{U_0}$$

where U_0 is the binding energy, a is a monotonic increasing function of m_t/m_i, which has a value 0 17 for m_t/m_i = 0 1 to 1 4 for m_t/m_i = 10

Table 1 2 below tabulates the sputter yield for a number of metals in argon as a function of projectile energy

Target	At Wt /Den	100eV	300eV	600eV	1000eV	2000eV
Al	10 00	0 11	0 65	1 20	1 90	2 00
Au	10 20	0 32	1 65	2 80	3 60	5 60
Cu	7 09	0 50	1 60	2 30	3 20	4 30
Ni	6 60	0 28	0 95	1 50	2 10	
Pt	9 12	0 20	0 75	1 60		
Si	12 05	0 07	0 31	0 50	0 60	0 90
Ta	10 90	0 10	0 40	0 60	0 90	
Ti	10 62	0 08	0 33	0 41	0 70	
W	14 06	0 12	0 41	0 75		

Table 1 2

Figure 1 3 below shows the general trend for sputter rate as a function of projectile impact energy

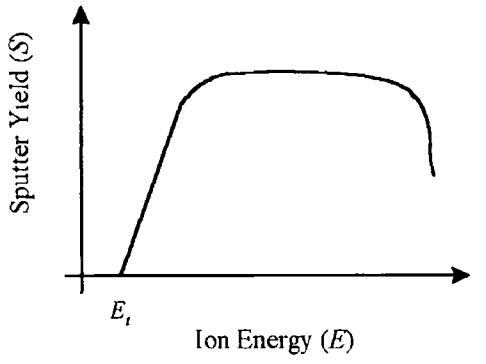

Figure 1 3 *Dependence of Sputter Yield on Incident Ion Energy*

Typically the sputter rate increases up to approximately 10KeV after which the sputter yield decreases rapidly This drop off in yield is due to ions becoming imbedded in the target material

The sputtering yield is also a function of the projectile impact angle This fact was first discovered by Fetz[15], who found that thin wires sputtered more quickly than thicker wires due to the larger percentage of oblique collisions

Figure 1 4 below shows the general trend for sputter rate as a function of projectile impact angle[16]

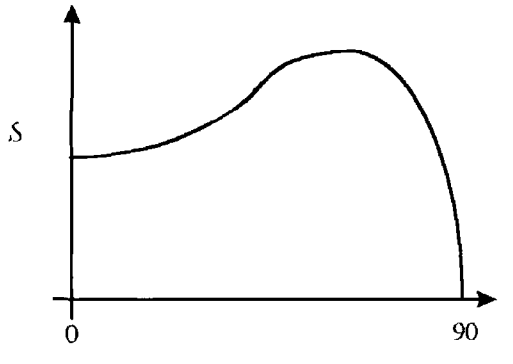

Figure 1 4 *Dependence of Sputter Yield on Incident Ion Angle*

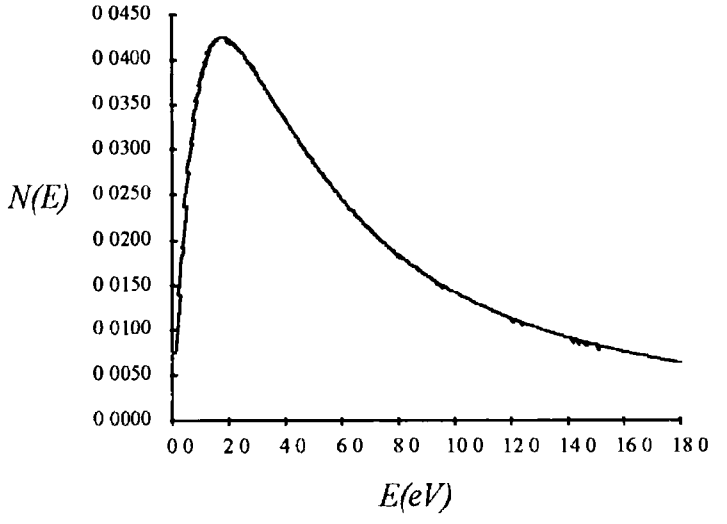

Figure 1 5 *Energy Distribution of Nascent Sputtered Flux*

Sputtered atoms are ejected from the target surface with an energy distribution approximated[17][18] by

$$f(E) \propto \frac{E_b E}{(E_b + E)^3}$$

The maximum of this energy distribution occurs at $E_b/2$, where E_b is the binding energy of the target atoms The distribution shown in figure 1 5 is the calculated distribution for a copper target The general shape of this distribution agrees with experimental observation[19]

The ejection angle of the sputtered atoms depends largely on the crystal orientation of the target[20] Experiment has shown that for crystalline and polycrystalline targets ejection occurs preferentially along close-packed directions in the target[21] For amorphous targets the ejection angle distribution can be *cosine* or *off-cosine* depending on the ion energy, mass and incident angle, see figure 1 6 for an illustration

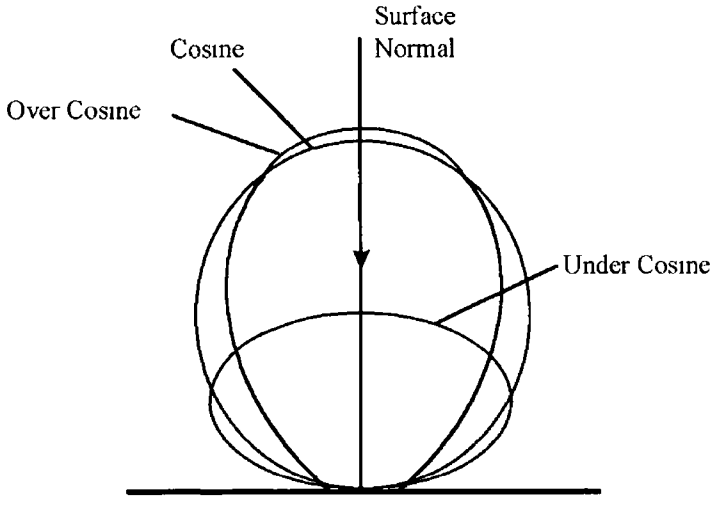

Figure 1 6 *Ejection Angle Distributions*

1 4 The DC Glow Discharge

A glow discharge is achieved by applying a potential between two electrodes in a gas Initially no current flows as all the gaseous atoms are neutral On the introduction of an electron (or other charged particle) into the gas, typically by ionisation of a gas atom by a cosmic ray, radioactive impurities, a charge multiplication process or background radiation, it will be accelerated by the electric field between the electrodes If the energy gained by the electron is sufficiently high, an inelastic collision with a gas atom may result in excitation or ionisation of the gas atom If ionisation takes place a second electron is released into the gas Subsequently both electrons will be accelerated again, creating a condition known as gas breakdown

The electrode potential difference required to ignite a discharge is known as the breakdown voltage and is a function of the gas pressure and the electrode spacing This relationship between pressure, spacing and breakdown voltage is known as Paschens relationship[22] The DC discharges of interest in film deposition are normally low density plasmas with neutral to ion ratios of the order of 10^4 The electrons and ions in the plasma eventually become lost to the discharge through collisions with surfaces, electron - ion recombination etc For the plasma to maintain itself there needs to be a balancing amount of ionising processes occurring in the discharge

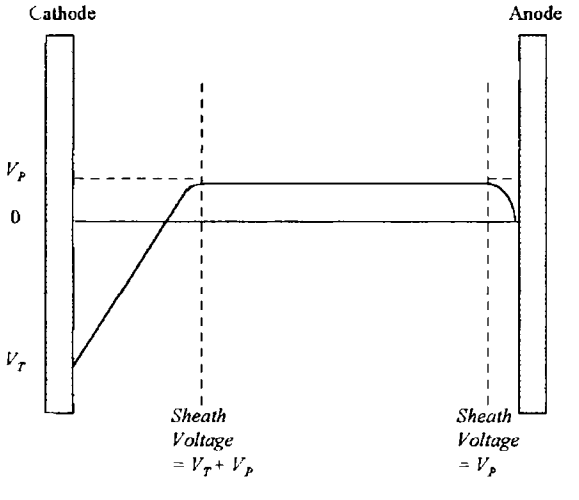

Figure 1 7 *Voltage Distribution in a dc glow discharge*

Figure 1 7 shows the voltage distribution in a dc glow discharge In a dc discharge the electric fields in the system are restricted to the sheaths The sheaths act to repel electrons at each electrode[23]

A floating substrate immersed in the discharge will also have a sheath and will be biased negatively with respect to the plasma The reason for this is due to the difference in the mobilities of the electrons and the ions in the plasma When a substrate is first immersed in the discharge it is subject to bombardment from electrons, ions and neutrals In this analysis only the charged particle fluxes are of interest, so the current densities to the substrate on initial immersions are

$$J_e = \frac{en_e\bar{c}_e}{4}$$

$$J_i = \frac{en_i\bar{c}_i}{4}$$

where J is the current density, n is the particle density and $\bar{c}$ is the average velocity Due to their smaller mass, the average velocity of electrons is much larger than that of the ions Due to this difference in velocities $J_e >> J_i$, the substrate immediately starts to build up a negative charge and potential with respect to the plasma Eventually a steady state is reached where the electron flux is reduced due to electrons being repelled by the negative charge on the substrate This means that a floating voltage V_f will have developed on the floating substrate It can be shown[24] that V_f is related to the electron temperature T_e and the ratio of the electron mass m and the ion mass M

$$V_f = \frac{1}{2e}kT_e \ln(\frac{\pi m}{2M})$$

Where e is the electronic charge and k is Boltzmann's constant Typical values for V_f in practical sputtering systems are -25V to -60V When the bias develops on the substrate it will be subject to ion bombardment from the plasma, the ions having an energy eV_f

A bias voltage can be applied to the substrate from an external dc or rf power source. The plasma potential stays the same but the voltage on the substrate V_b is now set by the external power source. This substrate bias can be a very influential parameter in determining the properties of the growing film. Under certain circumstances the net deposition rate can be reduced or even made negative (sputter etching).

1.5 RF Discharges

In some situations it is necessary to sputter non-conducting materials. A typical example would be SiO_2 sputter etching prior to metal deposition. Unfortunately applying a dc voltage to an insulating cathode will not ignite a plasma as the effective voltage on the cathode surface will approach zero due to the build-up of a surface charge of positive ions on the front side. This limitation can be circumvented by replacing the dc supply with an rf supply. Figure 1.8 shows a typical rf sputtering configuration. A blocking capacitor is placed between a matching network and the target. Typically, the target area is much smaller than the system anode (chamber walls etc.). This asymmetrical configuration induces a negative dc bias on the target which results in the sputtering of the target.

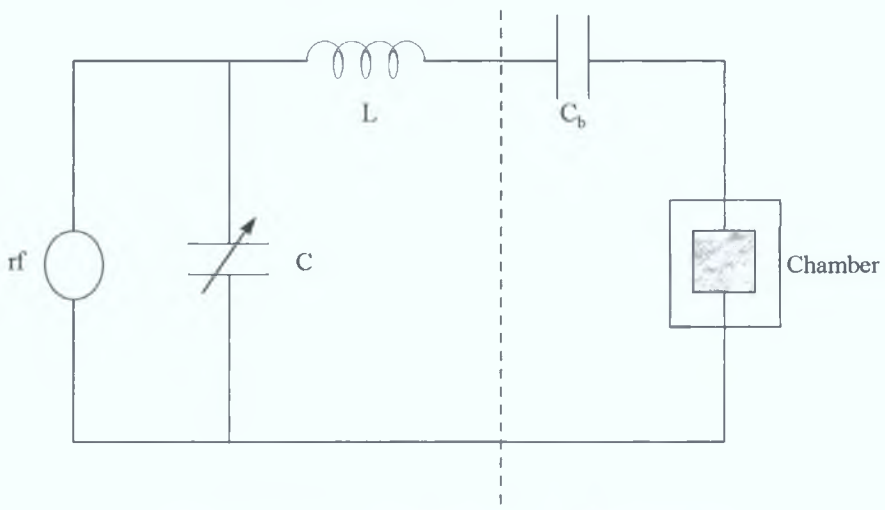

Figure 1.8 *RF Sputtering Configuration*

The introduction of the negative bias due to the asymmetric configuration is explained by the voltage distribution model developed by Koenig and Maissel[25]. This model

relates the ratio of the sheath voltage at the two electrodes to the electrode areas by the following equation

$$\left(\frac{V_c}{V_d}\right) = \left(\frac{A_d}{A_c}\right)^4$$

Where V_c is the voltage of the small capacitively coupled electrode (the target), V_d is the voltage of the large directly coupled electrode (the chamber walls), and A_c and A_d are the areas of the capacitively coupled and directly coupled electrodes respectively

1.6 Magnetron Sputtering

A magnetron discharge is a modification of the glow discharge which involves using magnets, normally placed at the rear of the cathode to reduce the electron mean free path and confine electrons in the region of the cathode The magnetic field effect can be used to significantly increase deposition rate and can reduce the minimum required operating pressure significantly Confining the electrons in the region of the cathode also has the added advantage of reducing the amount of electron bombardment of the substrate This effect is important when dealing with temperature sensitive substrates This decreased loss of electrons in the target region corresponds to an increased electron density in the discharge With this increased electron density it is possible to reduce the applied voltage to the plasma A typical diode sputtering system operates in the range 1000VDC to 10,000VDC whereas a magnetron plasma can operate typically between 200VDC to 800VDC The magnetron can operate at a lower pressure due to the fact that the mean free path of the electrons in the magnetic field is reduced Electrons in a crossed electric and magnetic field follow the motion of a spiral whereas in a simple electric field the motion is in a straight line

The force F acting on a particle of velocity v and charge q in a magnetic field B is given by

$$\underline{F} = q\underline{v} \times \underline{B}$$

The force F acts in a direction perpendicular to both the particle velocity and the magnetic field

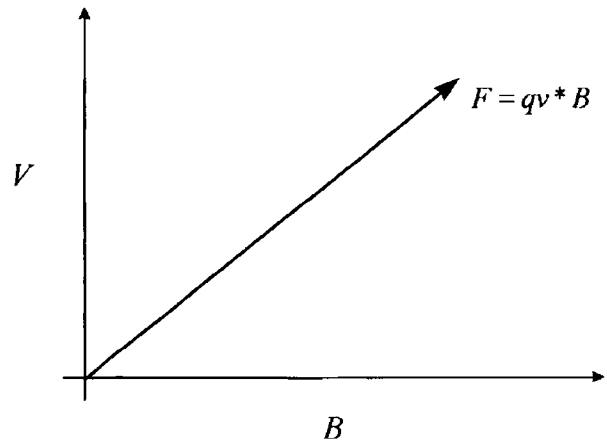

Figure 1 9 *Force on a charged particle in an EXB field*

An electron travelling at an angle Q relative to the magnetic line of force B, will be subject to a force F_B, where

$$F_B = BevsinQ$$

The velocity component in the direction of the magnetic field is given by

$$F = vcosQ$$

Coupling the above two velocities together, the general motion will be that of a helix along the magnetic line of force

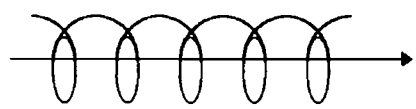

Figure 1 10 Helical Motion of a Charged Particle

The radius of the circular motion around the magnetic line of force (*gyroradius*) is a function of the strength of the magnetic field and the mass of the charged particle

Consider the centripetal acceleration of a body

$$a = v^2/r$$

where a is the acceleration

$$F = ma \Rightarrow F = m\, v^2/r$$

$$m(v\sin Q)^2/r = Bev\sin Q$$

$$\Rightarrow \quad r = mv\sin Q/Be$$

where e is the electronic charge

The gyroradius is a function of the mass and velocity of the charged particle In a typical sputter discharge the gyroradius of the gas and metal ions are approximately 300 times larger than that of electrons in equivalent conditions Therefore the ions move through the magnetron magnetic field and cathode dark space in essentially a straight line

Magnetrons are designed such that the magnetic field traps the electrons close to the target surface so as to increase their ionising effect The electron, once emitted from the surface is immediately under the influence of the magnetic field

The generally accepted current - voltage relationship in magnetron sputtering systems is given by the equation[26]

$$I_t = kV_t^n$$

Where I_t is the target current, V_t is the target voltage and k and n are constants The constants k and n depend on the gas-target combination and the magnetron design

Figure 1 11 is a schematic of a typical magnetron arrangement The magnetic lines loop between the inner and outer magnetic poles resulting in a closed magnetic field A disadvantage of the magnetron arrangement is that the target surface is etched away non-uniformly The electric and magnetic fields only confine the electrons in certain regions in front of the target surface, known as the racetrack region In practice magnetrons come in all shapes and sizes For large substrates the magnets are sometimes rotated at the back of the magnetron in order to optimise target utilisation

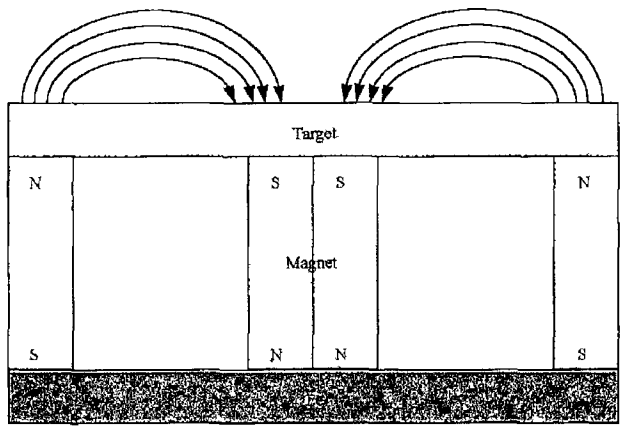

Figure 1 11 *Balanced Magnetron*

This type of magnetron design is optimised to confine the electrons in the region of the target With this design the electron and ion bombardment of the substrate is at a minimum as the plasma is confined by the magnetic fields to the target region In some situations ion bombardment of the substrate is desirable Ion bombardment can cause re-sputtering of the depositing film which can help to fill in voids It can also be used to modify the stoichiometry of the depositing film In the case of mechanical engineering films for wear resistant applications ion bombardment is used to densify and harden films The amount of ions available to bombard a substrate can be increased by modifying the magnetic field design so that either the outer or inner set of magnets is increased in magnetic field strength relative to the other set This type of magnetron was first proposed by Window and Savvides[27] and is known as an unbalanced magnetron A schematic is given in figure 1 12

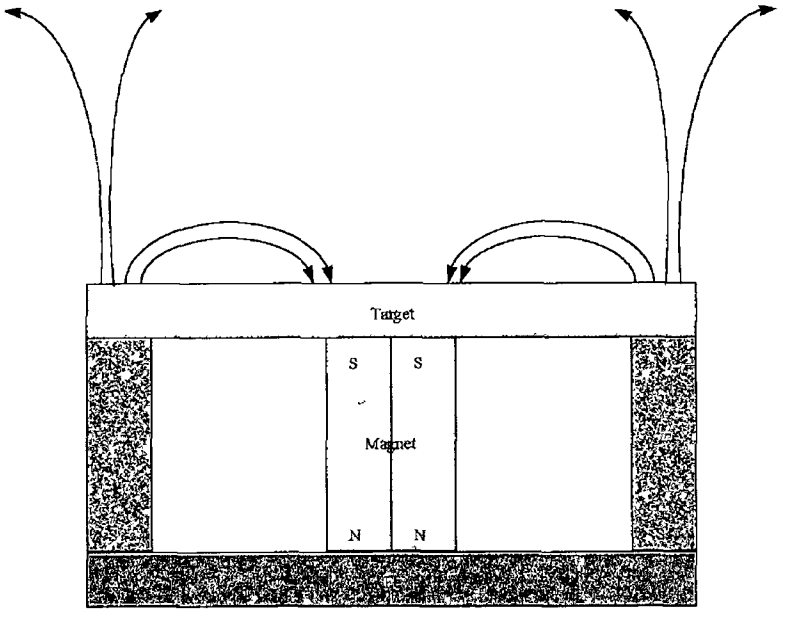

Figure 1 12 Unbalanced Magnetron

1.7 Variations of Magnetron Sputtering

Many variations of the physical vapour deposition process exist.

Collimated Magnetron Sputtering

This process has already been discussed earlier in this chapter and will be discussed in more detail in chapters 3 and 5. Basically it is an extension of the magnetron sputtering process where sputtered atoms at oblique angles relative to the target normal are filtered out.

Ionised Magnetron Sputtering

This process has already been mentioned earlier in this chapter and will be discussed in detail in chapters 3 and 6. Basically, the addition of an additional ionisation source in the region between the cathode and the substrate results in a large fraction of the depositing flux being ionised. The ionised material is then directed normal to the substrate due to the influence of the substrate sheath.

Long Throw Magnetron Sputtering

Long throw sputtering involves increasing the target - substrate spacing to distances much larger than are typically used. Typically the target - substrate is five times that of a conventional PVD chamber. The resulting flux at the wafer typically approaches the substrate surface more normal to the substrate than the standard process. Material sputtered at oblique angles deposits on the chamber walls before reaching the substrate[28]. Typically better bottom and step coverage can be achieved using this process.

Closed Field Magnetron Sputtering

For some applications ion bombardment of the substrate during film growth is very important. This is particularly true in cases where hard dense films are required i.e. wear resistant applications. The concept of the unbalanced magnetron was discussed earlier in this chapter and the ability of the unbalanced magnetron to extend the plasma region explained. Closed field magnetron sputtering involves positioning a number of unbalanced magnetrons symmetrically around the substrate in such a manner that the

magnetic field lines link in order to form a good magnet trap for the electrons An example of a four-magnetron system is shown in figure 1 13 Closing the magnetic field in this way results in a much higher plasma density in the substrate region and hence significantly higher ion currents to the substrate can be achieved Another variation of this technique is to place biasing magnets behind the substrate[29]

BIASED SPUTTERING

Biased sputtering involves placing a bias on the substrate during the deposition process to increase the amount of ion bombardment of the substrate The substrate bias is one of the most useful parameters to control during deposition Almost any film property can be modified by the application of a bias The particles impinging on the substrate during deposition include electrons and argon and sputtered material ions Applying a positive bias to the substrate increases the amount of electron bombardment and reduces the ion bombardment Applying a negative bias to the substrate reduces the electron bombardment and increases the ion bombardment It is the control of the ion bombardment which is useful in directly controlling film properties The amount of bias determines not only the ion current, it also determines the energy distribution of the impinging ions If the bias is too great, the film tends to be sputtered away from the substrate as fast as it arrives, so that little or no net deposition occurs Biasing the substrate more moderately (-20V to -200V) can have a number of effects on film properties

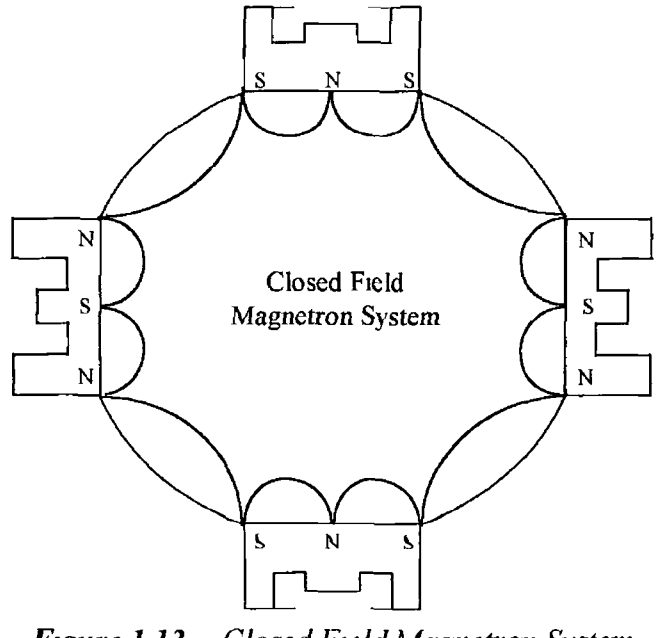

Figure 1 13 *Closed Field Magnetron System*

Ion bombardment changes the initial formation stages of the film (nucleation and growth phases) It can improve the step coverage due to the increased adatom mobility of impinging particles The density of deposited films are also significantly increased by ion bombardment of the growing film, which is particularly useful for mechanical engineering applications Ion bombardment also effects the crystallinity of the growing film The combined effect of the above means that by controlling the ion bombardment it is possible to influence the film mechanical and electrical properties

Reactive Sputtering

Reactive sputtering is a very important extension of the sputtering process because it allows the deposition of compound materials In this process a reactive gas is introduced into the process environment along with the sputtering gas The reactive gas reacts with the sputtered material at the surfaces to produce a compound film One of the most common and widely used reactively deposited materials is TiN This process is examined in more detail in appendix A

1 8 Thin Film Evolution and Growth and Particle Bombardment Effects

Thin films usually have properties that differ from the bulk material properties This is due to the influences of the surface and the interfaces and also the film structure, determined by the initial condensation process The film growth process involves the processes of initial nucleation and subsequent film growth Nucleation refers to the earliest steps of film growth where a sufficient number of vapour atoms or molecules condense on the substrate Soon after exposure to the incident flux a uniform distribution of small highly mobile clusters (or islands) form These clusters grow in size and density until the islands begin to merge in what is known as the coalescence phenomenon, which is liquid like in character (especially at high temperatures) Coalescence decreases the island density allowing further nucleation to occur Coalescence continues until a connected network with unfilled channels and voids develops Finally the voids are filled and a continuous film results

There are three generally agreed upon thin film growth modes, known as

1 Island Growth Mode (or Volmer-Weber)
2 Layer Growth Mode (or Frank van der Merwe)
3 Stranski - Krastanov Growth Mode

The type of growth mode is normally a function of the substrate / flux material interaction The following is a brief description of each of the growth modes

ISLAND

In the island growth mode the smallest stable clusters nucleate on the substrate and grow in three dimensions to form islands This happens when deposited atoms are more strongly bound to each other than to the substrate This growth mode is typical of metal on insulators

LAYER

In the layer growth mode the smallest stable clusters grow in two dimensions, resulting in the formation of planar sheets In this growth mode the atoms are more strongly

bound to the substrate than to each other An example of this growth mode is single crystal epitaxial growth of semiconductor films

STRANSKI - KRASTANOV

The Stranski - Krastanov growth mode is a combination of the island and layer growth modes In this case after the formation of one or more monolayers, subsequent layer growth becomes unfavourable and island growth begins This transition from two to three dimensional growth is not fully understood but is observed m metal - metal and metal - semiconductor systems

The resulting microstructure of thin films is a function of the interplay of the nucleation and growth processes The nucleation and growth processes are influenced by substrate temperature, film composition and the ambient However, independent of the specific deposition conditions, general trends in film microstructure are observed as a function of certain process conditions The most famous illustration of this phenomena is that first presented by Movchan and Demchishin[30] and later extended by Thornton[31], which represents schematically the influence of substrate temperature and argon gas working pressure on the microstructure of metal coatings deposited by sputtering (see figure 1 14)

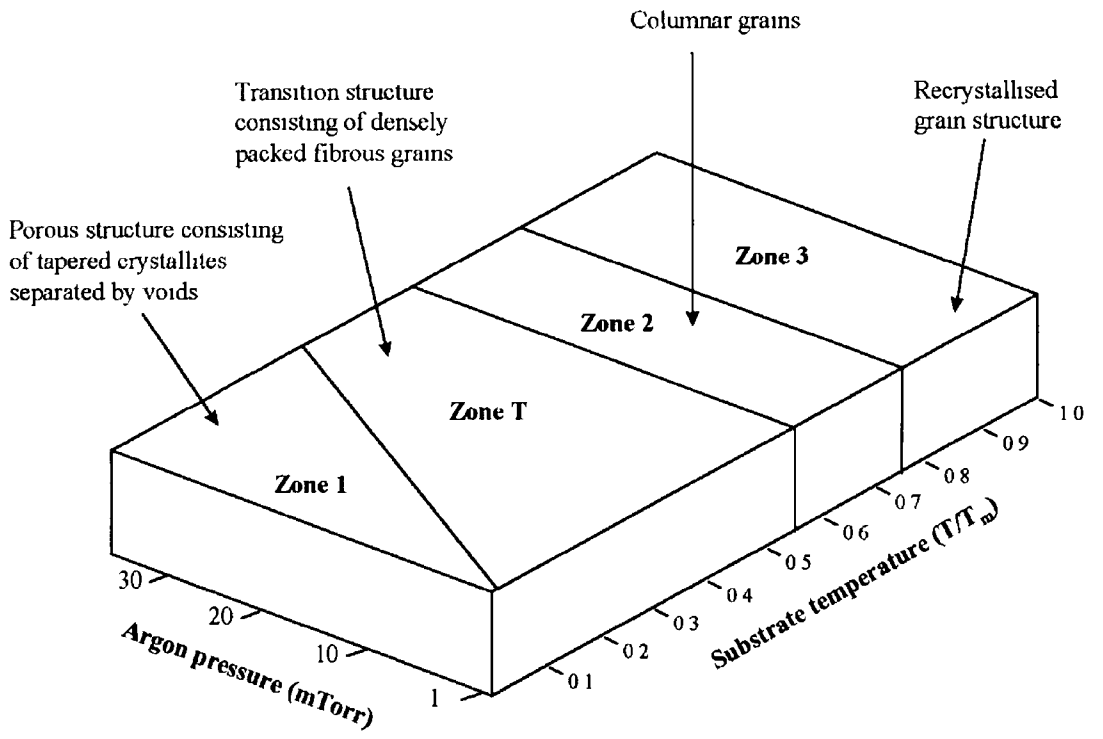

Figure 1 14 *Movchan et al Illustration of Film Microstructure*

In this representation, the microstructure characteristic of each range of substrate temperature and process pressure are classified into one of four 'zones' Zone 1 results when adatom diffusion is insufficient to overcome the effects of shadowing It normally forms at low temperatures and higher working gas pressures The zone 2 region is the range of temperature and pressure where the growth process is dominated by adatom surface diffusion The zone 3 region is the range of temperature and pressure where film growth is dominated by bulk diffusion, which is typical of high temperature aluminium deposition used for microchip interconnect via fill and interconnect applications The zone *T* region is transition region between zones 1 and 2 It has been defined as the limiting form of zone 1 at $T/T_m = 0$ and an infinitely smooth substrate

1.9 PVD in Semiconductor Fabrication

Many different thin film deposition techniques are used at various stages of the microchip fabrication process The 'Back End of the Line' or BEOL part of the fabrication process is the name give to the set of fabrication steps which interconnect the devices which have been formed on the silicon surface The following is a typical BEOL process flow for a multilevel metal system

1 Barrier and Glue Layer Deposition
2 Anneal Barrier (to improve contact resistance)
3 Blanket W Contact Fill
4 EtchbackW
5 Deposit Interconnect Metal (i e AlCu)
6 Deposit Anti-Reflection Coating (usually referred to as ARC)
7 Metal Patterning
8 Oxide Deposition and Planarisation
9 Via Opening
10 Barrier and Glue Layer Deposition
11 Blanket W Via Fill
12 W Etchback
13 For Metal 2,3,4, Goto Step 5
14 Passivation Deposition and Patterning

Metallisation refers to the barrier and metal interconnect deposition steps in the manufacturing process

The above process flow would typically use sputtering to deposit the barrier and glue layers, the AlCu interconnect and the ARC In this instance the W contact and via fill would typically be deposited using a chemical vapour deposition process

In the case of a PVD Al-plug process, steps 3, 4 and 5 of the above process sequence would be replaced by a single AlCu deposition step The same applies to steps 11, 12 and 13

1 10 PVD vs Alternative Deposition Processes (CVD, Electroplating)

Thermal or plasma enhanced Chemical Vapour Deposition (CVD) has been suggested as an alternative deposition processes to PVD for the various metallisation films This technique involves reacting the constituents of a vapour at a hot surface to deposit a thin film, one of the products of that reaction being the material to be deposited As atoms are deposited chemically onto the substrate surface, the films produced by CVD tend to be more conformal than can be achieved using PVD

In current metallisation processes tungsten is widely deposited using CVD techniques for contact/plug and first level metal applications The basic chemistry for CVD W is as follows

$$WF_6 + 3H_2 \Rightarrow W + 6HF$$

$$2WF_6 + 3Si \Rightarrow 2W + 3SiF_4$$

$$WF_6 + SiH_4 \Rightarrow W + SiF_4 + 2HF + H_2$$

$$2WF_6 + 3Si_4 \Rightarrow 2W + 3SiF_4 + 6H_2$$

The above reactions are thermally activated and have been studied extensively The deposited W has an electrical resistivity 1 5 - 2 times that of the bulk material due mainly to the incorporation of F in the film The W-plug contact and via fill process has proven to be a production worthy process and is still the technology of choice of a large number of chip manufacturers As technology moves forward and device sizes shrink W-plug technology is experiencing increased competition from lower resistivity materials such as Al and Cu

Al and Cu can also be deposited using CVD techniques however neither process is yet widely used in production

CVD Cu has a resistivity 10% - 20% higher than the bulk material Cu is also very vulnerable to corrosion and copper can diffuse easily into SiO_2, which means a diffusion barrier is required Materials such as Ta and TaN are marketed as production worthy diffusion barrier materials[4] and other materials such as WN are under development Cu metallisation is currently receiving a lot of attention due to its excellent conductivity and better electromigration resistance than Al Another reason for a renewed interest in Cu metallisation is the advent of chemical mechanical polishing (CMP) which eliminates the requirement for a chemical metal etch process One major disadvantage of Cu metallisation in the past has been the lack of a production worthy metal etch process

Al can also be deposited using CVD techniques Its resistivity is close to that of the bulk material and good quality films can be produced The major difficulty with CVD Al is the difficulty in including Cu in the film for improving electromigration resistance, or Si in the Al to reduce the risk of aluminium spiking One way around the Cu problem is to deposit 50% of the total thickness using CVD and the other 50% using PVD from an Al-Cu alloy target Subsequent heating of the aluminium stack will allow redistribution of the Cu throughout the entire film CVD Al is currently proving to be a very interesting process for depositing an Al seed layer on the walls of high aspect ratio features to provide a diffusion path for subsequent PVD deposited Al[32]

Diffusion barrier materials can also be deposited using CVD techniques CVD TiN is currently attracting a lot of attention as a barrier for Al in high aspect ratio applications where a conformal and smooth barrier film is required CVD TiN is a commercially available process and is used by a number of manufacturers throughout the world CVD technology plays a very important role in current metallisation processes and it is likely to remain very important for the foreseeable future However, some of the disadvantages of this process which have prevented it from replacing PVD are as follows

1 High cost of manufacture relative to PVD
2 Higher resistivity films which lead to higher contact and via resistances

3 Process Complexity

Electroplating is defined as the deposition of an adherent metallic coating upon an electrode Electroplating of metals requires a conductive substrate held at a negative potential and immersed in a bath containing metal ions Plating provides a low cost method for depositing thick metal layers over large areas and is used extensively in printed circuit board manufacture Up until now microchip interconnects have mainly been manufactured using PVD and CVD techniques However, the advent of low permittivity dielectrics limits the use of these technologies as existing low permittivity dielectrics are much more sensitive to high temperatures than the current widely used dielectrics[33] PVD and CVD processes, especially when used to fill sub-micron features such as contacts and vias, frequently require high substrate temperatures (>400C)[34] Plating of metal is an ideal low cost, low temperature alternative metallisation process

ForceFill™ metallisation is a PVD technology recently introduced as a means of achieving aluminium via fill and planarisation This technology involves compressing aluminium into an aluminium bridged feature ForceFill™ is typically performed in two steps The first step involves depositing an aluminium layer on the wafer (typically at 400 - 450°C) until a bridge is formed over the feature to be filled In the second step the wafer is exposed to a high pressure of approximately 700 atmospheres at a temperature between 430 - 450°C to force the aluminium into the features A schematic of the process is given in figure 1 15

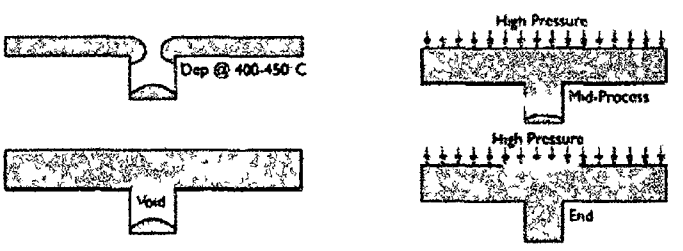

Figure 1.15

ForceFill™ has been patented by Trikon Technologies Inc

1 11 Step Coverage Definition

Up until now terms such as step coverage, bottom coverage etc have been used without any formal definition The exact interpretation of step coverage can vary so for the purposes of this study it is useful to define step coverage

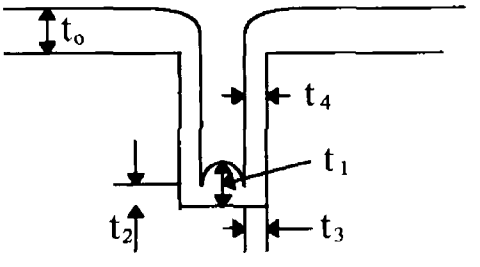

Figure 1 16

Step coverage is a figure of merit for the conformality of a film deposited over a feature The following is a list of definitions

Bottom Coverage	t_1/t_0
Step Coverage	t_3/t_0
Sidewall Coverage	t_4/t_0
Minimum Bottom Coverage	t_2/t_0

t_4 can be measured at any point along the sidewall but for consistency in this report assume t_4 is measured at the midpoint between the original bottom and top of the feature sidewall See figure 1 16 for an illustration

1 12 Moores Law / Technology Roadmap

This work is primarily concerned with PVD's role in the manufacture of semiconductor devices Throughout the work, the challenges facing PVD are mentioned again and again However, the obvious question to ask at this point is, why is the technology evolving as it is and why are feature sizes continuing to shrink ? To answer these questions the reasons for miniaturisation need to be understood The following is a list of reasons why miniaturisation is desirable

- Reduced Cost per Chip
- Reduction in Overall Device Size
- Improvement of Device Speed
- Reduction of Power Consumption

In 1965 Gordon Moore, then Head of Research at Fairchild Semiconductor Corporation predicted that the number of transistors per chip would double while the cost of the chip remains constant every year for the next ten years This prediction became known as Moore's Law The rate of rise was revised in the late 1970's to every eighteen months and it has proven to be surprisingly accurate This constant drive for miniaturisation has knock-on consequences for the metallisation process Based on resistive and capacative considerations the lateral dimensions of vias and contacts are scaled down much faster than the corresponding vertical dimensions So, as further miniaturisation takes place dramatic increases in contact and via aspect ratios can be expected Figure 1 17 is a forecast of contact aspect ratios for DRAM and logic IC's based on the Semiconductor Industry Association (S I A) roadmap As can be seen the expected increases in aspect ratios are dramatic

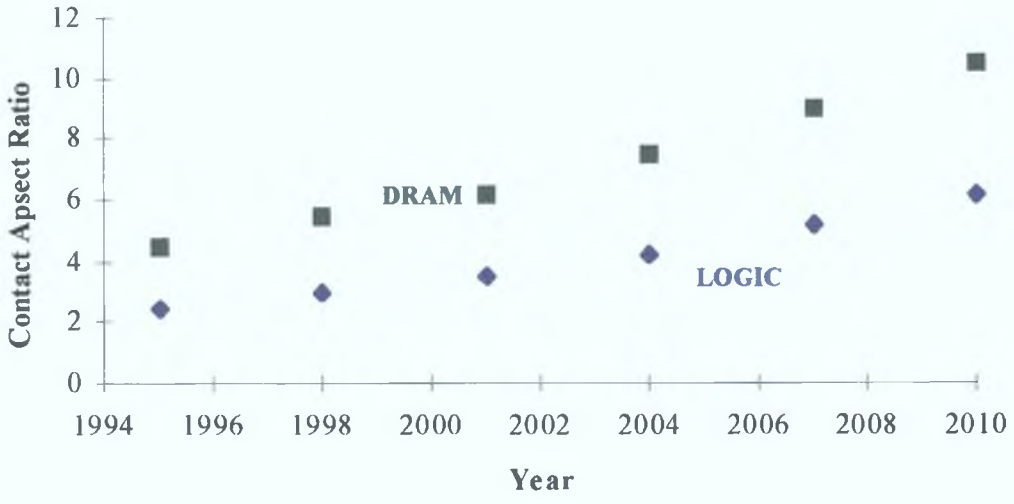

Figure 1.17

In the vast majority of ICs made today the interconnect wires are aluminium and the interlayer vias are tungsten. Eliminating the tungsten in vias and replacement with aluminium is in progress in many Fabs at the moment. Lowering the resistivity decreases wiring delays significantly, thus improving device speed. Recently much interest has been shown in copper metallisation. As an interconnect, lower resistivity of copper allows for higher performance at a given dimension relative to aluminium. The difficulties in working with copper are many, including its ability to contaminate nearby silicon. Recently IBM announced the replacement of aluminium with copper. A cross section of IBM's copper IC is given in figure 1.18. This chip has six layers of copper circuitry with circuit line widths of 0.20μm. The technique developed to prevent the interaction of the copper with the aluminium has not been released but is likely to be a PVD deposited Ta or TaN diffusion barrier.

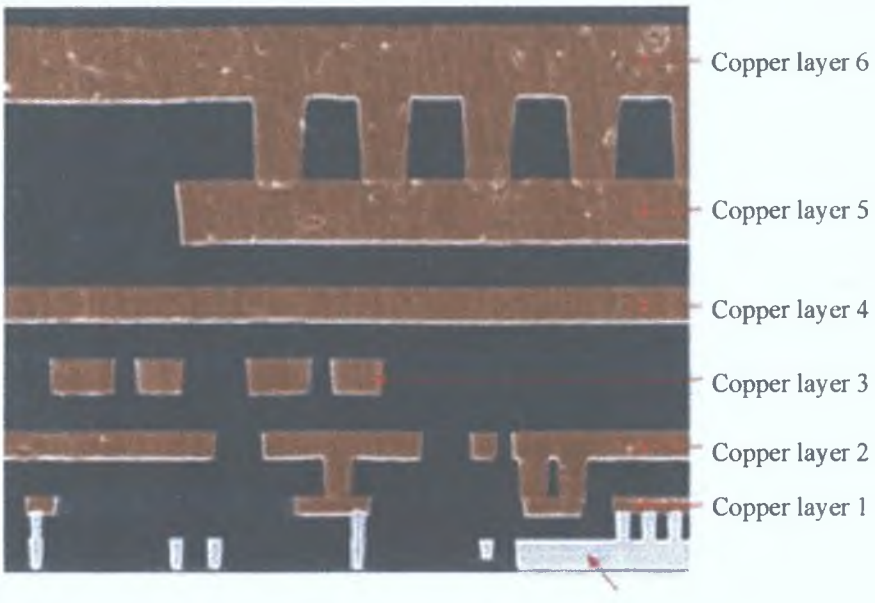
Copper layer 6
Copper layer 5
Copper layer 4
Copper layer 3
Copper layer 2
Copper layer 1
SEM cross-section
Local tungsten interconnect
Photo Credit: IBM

Figure 1.18

Chapter 2 Modelling the Sputtering Process

2.1 Introduction

The sputtering process has a very diverse range of applications, ranging from hard wear resistant coatings on drill bits to sub-micron high purity thin metal layers used in microchip fabrication[35][36]. Due to this diverse range of applications the size, shape and design of sputtering systems varies considerably. For this reason accurate models and simulations of the sputtering process can be of enormous benefit to both the system designer and the process engineer. A simulation package capable of providing information such as film non-uniformity, sputtered flux angular distribution, step coverage over sub-micron contacts and vias and the shadowing effects of clamps and shields would assist engineers in designing equipment and processes more rapidly and efficiently, minimising both development time and cost. Simulations and models also contribute significantly to the understanding of a process and the identification of trends which assist in process design.

A number of commercial sputter simulation packages exist, such as SIMBAD[37], DEPICT[38], EVOLVE[39] and SPEEDIE[40]. Commercial packages however tend to be limited in their scope of applications. Commercial simulation packages also tend to be very expensive and require powerful computers on which to run.

As the finance was not available for the purchase of a commercial sputter simulation package, a sputter simulation package called SPUTSIM was designed and developed in house[112][113]. The package was designed to be able to predict the properties of particle fluxes to surfaces in both 2D and 3D systems. The 2D and 3D simulation packages are known as SPUTSIM_2D and SPUTSIM_3D respectively. The motivation for the development of such a simulation was the requirement to study the deposition of thin films over a wide variety of features.

The SPUTSIM simulation software may not be as sophisticated as the professionally produced commercial simulation packages but it has advantages in terms of :

a) Cost

The software was developed on a PC using a C compiler As it was developed in-house it cost nothing only time and effort

b) Simplicity

The simulation runs on a PC and the I/O files are text based which interface easily with widely used office data analysis packages such as Microsoft Excel

c) Flexibility

The simulation was not designed with one particular application area in mind The philosophy was to simply predict fluxes to surfaces As will be shown throughout this work the simulation was as easily applied to a thin film uniformity problem over a 150mm substrate as it was to the film profile at the bottom of a sub-micron via feature

The SPUTSIM simulation simply predicts the properties of particle fluxes to the substrate It does not attempt to model or predict events that happen on the substrate surface Indeed, it would take a considerable effort to model and simulate events such as surface diffusion, surface self shadowing and nucleation phenomena with any degree of accuracy In chapters 4 and 5 of this work high temperature aluminium deposition into deep-sub-micron features is studied Under certain conditions surface diffusion lengths of sputtered adatoms are long with respect to sub-micron ULSI topography This is the case with high temperature aluminium deposition Therefore a more sophisticated simulation package is required to predict film coverage To study this phenomenon access was obtained to the SIMBAD film growth simulation package available at the Interuniversity Microelectronics Centre (IMEC) in Belgium

SIMBAD is a Monte Carlo film growth simulator which can be used to predict surface profiles and microstructures of thin films deposited over ULSI topography SIMBAD accounts for the effects of vapour flux shadowing and surface diffusion of the adatoms The simulation simulates 2-D hard disks launched from random points over the virtual feature The trajectory of each disk is tracked until it makes contact with the growing film On the film surface the incident disk is relaxed to the nearest cradle point with the largest number of nearest neighbours The relaxation process simulates surface

diffusion of the incoming particle that occurs in films to reduce the surface energy associated with areas of high surface curvature The trajectory of each disk does not represent the trajectory of an individual atom, but rather a large number of atoms that move through very similar trajectories The SIMBAD film growth simulation needs as input details of the fluxes of materials to the substrate surface This information can either be entered manually by the user or generated by another simulation package associated with SIMBAD known as SIMSPUD (SIMulation of SPutter flux Distributions)[41] SIMSPUD is a three-dimensional Monte Carlo simulation of the transport of sputtered material to the substrate The simulation tracks the individual sputtered particles from the time of their initial ejection from the target surface to their deposition on the substrate The inputs to the simulation include the system geometry, gas pressure, masses of the target and gas atoms and collision cross sections The software outputs data on the angular distribution of the material at the substrate surface, the relative flux densities at various points on the substrate and the energy distribution of the sputtered flux Details of the exact SIMSPUD process model have not been published so a comparison with the SPUTSIM process model is not possible The big advantage SIMSPUD has over SPUTSIM is software sophistication and ease of interface with the thin film growth simulation SIMBAD SPUTSIM however has the upper-hand when it comes to flexibility Figure 2 1 depicts the program structure of the complete SIMBAD simulation package

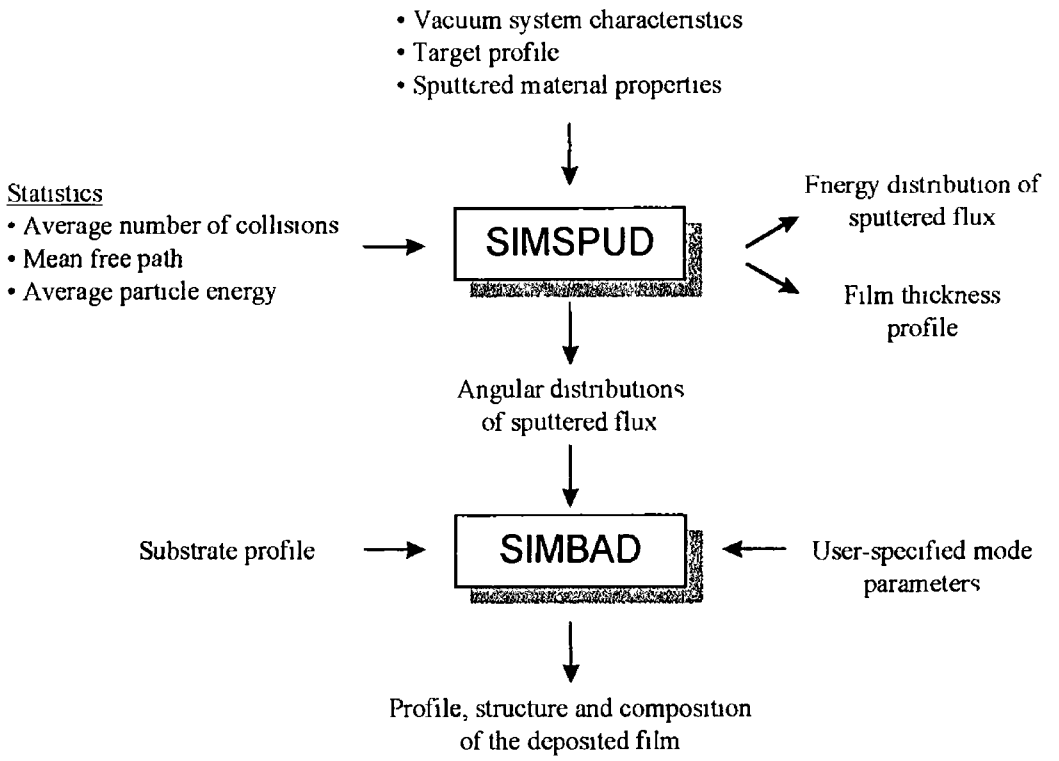

Figure 2 1 *SIMBAD Simulation Structure*

The EVOLVE, DEPICT and SPEEDIE packages mentioned earlier are designed exclusively for semiconductor manufacturing processes They are better described as film growth simulators rather than deposition process simulators Their approach is to divide the simulation task into two parts the process scale task and the feature scale task Both SPEEDIE and DEPICT address mainly the feature scale problem All of these packages predict the evolution of semiconductor surface structures during the various etch and deposition steps of the back-end production process PVD is just one of these deposition processes SPEEDIE, the Stanford Profile Emulator for Etching and Deposition in IC Engineering, uses surface kinetic models to convert local neutral and ion fluxes to etch or deposition rates

To model the complete magnetron sputtering process a large number of component processes must be taken into account, a number of which are

- Impinging ion flux energy and density
- Sputtering yield and secondary electron emission

- Sputtered atom ejection angles and energy
- Effect of cathode sheath
- Transport of particles through plasma / gas
- Ion bombardment of surfaces
- Sputtering due to energetic neutrals
- Magnetic field effects

Figure 2 2 shows a block diagram which breaks down the modelling task into a number of component parts

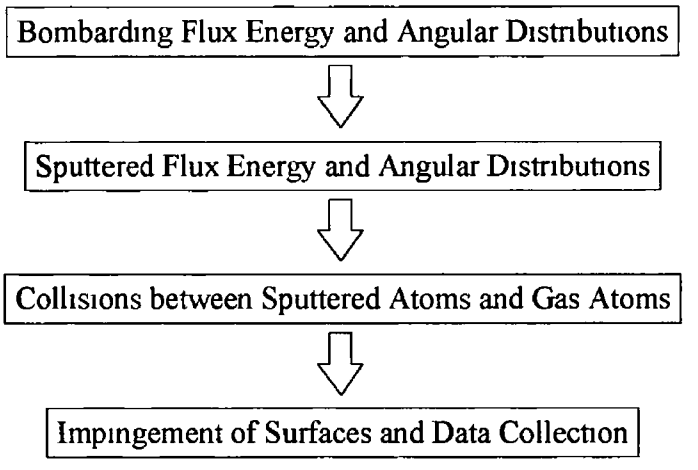

Figure 2 2 *Block Diagram of Sputter Modelling Task*

Over the past number of years much work has been carried out in modelling and understanding the above component processes

Goenecker et al[42] have simulated the ion dynamics in a magnetron system using Monte Carlo techniques and they have been able to predict the energy and angular distribution of the particles bombarding the target successfully

Particles are ejected from the cathode surface with a particular energy and angular distribution The energy distribution depends on the target material, the sputtering gas and the bombarding species' energetic distribution function Some previous simulations have assumed the ejected species to be monoenergetic[43][44] A more accurate

theoretical description can be obtained from the analytic expression developed by Thompson[45] This assumes that atoms are ejected due to random atomic collision cascades caused by the bombarding species, that the mean collision free path is independent of energy and that the existence of a surface binding energy causes refraction at the surface

The Thompson function provides expressions for the energy and angular distributions of the sputtered particles This function can be separated into two contributions, one for energy and one for emission angle

As an alternative to the Thompson distribution, Myers et al[46][47] have used fractal TRIM for the nascent sputter particle energy and angular distributions TRIM is a simulation of ion transport in matter developed by Biersack and Haagmark[48] TRIM is a Monte Carlo simulation of particle transport in the solid phase

The angle of emission generated by the Thompson function is therefore independent of the energy distribution Quite often the angular distribution is assumed to be a cosine distribution which agrees with experimental results Under different process conditions it has been shown that the angular distribution can vary from a cosine distribution[49]

After the sputtered atom is ejected from the target surface it must pass through the filling gas, undergoing collisions with gaseous atoms until it impinges on a surface On collision with another atom the direction and energy of the sputtered atom will be altered The mean free path of a particle passing through a gas can be generated from the kinetic theory of gases Many researchers have assumed the distance travelled by an atom between collisions to be a random fraction of the mean free path The accuracy of the model can be increased by making the mean free path a function of the kinetic energy in the system, as well as a function of the relative velocities of the colliding particles Gas phase scattering has been modelled by a number of different Monte Carlo models Motohiro[50] used both a hard sphere collision model and a potential interaction model based on Born-Mayer parameters Turner et al[51][52] used the 6-12 Lennard-Jones potential to describe collisions and Myers et al[46][47] used the 'universal' interatomic potential

2.2 Model of the Sputtering Process

The model used in SPUTSIM describes the motion of particles ejected from a target surface and passing through the filling gas, undergoing binary hard-sphere type collisions with the filling gas atoms, until eventual impingement on a surface The following simplifying assumptions were made

- The filling gas atoms are assumed to be stationary
- The collision cross-section between the sputtered particles and the background gas is assumed to be constant
- Only collisions between sputtered particles and background gas atoms are considered

Particles are ejected from a random point on the target surface In order to take into account the fact that the majority of the particles in a real system are ejected from the racetrack region, the probability distribution function could be weighted to increase the likelihood of ejection from the racetrack region of the target

It has been shown experimentally that the ejection angle of sputtered particles can be approximated be a cosine distribution[49] Therefore the ejection angle used in the Monte Carlo simulation is generated from

$$q = sin^{-1}(2*u3 - 1)$$

where $u3$ is a random number

Take cumulative distribution function (cdf) as a random variable between 0 and 1 For a $cos(Q)$ distribution

$$pdf\ p(Q) = kcos(Q)$$

$$cdf\ P(Q) = INT\ \{k\ cos(Q)dQ\} + m$$

$$cdf\ P(Q) = k\sin(Q) + m$$

$$P(-PI/2) = 0 = -k + m$$

$$P(PI/2) = 1 = k + m$$

$$\Rightarrow \quad m = \tfrac{1}{2} \qquad k = \tfrac{1}{2}$$

$$\Rightarrow \quad P(Q) = \tfrac{1}{2}(\sin(Q) + 1)$$

make $P(Q)$ a random variable

$$\Rightarrow \quad R = \tfrac{1}{2}(\sin(Q) + 1)$$

$$\Rightarrow \quad \sin(Q) = 2R - 1$$

$$\Rightarrow \quad Q = \sin^{-1}(2R - 1)$$

Figure 2.3 plots the ejection angle Q as a function of the random variable R.

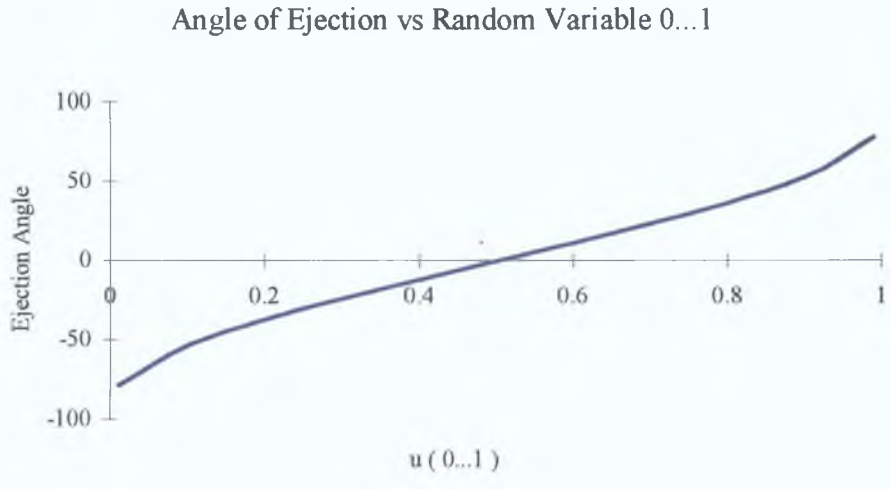

Figure 2.3

The initial energy distribution of the sputtered particles was generated using an approximation of the Thompson function. The Thompson distribution function for incident ions of several hundred eV's can be approximated by a simple cascade distribution[112]

$$P(E) = \frac{2E_b}{E^2(1+\frac{E_b}{E})^3}$$

Where P(E) is the relative probability of emitting an atom of energy E and E_b is the surface binding energy, which typically ranges from 1 - 4 eV. It was assumed that the incident flux was monoenergetic with an energy of 500eV. The software used a random variate generation method based on rejection to create a file of initial energies. Rejection techniques are commonly employed to sample complicated distributions where inversion of the distribution function is neither possible or practical. A computer program written in 'C' was written to carry out the necessary calculations. Details of the generation method are given in appendix B. Figure 2.4 graphs the output of the rejection algorithm computer program for titanium with a binding energy of 4.85eV.

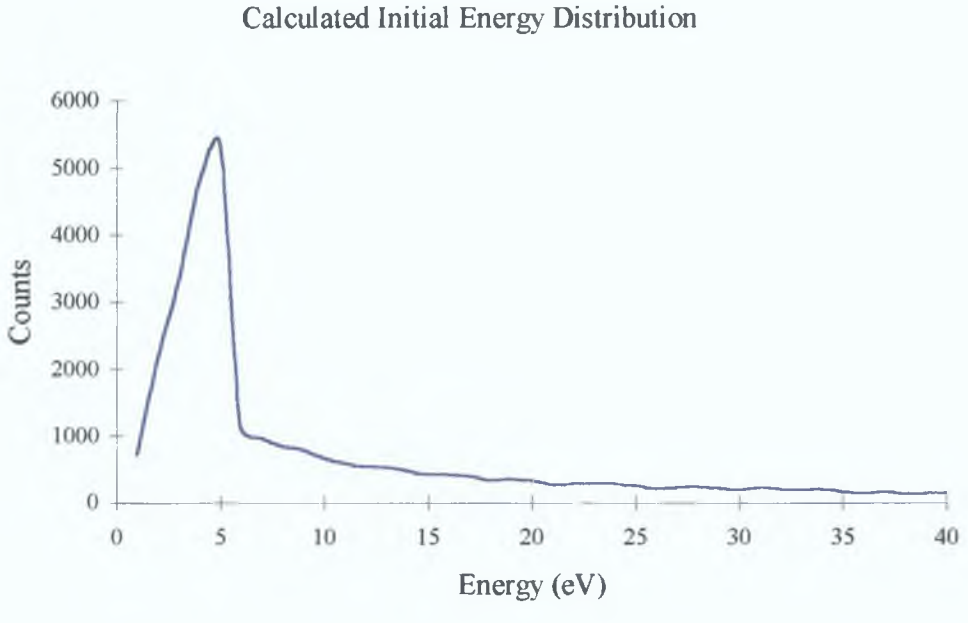

Figure 2.4 *Calculated Initial Energy Distribution of Sputtered Atoms*

2 3 The Particle Transport / Scattering Process

The mean free path, *mfp*, was generated from the kinetic theory of gases and for simplicity was assumed to be independent of energy The distance between collisions, L, was calculated from

$$L = \ln(1/(1-u_1)) * mfp$$

where u_1 is a random number generated uniformly between 0 and 1

For exponential *mfp* free path y

$$pdf \quad p(x) = k\, exp(-x/y)$$

$$cdf \quad P(x) = INT\ \{k\, exp(-x/y)\, dx\} + m$$

$$P(x) = -yk\, exp(-x/y) + m$$

$$P(0) = 0 = -yk + m$$

$$P(infinity) = 1 = m$$

$$\Rightarrow \quad k = 1/y$$

$$\Rightarrow \quad P(x) = -exp(-x/y) + 1$$

$P(x)$ is random variable R

$$\Rightarrow \quad R = -exp(-x/y) + 1$$

$$\Rightarrow \quad exp(-x/y) = 1 - R$$

$$\Rightarrow \quad -x/y = \ln(1 - R)$$

$$\Rightarrow \quad x/y = \ln(1 / (1 - R))$$

$$\Rightarrow \quad x = y \ln(1 / (1 - R))$$

Figure 2.5 plots the probability of collision as a function of distance travelled for a 200mm mean free path.

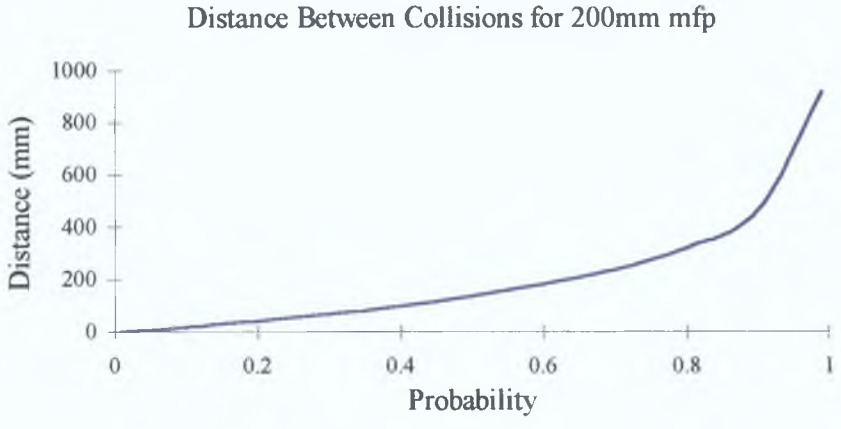

Figure 2.5

It is shown in appendix C that the mean free path can be approximated by the equation

$$\lambda = \frac{kT}{P} * \frac{1}{\sigma}$$

where k is Boltzmann's constant, T is the gas temperature, P is the pressure, and σ is the collision cross section. It is known that the collision cross section is a function of the energies of the colliding particles[53]. Unfortunately it is very difficult to find data on cross sections for energetic metal atoms colliding with inert gas atoms. To estimate the collision cross section an interpolation technique was used similar to that used by Somekh[43]. If the cross sections for two inert gases is known, the cross sections for the particles of interest can be approximated using the following equation:

$$C(E) = C_{Ar}(E) + [\, C_{Kr}(E) - C_{Ar}(E) \,] * (Z_1 - Z_2)/(Z_{Kr} - Z_{Ar})$$

where

$C_{Ar}(E)$ = cross section for argon

$C_{Kr}(E)$ = cross section for krypton

Z_1 = atomic number of metal atom

Z_2 = atomic number of gas atom

Somekh's cross sections were based on Robinson's original calculations for Ar, Kr and Xe Robinson presents data for the energetic collision cross section for Ar, Kr and Xe as a function of energy[54]

Taking data directly from the graphs presented, the following table approximates Robinson's results for momentum transfer

Energy (eV)	Ar	Kr
1	7 1	9 00
2	6 0	8 00
5	4 6	7 00
10	3 8	6 25
20	3 0	5 70
50	2 5	4 95
100	2 0	4 20
200	1 8	3 85
500	1 5	3 10
1000	1 1	2 80

Table 2 1 *Ar-Ar and Kr-Kr Collision Cross Section (Angstroms^2)*

Using the equation given above, table 2 2 is an approximation of the collision cross section between an Argon and Titanium atom over a range of energies

Energy (eV)	Ti/Ar Cross Section
1	7 54
2	6 46
5	5 15
10	4 36
20	3 62
50	3 06
100	2 50
200	2 27
500	1 87
1000	1 49

Table 2 2 *Ti - Ar Collision Cross Section (Angstroms^2)*

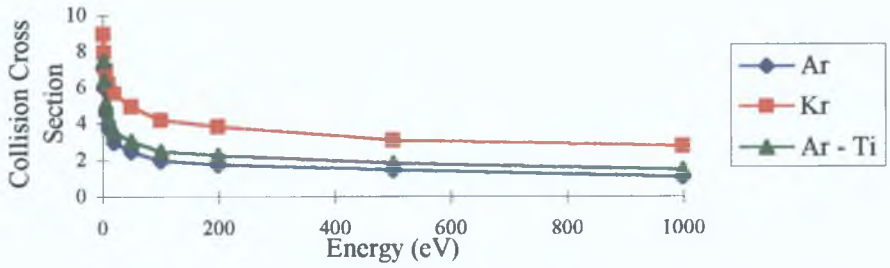

Figure 2.6 *Collision Cross Section Comparison (Angstroms^2)*

The energy dependent collision cross sections for Ar-Ar, Kr-Kr and Ar-Ti collisions are plotted in figure 2.6. The collision process was based on the hard sphere collision model used by Motohiro[50].

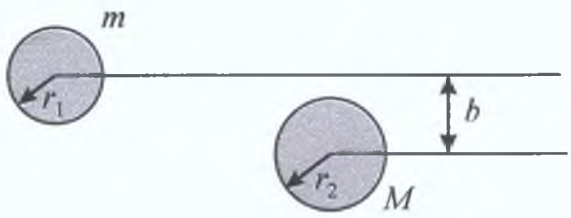

Figure 2.7 *Impact Parameter Illustration*

The scattering angle and the energy transfer was characterised by the impact parameter b as shown in figure 2.7.

$$b = (r_1 + r_2) * \sqrt{u_2}$$

where u_2 is a random number and r_1 and r_2 are the radii of the colliding particles.

The thermal motion of the gas atoms was neglected and the atomic radii were obtained by interpolation of experimentally determined radii of hard cores of several inert gas atoms under Sutherland's atomic model of '*Smooth Rigid Elastic Spheres Surrounded by Fields of Attractive Force*'[55][56].

Sutherland derived the following equation from measurements of the temperature dependence of the viscosity of gases

$$\delta(T) = \delta_m(1 + \frac{C}{T})$$

Where $\delta(T)$ is the radius of the gas molecules at a temperature T and C is a characteristic constant of the gas. From this equation $\delta(T)$ approaches δ_m as T increases, which corresponds to the radius of the hard core in the Sutherland approximation of the atomic potential. As the energy of the sputtered atoms is much greater than that of the thermalised gas atoms, δ_m will be an approximate value for the radius of the hard core in the Sutherland approximation of the atomic potential.

In this study the values for the radii of the argon and titanium atoms were taken from experimentally obtained δ_m values presented in reference[57].

$$r_{Ar} = 1.21\text{A}, r_{Ti} = 1.22\text{A}$$

From classical mechanics the scattering angle for a spherically symmetric atom - atom type collision in the centre of mass frame is given by

$$\chi(b) = \pi - \frac{2b}{r^2}\int_{r0}^{\infty} \frac{dr}{\sqrt{1-[V(r)/E]-[b^2/r^2]}}$$

Were $V(R)$ is the intermolecular potential (or the interaction potential), b is the impact parameter, and r_C is the distance of closest approach given by[58]

$$1 - \frac{\rho^2}{r_c^2} - \frac{V(r_c)}{\varepsilon} = 0$$

Numerous interaction potentials have been used by other authors in modelling atom - atom collisions in a sputtering process. The hard sphere potential used in this model, with its radius derived from viscosity measurements as described above, has the advantage that the scattering equation can be solved analytically. This type of potential is a reasonable approximation for the low energy collisions applicable to sputtering

deposition processes. Motohiro concludes in reference[50] that the results of the hard sphere collision model show little deviation from those of the more complex potential collision models. Yamamura et al[59] conclude that the hard sphere approximation gives reasonable results if its energy dependent collision diameter is properly selected. The computing time is much shorter than the TFM interaction potential and the Moliere interaction potential also investigated in Yamamura's paper.

For the hard sphere interaction potential model used the scattering angle is given by[60]

$$\theta = \arctan\left[\frac{M.\sin\{\pi - 2.\arcsin[b/(r_{Ar}+r_{Ti})]\}}{m + M.\cos\{\pi - 2.\arcsin[b/(r_{Ar}+r_{Ti})]\}}\right]$$

where θ is the scattering angle in the laboratory system, m is the mass of the sputtered atom and M is the mass of the sputtering gas atom.

A 'C' program was written to examine the relationship between the scattering angle θ and the impact parameter b.

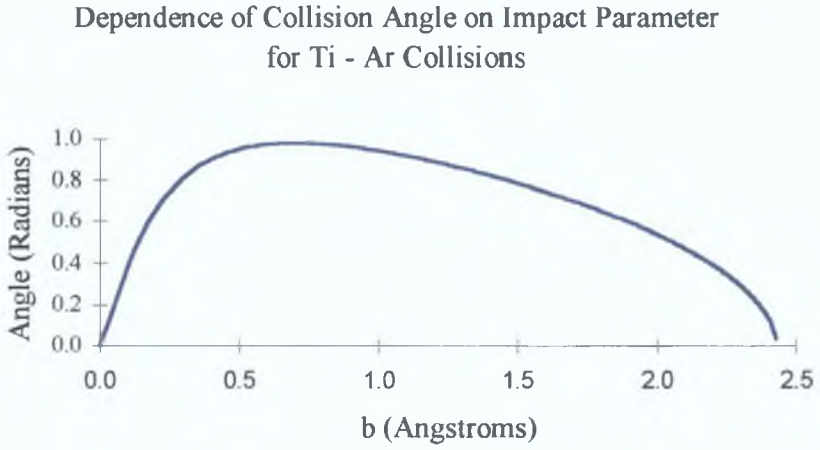

Figure 2.8

Figure 2 8 plots the scattering angle as a function of impact parameter, where the mass of the gas atom was 39 948g/mol and the mass of the metal atom (Ti) was 47 90g/mol

The energy loss rate is given by

$$k = [m_1^2 + m_2^2 - 2 * m_1 * m_2 \{1 - 2 * (b / (r_1 + r_2))^2\}] / (m_1 + m_2)^2$$

The trajectory of a particle was followed until it impinged on a surface If the particle impinged on the substrate surface, its position and energy was recorded
The simulation software was programmed in C on an IBM compatible PC A schematic of the software architecture is given in figure 2 9

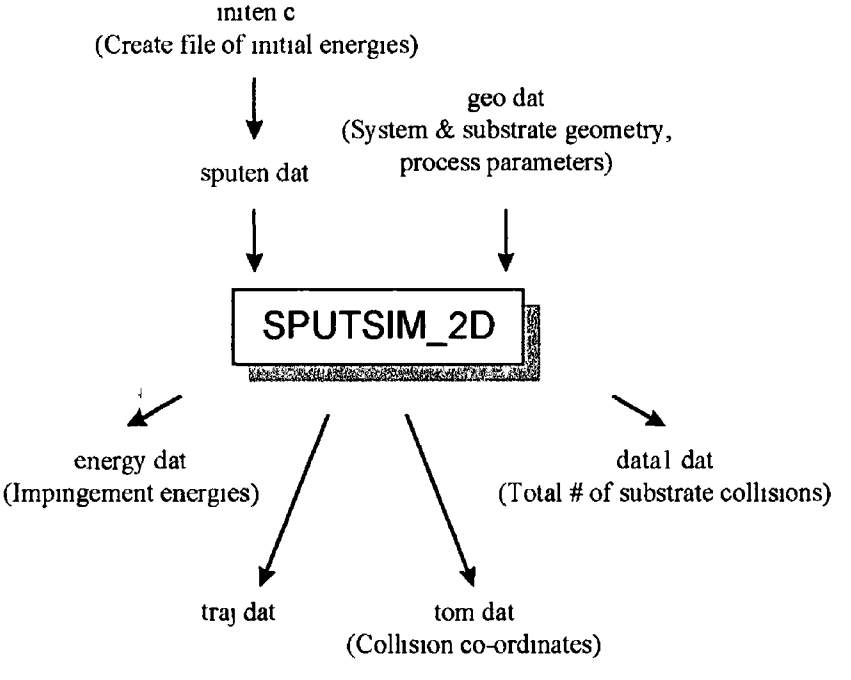

Figure 2 9 *Structure of SPUTSIM_2D Simulation Software*

2 4 SPUTSIM A 3-D computer simulation of sputtered atom transport in a sputter discharge using Monte Carlo techniques

This section describes the development of a 3D simulation package which simulates the ejection of sputtered atoms from the surface of a target and their transport through a plasma

2 4 1 Software

The 3-D system is described by Cartesian geometry with x, y and z axes The target is located in the y-z plane at $x = 0$ and it is centred at (0,0,0) The dimensions of the target are input by the user while running a simulation The 'virtual' system is rectangular in shape, 20cm long in the x direction, 26cm in the y direction and 26cm in the z direction

When a particle collides with a gaseous atom, it is scattered and its direction and energy are altered The following section explains how a particle's trajectory is calculated in 3D on emission from the target surface and on collision with another particle

2 4 2 3D Particle Trajectory after a Collision

The following is an explanation of how the particle trajectory after a collision is calculated by the software See figure 2 10 for an illustration

Particle A_1 is at a point p_1 It travels in the direction of a second particle A_2 which is stationary and located in space at a point p_2 When the particles collide, A_1 moves away from the point p_2 with a known velocity and at a particular point in time its position in space is p_3 From a knowledge of p_1, p_2, *mfp* and the scattering process, p_3 can be calculated

Parametric equations can be used to describe the equation of a line passing through points p_1 and p_2

$$x = f(t),\ y = g(t),\ z = h(t)$$

Define L_1 as the line passing through p_1 and p_2

The collision process described earlier describes an angle of deflection after a collision has taken place between two 2D disks However 3D collisions need to be considered To do this consider a cone with its apex at p_2 and its axis along L It can be assumed that the trajectory of the particle A_1 after collision is a straight line along the surface of the cone, p_3 is therefore a random point on the circle characterised by the base of the cone The angle of the cone is a function of the scattering angle generated by the collision model and the depth of the cone is a function of the distance travelled by the particle after the collision before it collides with another particle at p_3

Next find the equation of a plane which contains the point p_3 In particular it would be useful to find the equation of the plane containing p_3 which is perpendicular to L_1 The equation of the line L_1 is known and from this and a knowledge of the *mfp* and θ, the co-ordinates of the point p_4 can be found, which is the point at which L_1 intersects the plane $PL1$ From vector algebra, if there is a point on a plane and it is known that it is normal to a known vector, the equation of that plane can be calculated The base of the cone is on the plane PL_1 Also the centre point of the circle where the cone intersects the plane is known and from θ and the *mfp* ,the radius of the circle which defines the base of the cone can be found

It now remains to find a random point on this circle C_1 Consider a random point p_5 on the plane PL_1 Draw a line from this point to p_4, the centre of the circle From p_4 and p_5 the equation of a line L_2 can be generated This line intersects the circle C_1 at two points Moving away from p_4 along L_2 for a distance r_1 (the radius of the circle) the co-ordinates of a random point p_3 on the circle can be found

Therefore the line joining p_2 and p_3 is the trajectory of the particle after collision with a particle at point p_2 The particles next point of collision is at the point p_3

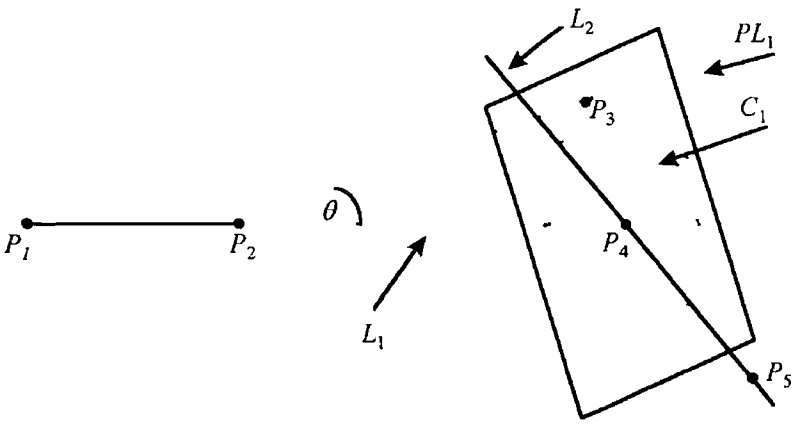

Figure 2 10 *Particle Trajectory After Collision*

2 4 3 Software Features

The code for SPUTSIM was implemented in C The code has the following capabilities

- Particles can be ejected from random points on a target surface or from a specified racetrack region
- The variables sputter pressure, sputter gas, target material, number of particles to simulate, target and racetrack geometry and substrate geometry are input to the program via a data file
- The substrate is considered by the software to be a set of surfaces Any number of surfaces can be considered with the limitation that each surface must be parallel to either the *x*, y or z plane
- The average energies of the particles leaving the target surface are generated by a program *sputen c* This program creates a data file of random energies based on the Thompson distribution function, with target material and target voltage as input parameters
- The energy of every particle impinging on the substrate surface is output to a data file with details of the surface number and the exact co-ordinates of the intersection
- The angle of impingement of each impinging atom is recorded with the surface number and exact co-ordinates
- Numerous graphical outputs are available For example *displ c* outputs a bar chart comparing the number of atoms impinging on each surface, *surfdis c* looks at the shape of a film on a specified surface while *uniform c* calculates the uniformity of a film on a specific surface

2.5 SPUTSIM Application. Material Deposited on Chamber Walls during the Sputter Etch Process

2.5.1 Introduction

Sputter Etching is the process of bombarding a substrate with ions with the object of removing a certain amount of the substrate surface material by physical means Typically an rf or dc source is used to bias the substrate negatively relative to an anode and a discharge is sustained with the substrate acting as the cathode This technique is most frequently used to clean a substrate in a vacuum environment prior to film deposition In semiconductor manufacturing the sputter etch process is used to remove native oxide and post etch fluorocarbon residue from contacts and vias on device wafers prior to metallisation[61]

When a wafer is being sputter etched prior to deposition of interconnecting metals, the vast majority of the material exposed to the plasma is SiO_2 (or SiN) It is expected that the majority of the material deposited on the shields and walls of the sputter etch chamber will be Si, and / or SiO_x In this study the material deposited on chamber walls after etching SiO_2 and SiN in Ar and $Ar/H_2(5\%)$ plasmas will be examined The thickness of the deposit as a proportion of the overall amount of etched material is measured and the accuracy of the SPUTSIM-2D model and simulation in predicting the amount of deposited film will be examined

2 5.2 Experimental

The sputter etch chamber used was the commercially available Preclean II™ process chamber available from Applied Materials This chamber consists of an upper coil powered by a 400kHz supply and a cathode powered by a 13 56mHz rf supply The cathode supply is used to generate a negative bias on the wafer to attract ions from the plasma and the coil is used to increase the density of the plasma, making more ions available for the etching process A schematic of the chamber is shown in figure 2 11

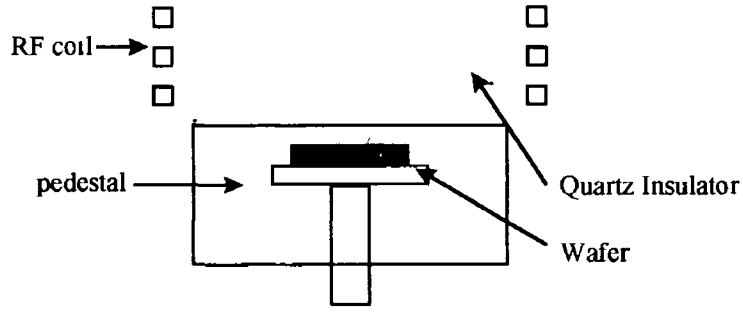

Figure 2 11 *Diagram of Sputter Etch Chamber*

Small pieces of crystalline <100> Si were placed at various points in the process chamber The Si pieces were dipped in HF prior to placement in the chamber in order to remove any native oxides The chamber was then pumped down to high vacuum and allowed to sit at high vacuum for a number of hours in order to give the various components in the chamber time to out-gas

Four experiments were run using different plasma / substrate combinations The plasma was either an Ar plasma or an Ar/H_2 (5%) and the substrate was either SiO_2 or SiN

For each process split eighteen 150mm diameter SMF(semi-major flat) wafers were etched consecutively The etched process removed approximately 300nm per wafer at a DC bias of 180V After the eighteen wafers had been etched the chamber was vented and the Si pieces removed The thickness and composition of the deposition on the Si pieces was measured using RBS

The SPUTSIM-2D simulation package was used to predict the amount of Si deposited on the Si pieces Approximate wafer and chamber geometries were input to the program and the simulation was run for 30,000 particles

2.5 3 Simulation

The wafer was located along the x-axis at $x = 0$ The wafer was 15cm long, from +7 5 to -7 5 on the y-axis The simulation software was unable to deal with the curved surface of the bell jar, so this was approximated by a rectangular piece of approximately the same height The substrate was 3cm long located at (2 6,9 6) -> (2 6,12 6) See figure 2 12 for an illustration

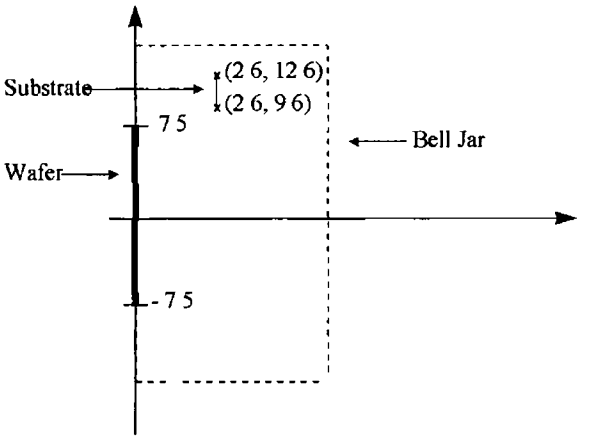

Figure 2 12 *Diagram of Virtual Chamber*

2.5 4 Results

The simulation was run for 30,000 particles at a process pressure of 0 5 10^{3}mbar which corresponded to a mean free path of approximately 13mm Of the 30,000 particles ejected from the wafer surface, 1095 particles impinged on the substrate The simulation is in 2D For the results to be meaningful, the results need to be interpreted in 3 dimensions The line defining the substrate in 2D can be considered a circular band in 3D, the area of which is defined by

$$A_{band} = \pi(r_1^2 - r_2^2)$$

The area of the target (wafer) is simply πr^2

In the specific case being considered,

$$A_{band} = 203\ 48\text{cm}^2$$

$$A_{target} = 176\ 65\text{cm}^2$$

The volume of material etch from the wafer surface is given by

$$V_{target} = A_{target} * t_{etch}$$

where t_{etch} is the total thickness of material etched

The percentage of material ejected from the target / wafer which impinges on the substrate is 3 65% So the volume of material which impinged on the substrate V_{sub} is given by

$$V_{sub} = 3\ 65\ *\ V_{target} / 100$$

The thickness can then be calculated from

$$t_{dep} = V_{sub} / A_{band}$$

The results of the measured and simulated film thicknesses are tabulated in table 2 3

Film	Plasma	Thickness Etched (μm)	Composition	Thickness Measured	Simulated Thickness
SiO_2	Ar	5 4	SiO_2	0 07-0 12	0 16
SiO_2	Ar/H_2	5 4	SiO_2	0 06-0 12	0 16
SiN	Ar	5 0	SiN	0 06-0 11	0 14
SiN	Ar/H_2	5 0	SiN	0 06-0 12	0 14

Table 2 3 *Measured and Simulated Thickness (μm)*

The simulated thickness is very comparable to the actual measured thickness for each of the four processes, especially given that the deposit on the samples is very non-uniform This indicates that the simple SPUTSIM-2D model is accurate in the 10^{-3} mbar pressure regime

This experiment also illustrates how SPUTSIM can be usefully applied to a real life situation The amount of deposition on the shields is an important parameter to consider in a production process as under normal circumstances there is a limit on the amount of deposit on a kit before it starts to flake, leading to unacceptable levels of particle contamination

2.6 SPUTSIM-3D Application. Examination of Thin Film Uniformity at the Bottom of a Hole.

2.6.1 Introduction

In any thin film application it is important to ensure that the properties of the film are consistent over the entire substrate surface of interest This constraint may be difficult to achieve on large substrates or substrates with complex geometries Frequently it is necessary to ensure a uniform film thickness over a substrate surface Uniform film thickness may be necessary to ensure consistent mechanical or electrical properties

The SPUTSIM-3D simulation package described earlier simulates in 3D the flux of sputtered atoms from a target surface For a given set of process parameters and system geometries, the simulation will predict the intensities and energies of the fluxes of sputtered atoms to each surface of a specified 3D substrate Details of the model on which SPUTSIM is based have been discussed earlier

In this section SPUTSIM-3D is used to examine the thickness uniformity of a film at the bottom of a 'hole' structure as a function of process pressure, target racetrack geometry and hole depth The simulated 'hole' structure approximates the typical arrangement in a commercial sputtering system used, for example, to deposit metal layers on a silicon wafer The hole walls correspond to the chamber walls and shields etc , the bottom of the hole corresponds to the wafer surface

The trends in uniformity predicted by the simulation are compared to trends in a real sputter system

2 6 2 Description of the Simulated System

The virtual system on which the simulation was run is a rectangular chamber 26 cm long in the x direction, 20 cm high in the y direction and 20 cm wide in the z direction The target is positioned on the y-z plane at $x = 0$ It is centred at $x = 0$, $y = 0$, $z = 0$ The substrate is an open box type structure with the open end facing the target The open face is a square with side length 4 cm The racetrack geometry will be experiment specific and it is assumed that all particles sputtered from the target are sputtered from

the racetrack region The simulated target material is titanium and the process gas is argon A diagram of the system is given in figure 2 13

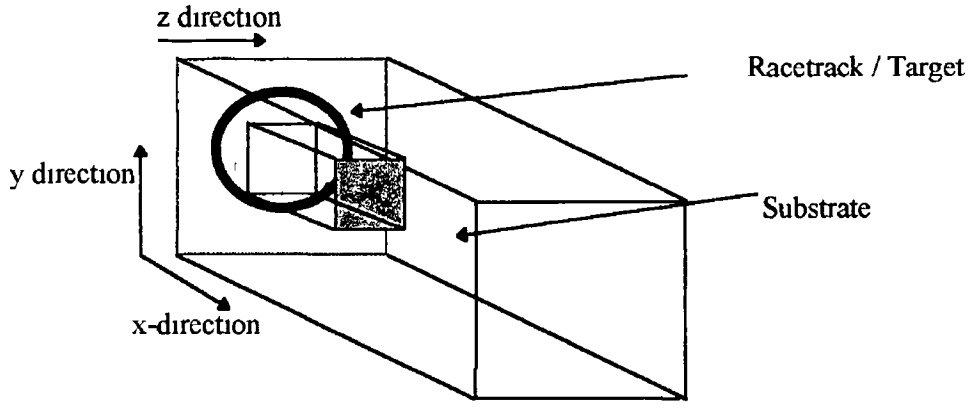

Figure 2 13 *Diagram of the Simulated System*

2 6 3 Experimental Set-up

The tests were run in a commercially available PVD system on 200mm bare silicon wafers The sputter chamber was evacuated using a cryo pump and the base vacuum was in the 10^{-8}mbar range The chamber was fitted with a titanium target with a specified purity of 99 9995% The magnetron used was also commercially available from the equipment supplier A schematic of the sputter chamber is shown in figure 2 14

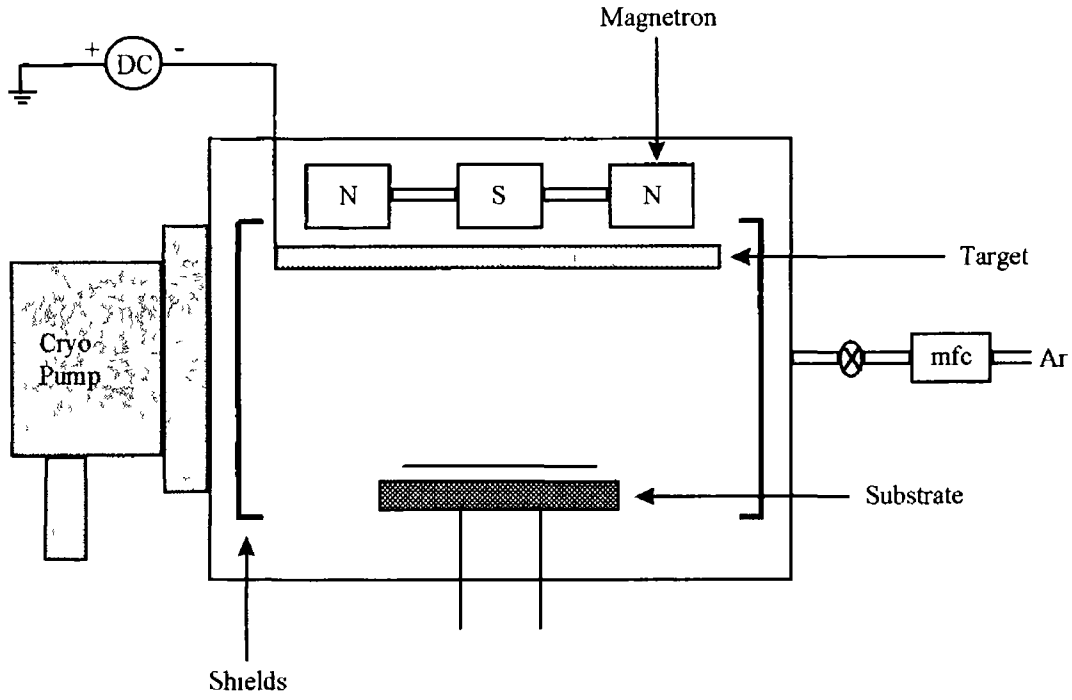

Figure 2 14 *Schematic of Sputter Chamber*

2 6 4 Results

For each of the simulations the total number of particles simulated was 90,000 It was assumed that the sticking coefficients of particles impinging on any surface was unity

In order to calculate the film uniformity the following formula was used

$$Sigma = \sqrt{\frac{(M1 - Mean)2 + (M2 - Mean)2 + \qquad (Mn - Mean)2}{n - 1}}$$

$$Sigma(\%) = (Sigma/Mean) * 100$$

Where *Sigma* is the non-uniformity and n is the number of measurement points on the surface

In these simulations nine surface sites were 'measured' The substrate surface was divided into nine squares of 1 33 cm side length The centre of each square corresponded to a measurement site

2.6.5 Film Uniformity as a Function of Process Pressure

In this experiment the process pressure was varied between 0.5 10^{-3} mbar and 6.0 10^{-3} mbar. All other parameters were kept constant. The hole depth was 4 cm. The racetrack configuration was set to be a circular ring with inner diameter 4 cm and an outer diameter of 4.5 cm. All the particles from the target surface were assumed to be ejected from the racetrack region. The results of the simulations are displayed in figure 2.15.

It can be seen that the non-uniformity generally decreases as the system pressure is increased (the increase at a pressure of 1 10^{-3} mbar is an artefact due to the limited number of particles in the experiment). The only parameter in the model which changes in these simulations is the mean free path of the sputtered particles. As the pressure is increased, i.e. the mean free path is reduced, the sputtered atoms undergo more collisions before reaching the substrate and hence there is more randomness in their direction and more even distribution. It should be pointed out, however, that the thickness of the film also decreases with increasing pressure since more atoms are scattered away from the substrate on to the chamber walls.

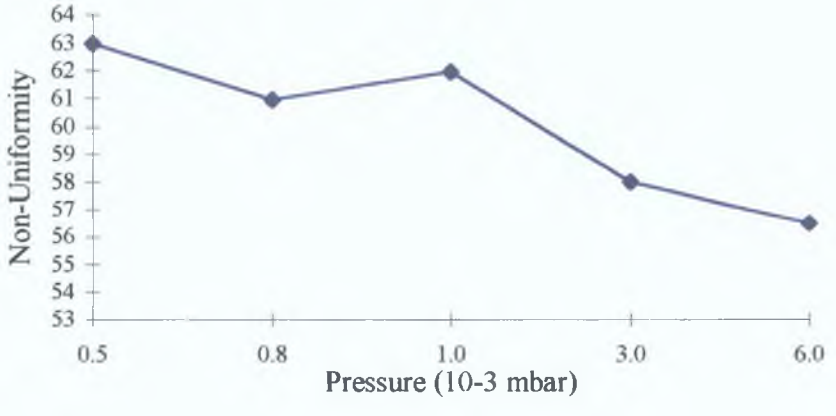

Figure 2.15 *Non-Uniformity vs Pressure*

In order to verify the validity of the simulation predictions, the relationship between non-uniformity and process pressure in a real sputter system was examined. The

process pressure was varied by controlling the flow of argon gas into the chamber using a mass flow controller The titanium film deposited had an approximate thickness of 1000 angstroms The variation in thickness across the wafer was interpolated from 4-point probe sheet resistance measurements taken at nine points on the wafer surface using a prometrix automated sheet resistance measurement tool

The process pressure was varied between 0 5 10^{-3}mbar and 6 0 10^{-3}mbar and the deposition temperature for each wafer was kept constant at 150°C The target to wafer spacing was set to 40mm The results are presented in figure 2 16

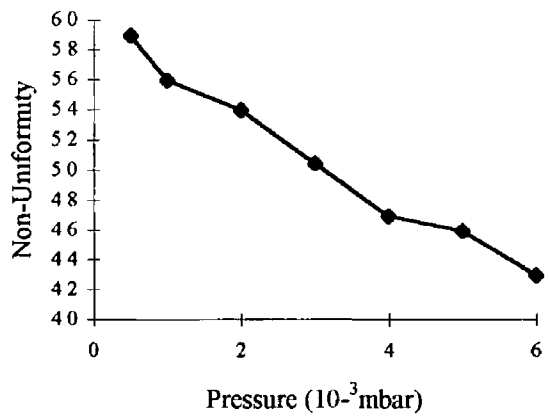

Figure 2 16 *Measured Non-Uniformity vs Pressure*

The results show the downward trend in non-uniformity with increasing pressure as predicted by the Monte Carlo simulations The actual non-uniformity figures differ between the simulation and experiment This is expected as the racetrack geometry of the real target differs considerably from that of the simulated target The important trend however is the decrease in uniformity with increasing pressure

With increasing pressure the number of collisions a sputtered particle is likely to undergo before impingement on the substrate increases Therefore it is more likely that more particles stick to the shields, resulting in fewer particles on the substrate The average sheet resistance of each wafer is plotted in figure 2 17 The increasing sheet resistance corresponds to decreasing film thickness

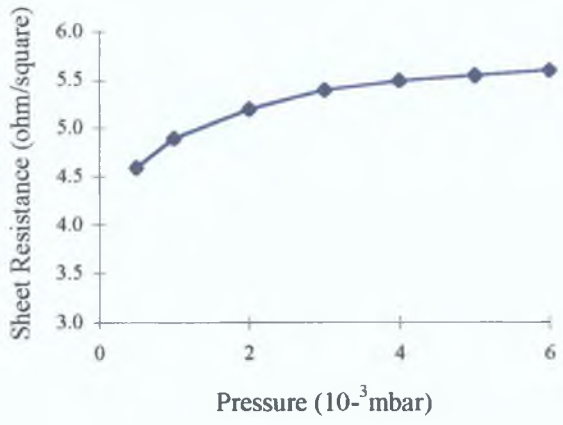

Figure 2.17 *Film Sheet Resistance vs. Pressure*

2.6.6 Film Uniformity as a function of Racetrack Geometry

The purpose of this experiment is to examine how the film uniformity at the bottom of the hole varies with the racetrack geometry. For this experiment the pressure was kept constant at 310^{-3} mbar. The racetrack is a 0.5 cm thick circular ring. By varying the inner and outer diameters the size of the racetrack was varied. The following geometries were simulated

#1	r_1= 2.0cm, r_2 = 2.5cm
#2	r_1 = 2.5cm, r_2 = 3.0cm
#3	r_1 = 3.0cm, r_2 = 3.5cm
#4	r_1 = 3.5cm, r_2 = 4.0cm
#5	r_1 = 4.0cm, r_2 = 4.5cm
#6	r_1 = 4.5cm, r_2 = 5.0cm

where r_1 is the inner diameter and r_2 is the outer diameter. It has been assumed that the flux of sputtered atoms is emitted uniformly from all parts of the racetrack region. In reality, the flux from a magnetron target will show a peak at the diameter of the racetrack and will decrease gradually at greater or lesser diameters, the exact shape of the distribution depending on the magnet configuration in the magnetron. It is intended to incorporate such a variation in the flux model, however, at present assuming a uniform flux distribution gives a reasonable approximation to this. It is likely that the non-uniformity may be rather overstated in the existing model since it will give too

abrupt a change between the racetrack and the rest of the target. The results of the simulations are shown in figure 2.18. From the results it is seen that the optimum uniformity is achieved at racetrack geometry #5. Here the racetrack outer diameter is slightly greater than the hole orifice. It can be seen that the best uniformity, unsurprisingly, occurs when the racetrack region is centrally placed above the hole. This highlights the difficulty which will be achieved in coating inside an aperture which is not in line of sight with the emitting area of the magnetron target.

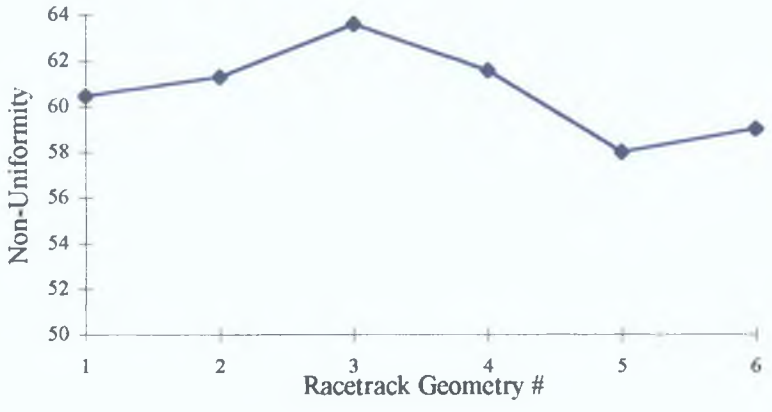

Figure 2.18

2.6.7 Film Uniformity as a function of Hole Depth

In figure 2.19 the uniformity of the film on the bottom surface of the hole is examined as a function of the hole depth at a constant pressure of 3 10^{-3} mbar. The racetrack geometry was set to inner and outer diameters of 4.0 and 4.5 cm. Simulations were carried out for hole depths of 2 to 10cm at 2cm intervals.

It is evident that the non-uniformity of the film thickness decreases as the hole depth increases. This can be understood as follows. As the hole depth increases, the flux of atoms arriving at the bottom surface will become more perpendicular to it since oblique-angled atoms will tend to collide with the hole walls and thus become filtered out i.e. it behaves like a collimator. However, as shown in figure 2.20, the film thickness at the centre of the bottom surface also decreases markedly as a function of hole depth due to increased scattering of the sputtered atoms and their subsequent collision with the hole walls. At a point in the centre of the bottom surface, the

simulation predicts that at a distance of 10cm the film thickness is only 12% of that at a distance of 2cm. Moreover, at a hole depth of 10 cm, only 2% of the sputtered atoms reach the bottom surface. Under these circumstances it is difficult to obtain an accurate description of the topology or uniformity from the simulation because of the relatively few atoms arriving on the surface.

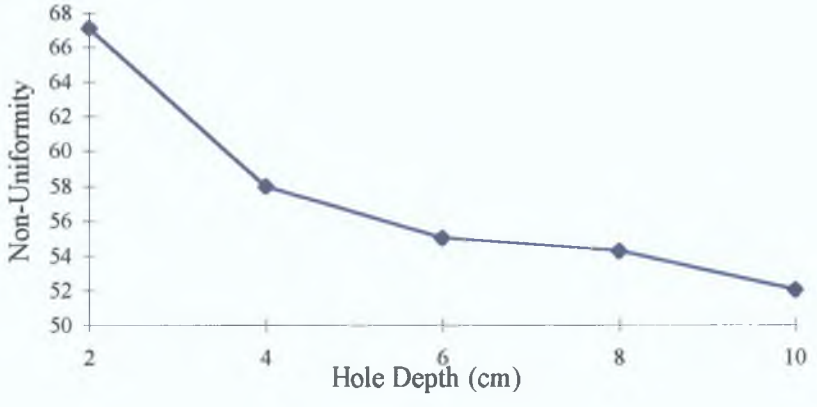

Figure 2.19 *Non-Uniformity vs. Hole Depth*

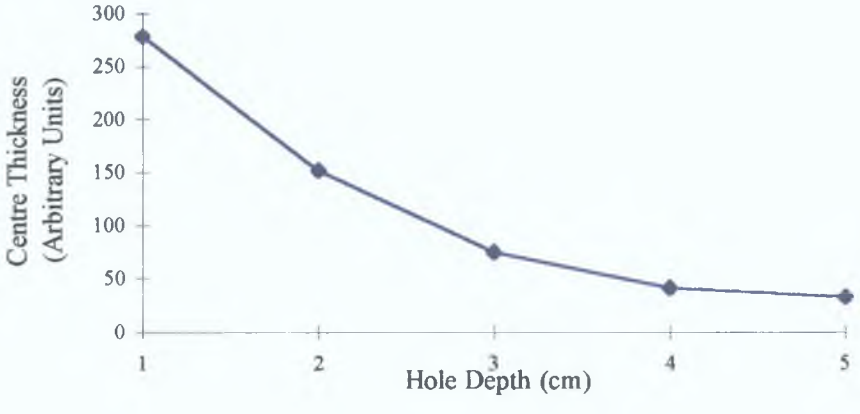

Figure 2.20 ***Film*** *Centre Thickness vs Hole Depth*

In this case hole depth is analogous to target to substrate spacing. The process pressure was kept constant at 3 10^{-3}mbar and the target to substrate spacing varied between 4 and 7cm. This spacing range was limited by the process chamber hardware. The non-uniformity as a function of spacing is shown in figure 2.21.

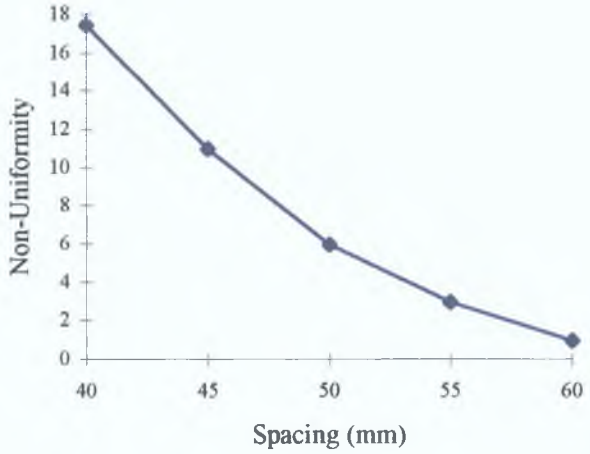

Figure 2.21 *Measured Non-Uniformity vs. Spacing*

The downward trend in non-uniformity with process spacing agrees with the earlier simulation results.

In practice of course the target - substrate spacing is limited by a number of factors, particularly the fall in deposition rate. The greater the target to substrate spacing the greater the average number of collisions a sputtered particle is likely to have before reaching the substrate and hence the more likely it is for the particle to be scattered to the chamber walls or to the process chamber shields. The normalised film thickness for each of the wafers is plotted in figure 2.22.

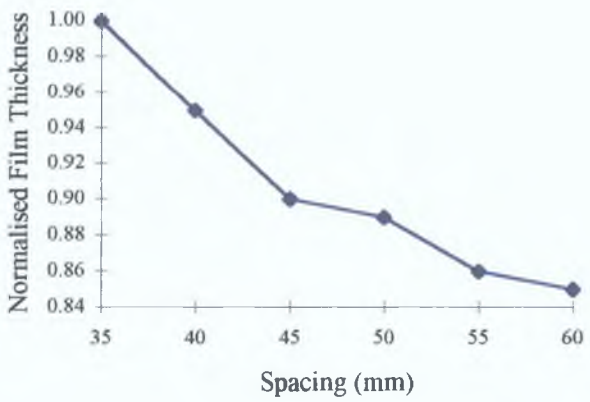

Figure 2.22 *Film Thickness vs. Spacing*

2 6 8 Summary of Simulation Results

The above simulations illustrate how predictions can be obtained of the substrate coverage on substrates with complex geometry The process was applied to a 'hole' structure but the simulation package could just as easily have been applied to a substrate of any particular shape or size The importance of configuring the system such that the emitting area of the target is adjacent to the surface was demonstrated In particular a re-entrant surface is necessary to obtain good coverage The importance of rotation is evident for this type of substrate The model also predicts the improvement in uniformity which can be obtained by operating at increased pressure where possible The simulation model correctly displays the features which occur in real sputtering systems Further extensions of the model are planned to take into account the effect on the stoichiometry of the films of substrate topology during reactive sputtering

2 7 Summary

In this chapter justifications for modelling the sputtering process were put forward and examples of the usefulness of a sputter simulation package discussed The SPUTSIM simulation was inexpensive to develop relative to commercial simulation packages and is flexible and runs on standard IBM compatible personal computers The model employed, though reasonably simple, provides accurate predictions of particles fluxes

Chapter 3 Conformal Liners, Barriers and Wetting Layers for Deep Sub-Micron Features

3 1 Introduction

Film conformality over small contact and via structures is of critical importance in modern day semiconductor metallisation processes As feature sizes shrink, good conformality becomes more difficult to achieve, especially with PVD-type processes[62] The primary shortfall of PVD type processes is the requirement to deposit excessively thick nominal film thicknesses in order to achieve the required bottom and sidewall film thicknesses in high aspect ratio features The reason for the poor step coverage is the wide angular distributions of the depositing flux This wide distribution results in shadowing at the top of the feature The thicker the deposited film the more the film overhangs across the mouth of the feature The overhang alters the shape of the feature, possibly leading to a re-entrant profile which may cause problems for subsequent processing steps Figure 3 1 illustrates the effect of a sputtered film on the shape of a via feature The initial via sidewall slope is determined by the via photo-lithography and via etch processes As can be seen from figure 3 1, if an initial slope of 90° is employed the slope after deposition of the sputtered film is > 90° In this case a void-free CVD - W film is not obtained Therefore a tapered via is usually preferred with a slope of 86° - 88°[63]

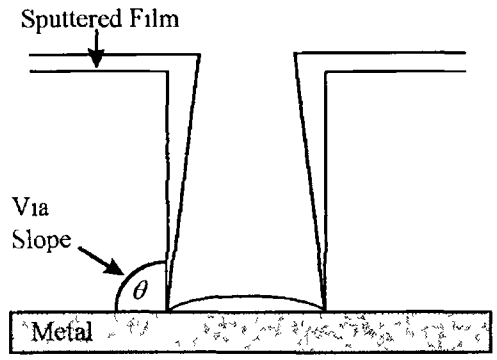

Figure 3 1 *Effect of Sputtered Film on Feature Profile*

For W-plug contact and via applications a Ti/TiN film stack is typically used as both a diffusion barrier to protect underlying layers such as silicon and titanium from attack by WF_6 reactants present during the tungsten CVD process and as an adhesion layer for the tungsten, which tends to adhere poorly to Si and SiO_2 The titanium layer acts both as an adhesion layer between the TiN and the Si or SiO_2 and also as a getter of surface contamination of the underlying material at the bottom of the via or contact Sufficient Ti at the bottom is normally required to achieve good via and contact resistances Insufficient Ti leads to high contact resistances[64] and insufficient TiN leads to defects such as wormholes and volcanoes[65] Figure 3 2 is a photo of volcanoes on vias where the TiN barrier has failed and WF_6 used in the W deposition process has reacted with the underlying Ti

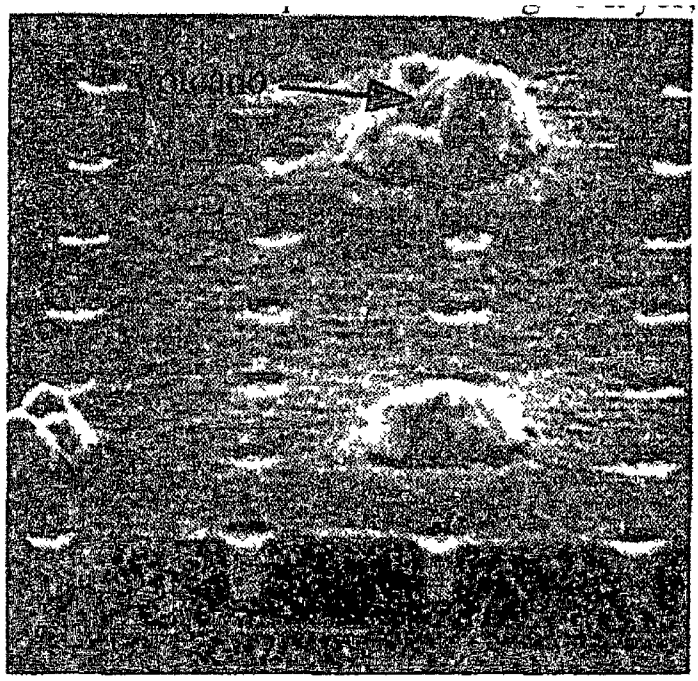

Figure 3 2 *Volcano Formation on Tungsten Plugs*

For aluminium plug contact and via fill applications a Ti/TiN/Ti stack is normally used at the contact level[66] The first Ti layer is again used as a contamination getter, the TiN serves as a diffusion barrier to avoid aluminium spiking and consequent junction leakage[67] and the top Ti layer is used as a wetting layer for subsequent hot aluminium deposition At the via level there is normally no requirement for a diffusion barrier so only the Ti wetting layer is required, however in some instances a Ti/TiN/Ti

layer is used The TiN serves to isolate the wetting layer from the substrate if the substrate tends to out-gas and also to compensate for any sidewall imperfections such as bowing before wetting layer and aluminium deposition[68]

For copper interconnect applications tantalum has been suggested as the most suitable diffusion barrier material Tantalum is attractive because of its high melting point and its immiscibility with copper Tantalum also allows low contact resistance and excellent adhesion to copper[4]

Electroplating is currently the favoured method for depositing the bulk of the interconnect and plug copper PVD and CVD methods can also be used but electroplating has advantages in terms of cost and simplicity However, an electroplating process requires a seed layer (conducting layer) to be deposited conformally over the feature to be electroplated Therefore, the electroplating process will only be able to work in partnership with an alternative deposition process capable of depositing a conformal seed layer over high aspect ratio features Both CVD and ionised PVD have been suggested as possible seed layer deposition processes[69][70]

In this chapter, four different PVD processes are examined in terms of step coverage / film conformality The angular distributions of atoms arriving at the substrate surface are estimated and a simulation package is then used to estimate the film conformality on a 3 1 aspect ratio structure as a function of these angular distributions An experiment to determine the actual film profiles is described and the experimental and theoretical results compared

Finally, the extendibility of PVD processes to higher aspect ratios is considered Further simulations are run at higher aspect ratios and general expressions for film overhang and film bottom coverage are developed

3 2 Experiment

Each of the films deposited were deposited in an Endura HP™ PVD system This is a commercially available multi-chamber deposition system used widely throughout the semiconductor industry for depositing metal thin films The base vacuum achieved in the deposition chambers was in the 10^{-9}torr range The standard chamber was fitted with a titanium Durasource™ target manufactured by Tosoh which had a purity of 99 9995% The magnet used was an Applied Materials Durasource™ magnet which was rotated at the back of the water-cooled target The collimated chamber used the same target and magnet and a 1 1 honeycomb shaped stainless steel collimator was inserted between the target and the wafer The ionised PVD chamber was fitted with a target manufactured by Heraues and an Applied Materials RH™ magnet The coil used for ionising the sputtered atoms was fitted between the target and the wafer and was manufactured from the same material as the target A schematic of the three experimental set-ups is given in figure 3 3 Details of the process parameters are given in table 3 1

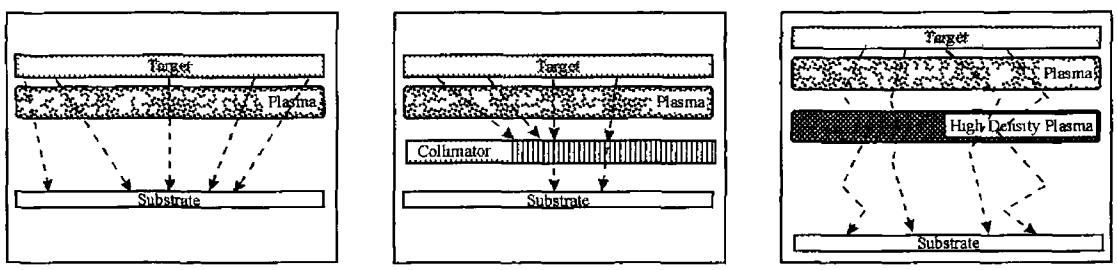

a) Standard PVD Process *b) Collimated PVD Process* *c) Ionised PVD Process*

Figure 3 3 *Sputter Process Configurations*

	Std Ti	Std TiN	Coll Ti	Coll TiN	IPVD Ti	IPVD TiN
Pressure	2mT	4mT	2mT	3mT	15mT	35mT
T-S Spacing	56mm	65mm	55mm	55mm	140mm	140mm

Table 3 1 *Std, Coll and IPVD Process Parameters*

3 3 Measurement of Film Conformality

In order to compare the film conformality associated with the different PVD type processes, patterned wafers were obtained and a split was run between the standard, collimated, ionised and biased ionised PVD processes In each case a Ti/TiN film stack with an approximate field thickness of Ti-20nm/TiN-80nm was deposited Detailed TEM analysis was carried out on features with varying aspect ratios and each film was characterised in terms of the following

- Bottom Coverage
- Step Coverage
- Sidewall Coverage
- Sidewall Top / Bottom Ratio
- Bottom Centre / Corner Ratio
- Degree of Overhang

Note the bottom, sidewall and step coverages are as defined in chapter 1 The aspect ratios of the features varied greatly (1 5 1 → 4 4 1) but in order to compare the different processes to one another, features with aspect ratios of approximately 3 1 were chosen Photographs of the coated features are presented in figures 3 4 to 3 7

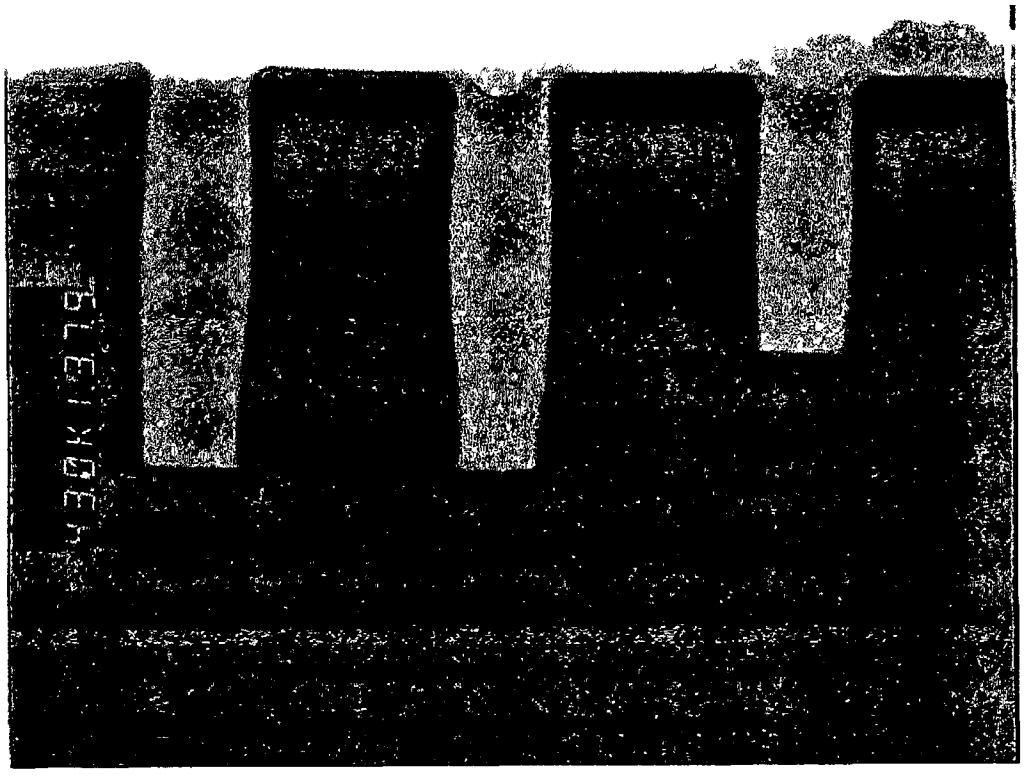

Figure 3 4 *Standard PVD*

Figure 3 5 *Collimated PVD*

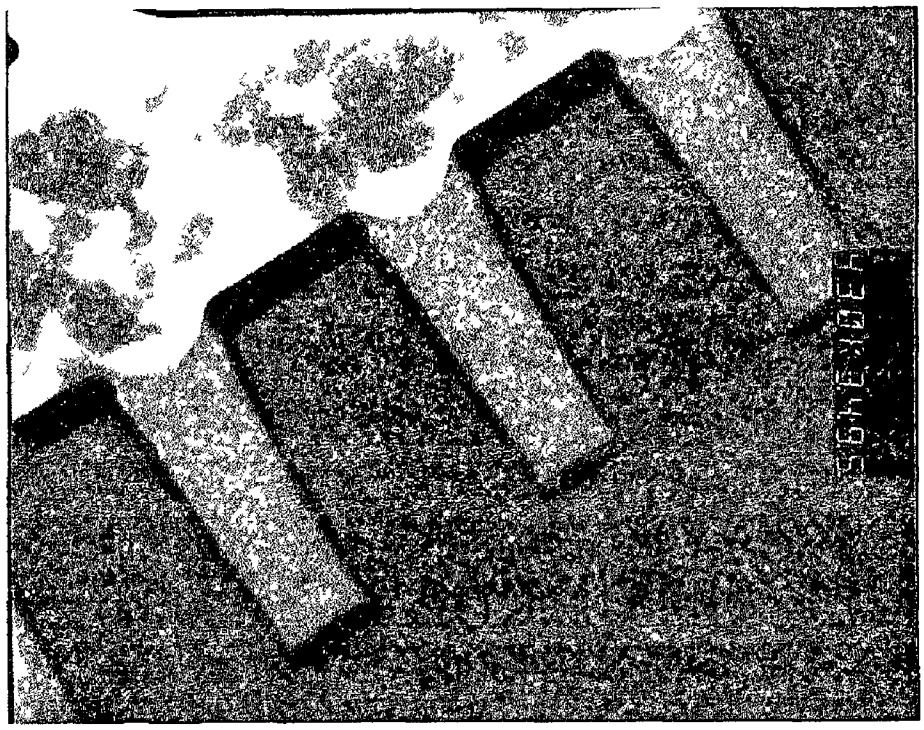

Figure 3 6 *Ionised PVD*

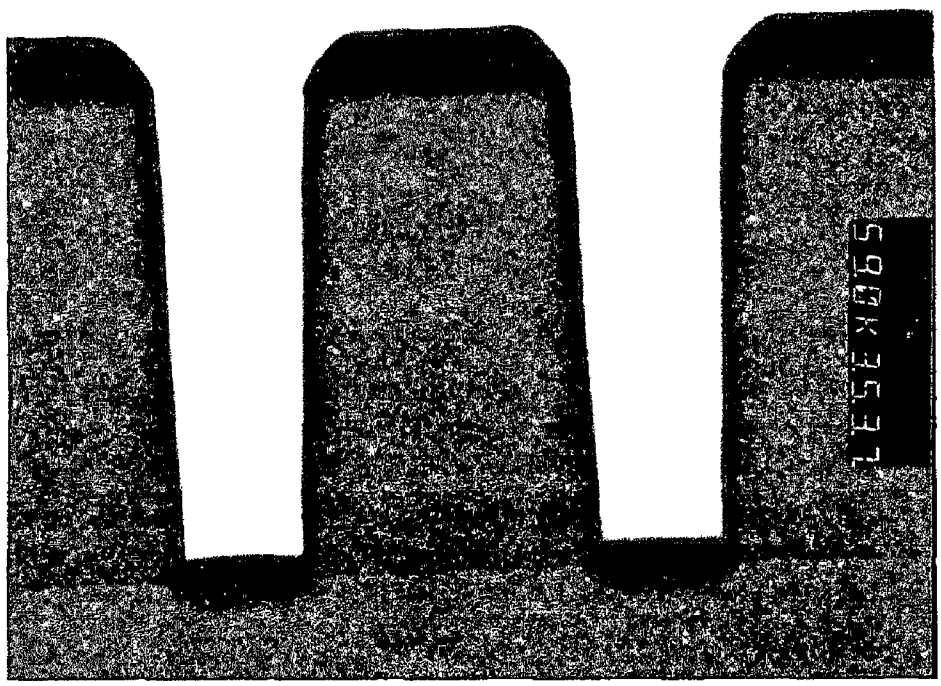

Figure 3 7 *Biased Ionised PVD*

Table 3 2 presents profile data for each of the processes on a 3 1 aspect ratio feature Note that the sidewalls were etched to an angle slightly less than 90° (~ 87°) which means that the coverage is better than that achieved on a true 90° sidewall and the feature profile is slightly more relaxed than that simulated in the following simulation discussion In the case of the ionised + biased process the bias voltage was -40V during deposition of the titanium film and -100V during deposition of the titanium nitride film

	Standard	Collimated	Ionised	Ionised + Biased
Bottom Coverage	15%	30%	50%	55%
Step Coverage	10%	25%	25%	23%
Sidewall Coverage	20%	25%	25%	23%
Side Bottom/Top	0 25	0 70	0 90	1 00
Bottom Centre/Corner	1 00	1 00	1 20	1 20
Overhang	5	+ 4	+ 4	+

Table 3 2 Step Coverage for PVD Processes

3.4 Analysis of Experimental Results

The superior bottom coverage achieved with the ionised processes is in agreement with the results obtained by other researchers[72] The collimated bottom coverage is considerably less than that achieved with ionised sputtering, however it should be remembered that the aspect ratio of the collimator is 1 1 Considerably better bottom coverage could have been achieved using higher aspect ratio collimators The standard process step coverage is considerably lower than that achieved with the other processes but it is still higher than expected Results reported by other authors suggest a bottom coverage of the order of 5% for this type of aspect ratio[72] The higher than expected bottom coverage is probably due to the fact that relatively low process pressures and large target substrate distances were used, moving the process towards the 'Long Throw' process regime[73]

For the 3 1 aspect ratios studied the step coverage for the ionised and collimated processes is about 25% and the standard process is much lower at ~ 10% It is likely

that at higher aspect ratios the step coverage of the standard process will drop off more relative to the other processes

A major disadvantage of a non-conformal deposition process such as PVD is the tendency of the growing film to bottleneck the top opening of the feature, leading to a re-entrant profile This build up is a problem particularly if the feature is subsequently to be filled with, for example tungsten using a CVD process The re-entrant profile could lead to key-hole formation in the tungsten plug and the associated reliability problems[74] It is an even greater problem if the feature is to be filled with a material using a PVD process, such as in the case of aluminium plugs In any PVD process there will be a certain amount of overhang at the top of a feature In practice this is compensated for by tapering or rounding the top of the feature, preventing the excess film growth at the top from causing a re-entrant profile This rounding effect is typically achieved by a sputter etch process prior to film deposition This subject is dealt with in more detail in chapter 4 Examining the profiles of the films in figures 3 4 to 3 7, the overhang associated with each type of process can be observed Although the thickness of the film at the top of the sidewall is less for the collimated process than for the standard process, the profile is more re-entrant due to what looks like an undercut at the top corner of the feature The non-biased ionised process profile is similar to the collimated process but the 'undercutting' effect is less pronounced This is probably due to the effects of re-sputtering of the growing film due to ion bombardment The profile of the ionised process with bias is very different to the other processes The facetting of the film is due to the high degree of sputter etching taking place in conjunction with the deposition process The slope of the material at the mouth of the feature is characteristic of the material / bombarding ion combination The slope is related to the angle at which sputtering / sputter etching is optimal Recall the general trend from chapter 1 figure 1 4

The SIMBAD simulation package supports the inclusion of ion bombardment effects during film growth Figures 3 8 and 3 9 present the results of two SIMBAD simulations of a 0 2μm titanium film grown over a 3 1 aspect ratio contact Figure 3 8 shows the overhang typically associated with the standard sputtering process and

figure 3.9 shows the effects of including the ion bombardment. The results of the simulation support the ion-bombardment theory.

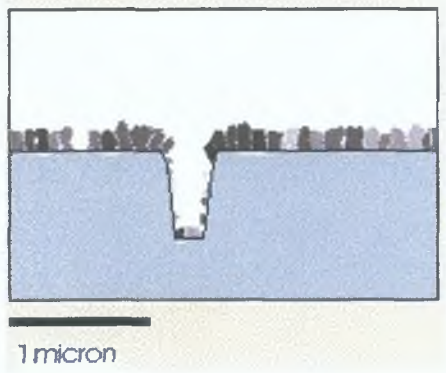

Figure 3.8 *SIMBAD Simulation : No Ion Bombardment*

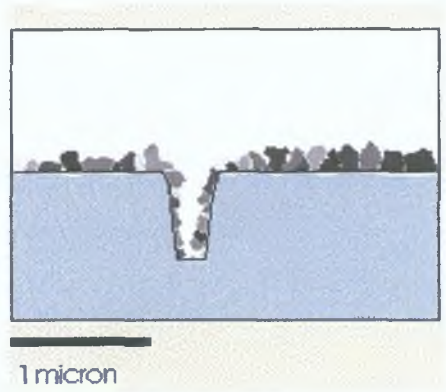

Figure 3.9 *SIMBAD Simulation : With Ion Bombardment*

The tendency to overhang prevents the standard process from being extended indefinitely. Without overhang, by depositing a sufficiently thick film, enough material could be deposited at the bottom of a feature.

3 5 Simulation of Film Conformality

The model used to examine step coverage assumes the particles are emitted from an infinite plane which lies parallel to the substrate surface The infinite plane assumption is valid as the dimensions of a feature are in the sub-micron range whereas the flux of material arriving at the substrate is assumed to be spread over an area of the order of centimetres The emission angle is related to the impact angle by the equation

$$\vartheta = \pi / 2 - \chi$$

The emission angle was calculated from the impact angle which was generated randomly based on a defined distribution function, which will be discussed in the following paragraph The sticking coefficient of the depositing particles is assumed to be unity and the particles are assumed to be infinitely small The effects of film build up are ignored which is a major simplification and compromises the accuracy of the simulation It was already mentioned that film build up / overhang at the feature opening tends to modify the geometry of the feature It will be shown in this section that the degree of overhang is a function of the width of the impinging flux angular distribution A modification of the SPUTSIM-2D software was used as a platform for the simulation The model used was very simple and ignored such processes as surface diffusion and film overhang However the model is likely to be reasonably accurate for very thin films (or the nucleation layer of thicker films) sputtered in conditions where surface diffusion is at a minimum

In order to correlate the angular distribution of the depositing atoms with step coverage, a number of different distribution functions were considered To illustrate the relation between step coverage and angular distribution, five simple distributions were investigated These distributions assume an even distribution over a given range of angles as illustrated in figure 3 10 Depending on the specific process conditions, the width of the angular distributions can vary from a few degrees (IPVD) to < 90 degrees (high pressure PVD) The shape of the distributions can vary but a uniform distribution over a specific range is a reasonable approximation The use of the uniform distribution

enables the results relating to distribution function width to be more general The purpose of this work is to look for general trends rather than the details of a specific process Also, the results of the simulations from uniform distribution functions can be interpreted to examine more complicated distribution functions, as described in section 3 5 9

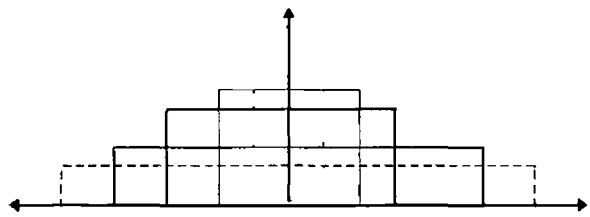

Figure 3 10 *Angular Distributions*

Distribution 1

$$P_1(\vartheta) = k, -10^o < \vartheta < 10^o, else \vartheta = 0$$

Distribution 2

$$P_2(\vartheta) = k, -20^o < \vartheta < 20^o, else \vartheta = 0$$

Distribution 3

$$P_3(\vartheta) = k, -30^o < \vartheta < 30^o, else \vartheta = 0$$

Distribution 4

$$P_4(\vartheta) = k, -40^o < \vartheta < 40^o, else \vartheta = 0$$

Distribution 5

$$P_5(\vartheta) = k, -50^o < \vartheta < 50^o, else \vartheta = 0$$

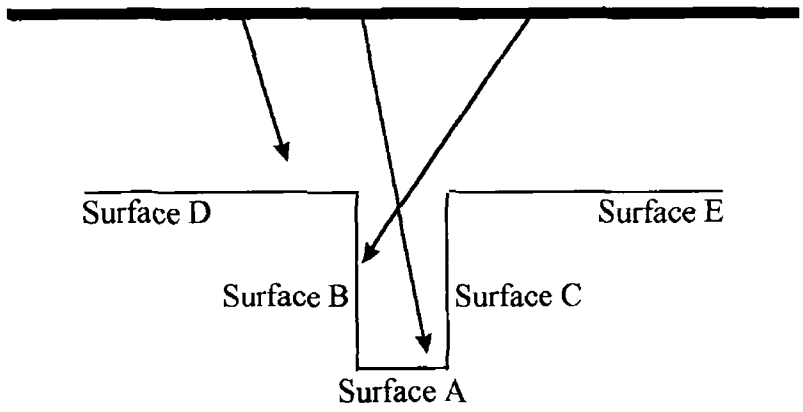

Figure 3 11 3 1 Aspect Ratio Feature

3 5 1 Simulation Results

The simulation was run for a structure with a 3 1 aspect ratio, as shown in figure 3 11 For each simulation 30,000 particles were run The results for each simulation are summarised in table 3 3 In order to compare the fluxes to each surface, the length of each surface must be taken into account Table 3 4 shows the data in table 3 1 as a function of unit length

	Distribution 1	Distribution 2	Distribution 3	Distribution 4	Distribution 5
Surface A Bottom	103 1	69 7	42 8	33 2	26 0
Surface B Left	18 7	35 4	52 0	57 8	60 0
Surface C Right	17 6	37 3	51 8	55 8	55 7
Surface D Left	371 9	371 4	365 4	366 9	375 5
Surface E Right	373 1	366 8	371 9	369 7	370 0

Table 3 3 Average Number of Impingements on Each Surface

	Distribution 1	Distribution 2	Distribution 3	Distribution 4	Distribution 5
Surface A Bottom	103 1	69 7	42 8	33 2	26 0
Surface B Left	6 2	11 8	17 3	19 3	20 0
Surface C Right	5 9	12 4	17 3	18 6	18 6
Surface D Left	148 8	148 6	146 2	146 8	150 2
Surface E Right	149 2	146 7	148 8	147 9	148 0

Table 3 4 Flux Density to each Side of the Feature

	Distribution 1	Distribution 2	Distribution 3	Distribution 4	Distribution 5
Surface A Bottom	0.696151	0.470628	0.288994	0.224173	0.175557
Surface B Left	0.042066	0.079676	0.117016	0.130047	0.135044
Surface C Right	0.039568	0.083930	0.116543	0.125591	0.125321

Table 3.5 *Flux to Bottom and Side Walls as a Fraction of Field Thickness*

3.5.2 Analysis of Simulation Results: Bottom Coverage

Table 3.5 expresses the bottom coverage and sidewall coverage data as a fraction of the field thickness, where field thickness is an term frequently used to describe the thickness of the material deposited on the flat areas of the substrate.

Average Bottom Coverage is the average thickness of the film at the bottom of the feature. It will be shown later that in reality the thickness of the film at the bottom of a feature is non-uniform. Centre Bottom Coverage refers to the ratio of the thickness of the centre of the film at the bottom of the feature to the field thickness. Figure 3.12 is a plot of the average bottom and the centre bottom coverage as a function of angular distribution.

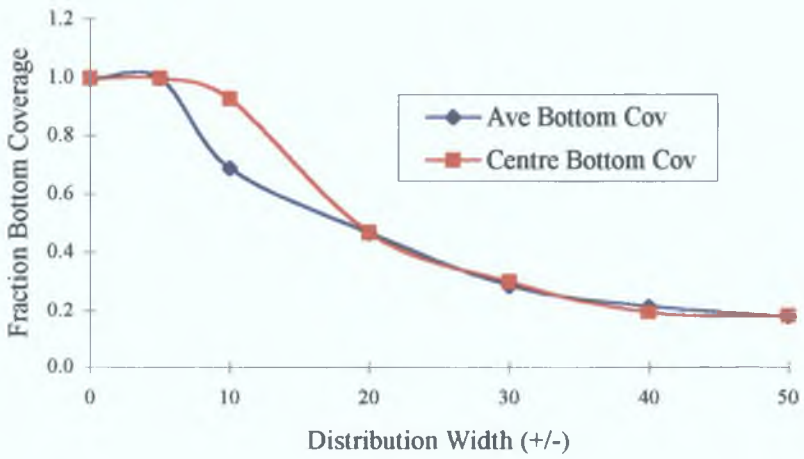

Figure 3.12 *Bottom Coverage versus Angular Distributions*

To better understand the relationship between bottom coverage and the width of the angular distribution (and hence the shape of the graph) an analytic expression relating the two was derived.

Consider the 2-D rectangular feature shown in figure 3 13 The diameter of the feature is given as d and the height of the feature is h

So,

$$\text{Aspect Ratio } AR = h/d$$

Let p_1 be the point at the bottom of the feature L_1 is the distance from p_1 to the left corner of the feature and L_2 is the distance from p_1 to the right corner of the feature Consider the flux of material impinging on the feature as two fluxes, F_1 and F_2 where F_1 emanates from the left of the normal and F_2 emanates from the right of the normal The angular distribution is a normal distribution with a width $2x$

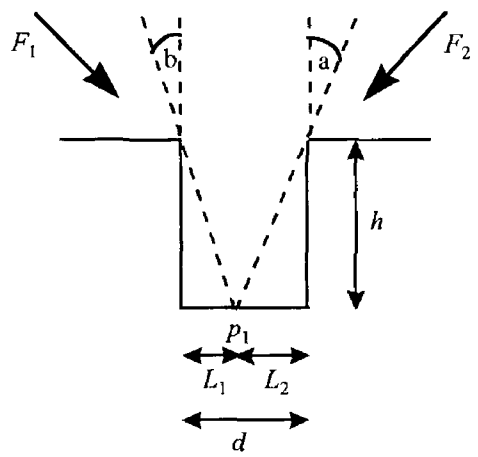

Figure 3 13

For F_1, only particles with an angle to the normal < b can reach p_1 where,

$$b = tan^{-1}(L_1/h)$$

So, if $x < b$ the bottom coverage due to flux $F_1 = t_1$, where t_1 is the field thickness due to F_1

If $x > b$ the bottom coverage due to $F_1 = t_1 * b / x$

Similarly for F_2

$x < a$, bottom coverage due to $F_2 = t_2$,

$x > a$, bottom coverage due to $F_2 = t_2 * a / x$

where $a = tan^{1}(L_2/h)$

Total flux $F = F_1 + F_2$ and total field thickness $t = t_1/2 + t_2/2$, $t_1 = t_2$

So, total bottom coverage = $t*(a + b) / (2*(x))$

This shows that there exists an inverse relationship between the bottom coverage and the angular distribution

$$B\,C \sim A/x$$

This inverse relationship only exists above a certain critical angle a, where a is defined by the aspect ratio of the feature On examination of the data presented in figure 3 12 the graphs change shape at ~9° This is in good agreement with the calculated critical angle for a 3 1 aspect ratio

$$a = tan^{1}(0\ 5/3) = 9\ 46°$$

Fitting trend lines to the data yields the following

Average Bottom Coverage, $ABC = 5\ 36\ x^{0\ 86}$ where $x > 9\ 46°$ ($R^2 = 97\ 84\%$)

$ABC = 1$ where $x <= 9\ 46°$

Centre Bottom Coverage, $CBC = 10\ 51\ x^{1\ 01}$ where $x > 9\ 46°$ ($R^2 = 99\ 11\%$)

$CBC = 1$ where $x <= 9\ 46°$

Here $2x$ is the width of the angular distribution (+/-) and R^2 is a measure of the goodness of fit

The simulation software also provided the capability of examining film thickness profiles on any specified surface. This is useful for examining the non-uniformity of films. Figure 3.14 graphs the film profiles at the bottom of the 3:1 aspect ratio feature for each of the distribution functions used.

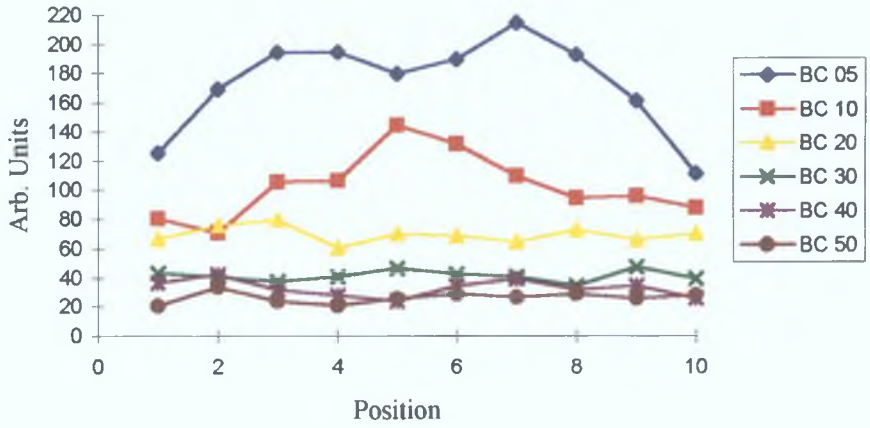

Figure 3.14 *Bottom Coverage Profiles*

This data shows that there is a thickness variation from the centre to the edge of the bottom film, with the centre being thicker than the edge. To explain this consider a 3:1aspect ratio feature and an impinging flux with an angular distribution of $2x$.

Flux reaching the corner of the feature can only come from flux from one side of the normal with an angle $< \beta$, where $\beta = tan^{-1}(w/L)$.

Flux reaching the centre of the feature can come from both sides of the normal with an angle $< \alpha$, where $\alpha = tan^{-1}(2w/L)$.

Define t_c as the thickness in the centre and t_e as the thickness at the corner,

$$t_c/t_e = 2\alpha / \beta$$

$$t_c/t_e = 2tan^{-1}(L/w) / tan^{-1}(L/2w)$$

$$t_c/t_e = 2 * 9.5 / 18.5$$

$$t_c/t_e = 19/18.5$$

This shows that the centre thickness will always be thicker than the edge thickness which agrees with the simulation results.

The simulated bottom coverages are very similar to the measured bottom coverages for the different PVD processes. The standard, collimated and ionised processes have bottom coverages of 15%, 30%, and 50% respectively. Distributions 4, 3 and 2 have simulated bottom coverages of 22%, 29% and 47% respectively. Of course, a more accurate description of the angular distribution of the depositing material would boost the accuracy of the simulated results.

3.5.3 Analysis of Simulation Results: Side Wall Coverage

Figure 3.15 shows the dependency of the average sidewall thickness on angular distribution. Note that this is a measure of the amount of material to the sidewall. The thickness of the material on the sidewall tends to be significantly non-uniform from the top to the bottom of the sidewall. The sidewall coverage is proportional to the width of the angular distribution up to approximately -30°, after which the curve evens out.

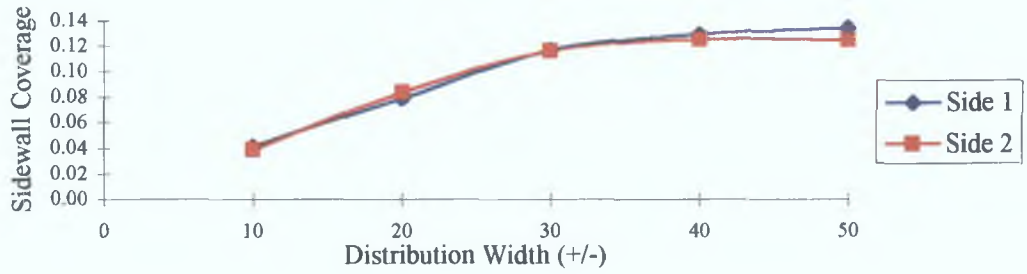

Figure 3.15 *Total Sidewall Coverage versus Angular Distributions*

Thickness profiles of the simulated sidewalls are presented in figure 3.16. It can be seen that the non-uniformity of the side wall coverage increases as the width of the distribution function increases. For the smaller angular distributions there is very little difference between the thickness at the bottom of the side wall when compared to the thickness at the top of the side wall. However, at the broader angular distributions severe variations in thickness are observed.

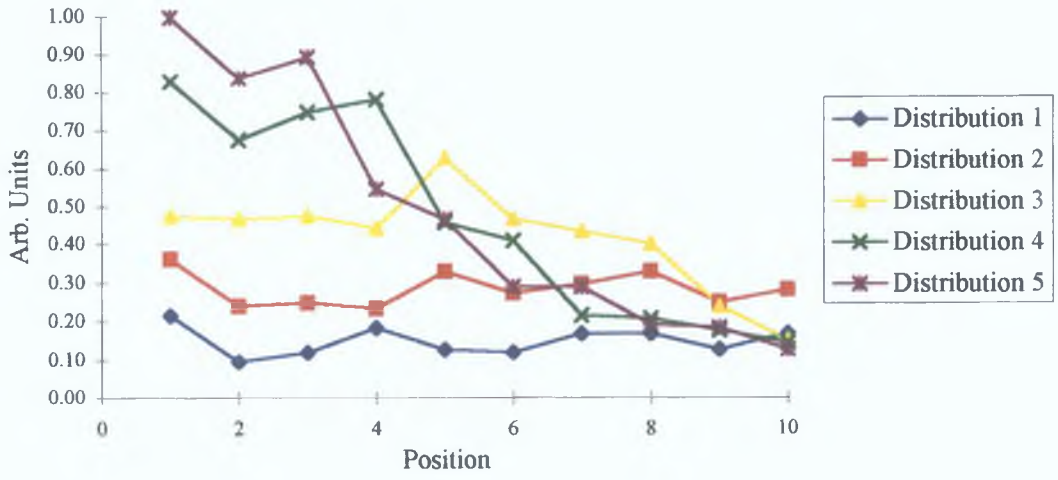

Figure 3.16 *Sidewall Film Profiles*

Table 3.6 shows the ratio between the top sidewall thickness and the bottom sidewall thickness for each of the distributions. For comparison, the corresponding experimental data discussed in section 3.3 is tabulated also (table 3.7).

	Dist. 5	**Dist. 4**	**Dist. 3**	**Dist. 2**	**Dist. 1**
Sidewall Bottom/Top Ratio	0.15	0.18	0.36	0.78	0.90

Table 3.6

	Standard	**Colimated**	**Ionised**	**Ionised + Bias**
Sidewall Bottom/Top Ratio	0.25	0.70	0.90	1.00

Table 3.7

The predicted sidewall thickness non-uniformities are what would be intuitively expected. Particles arriving at oblique angles relative to the surface normal can only deposit on the upper regions of the sidewall. The wider the angular distribution the more particles arriving at oblique angles, resulting in relatively more material deposited on the upper region of the sidewall.

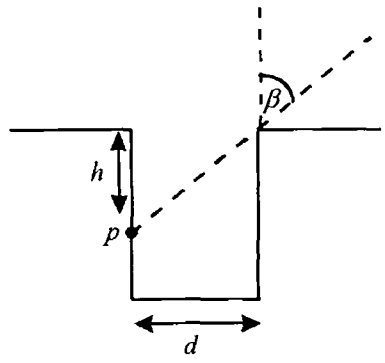

Figure 3 17

Figure 3 17 illustrates the flux contribution to the sidewall film Assuming the angular distribution of the impinging flux is symmetrical around the surface normal, particles impinging on the sidewall can only come from half the total flux (assuming no contribution from re-sputtering) At a point p on the sidewall only atoms with an angle $< \beta$ can impinge at p Therefore, the thickness of the film at point p is

$$t_p \propto t_f \beta / x, \qquad x > \beta$$
$$t_p \propto t_f \qquad x < \beta$$

where $2x$ is the width of the angular distribution and the angular distribution is assumed to be uniform, t_f is the field thickness and $\beta = tan^{-1}(d/h)$ where d and h are as defined in figure 3 17

These relationships explain the sidewall non-uniformities seen in figure 3 17 The more normal distributions result in more uniform sidewall films than the more oblique distributions

3 5 4 Effects of Re-Deposition

This model ignores the effects of re-sputtering of the growing film This phenomena can be important, especially during the higher energy ionised sputtering process Re-sputtering can result in material deposited at the bottom of the feature being re-sputtered onto the feature sidewalls The SPUTSIM simulation can be used to estimate the contribution of the re-sputtered material at the bottom of the feature to the sidewall by running a separate simulation with the bottom as the target The SIMBAD

simulation package can also be used to model the effects of re-sputtering SIMBAD includes the effects of ion bombardment during deposition through the addition of ion disks to the substrate Each disk represents a statistical average of a large number of physical ions The ion disks are intermittently launched at a specified angular distribution just above the film surface

When an ion strikes a film it can either be re-sputtered or reflected, depending on the angle of incidence and energy

The amount of re-sputtering that takes place is determined by the amount of ion bombardment As the flux density of the sputtering gas ions (Ar) is typically more dense than the metal ions the majority of the re-sputtering is as a result of the gas ion flux The voltage above which re-sputtering starts to occur is a function of the material / bombarding ion combination Typically for Ti in Ar re-sputtering starts to occur above 50V - 60V, for TiN re-sputtering starts to occur above 70V - 90V

The SIMBAD simulation requires as an input, the relative impingement rates of the depositing metal species and the bombarding ions For comparison with experimental films, the ion flux rate can be inferred from the net decrease in deposition rate of both simulated and experimental films

To illustrate the effect of re-sputtering of material from the bottom of a feature to the lower sidewall a SIMBAD simulation was carried out The ion disk flux was taken to be 0 77 relative to the film flux density The simulation was run twice, once without the ion flux and the second time with the ion flux present The results can be seen in figures 3 8 and 3 9 The sidewall thickness is about twice as thick with ion bombardment as it is without This subject is studied in more detail in chapter 6

3.5 5 Film Overhang

The amount of material overhanging at the mouth of the feature can also be interpreted from the data Figure 3 18 graphs the overhang (overhang = fraction of material at top / field thickness) as a function of angular distribution By fitting a line to the data, a relationship between overhang and distribution can be obtained

$$y = 0.007x - 0.017 \qquad (1)$$

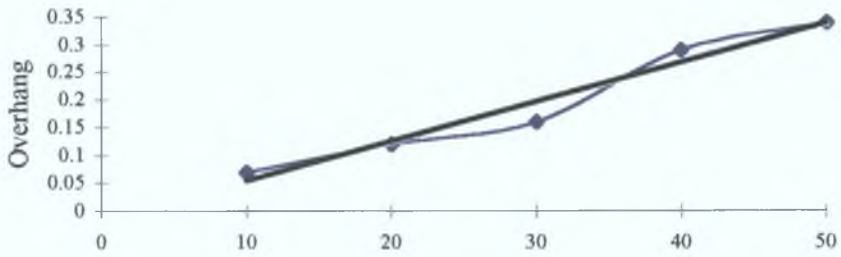

Figure 3.18 *Film Overhang versus Angular Distribution Width*

This compares with a measured overhang for the PVD processes of the following:

- Standard PVD 0.5
- Collimated PVD 0.5
- Ionised PVD 0.4
- Biased Ionised PVD 0.25

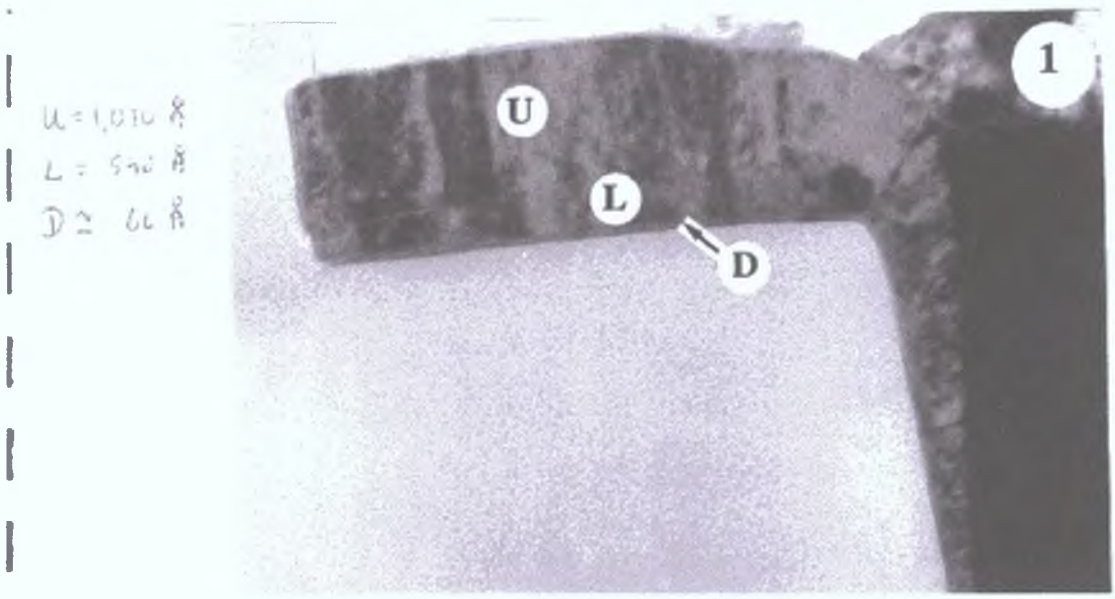

Figure 3.18 *Cross Section TEM of Standard Film Overhang*

Figure 3.18 shows a high resolution TEM of the opening of a feature which has been coated with a standard Ti/TiN liner and filled with CVD tungsten. The measured

overhang of the Ti/TiN is 0 45 This picture clearly shows the profile of the film along the sidewall The dramatic reduction in film thickness with distance along the sidewall is apparent

U - TiN

L - Ti

D - Ti/SiO_2 Interfacial Layer

1 - W Plug

3 5 6 Interpretation of Simulation Results

The above results show the relationship between step coverage and angular distribution for a 3 1 aspect ration feature It is important however to relate these results to what happens in a real sputter system In a real PVD process the angular distribution is unlikely to be evenly distributed over a particular range For each PVD process the angular distribution is a function of process parameters such as pressure, the mass ratio between the metal atom and the gas atom, target crystalline orientation, system geometry etc A general guideline for the angular distributions for each process is as follows

Ionised Sputtering	+/- 10° from Normal
Collimated Sputtering	+/- 30° from Normal
Standard Sputtering	+/- 40° from Normal

See figure 3 19 for an illustration

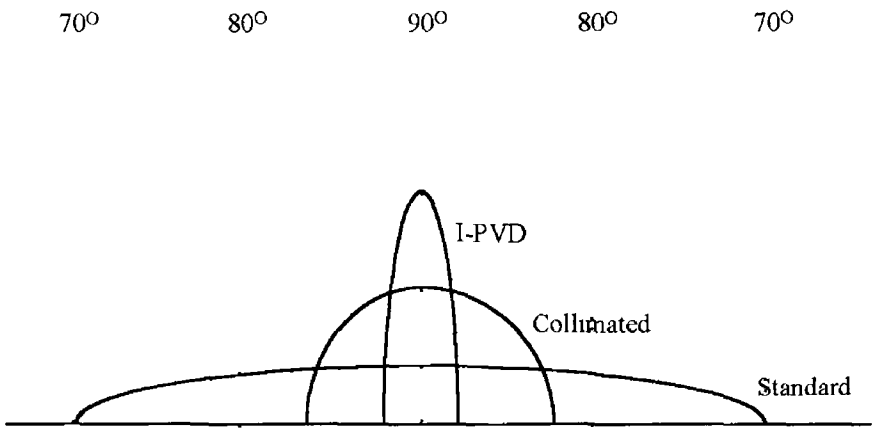

Figure 3 19 *Incident Angular Distribution on Substrate for Various Processes*

Without a more detailed knowledge of the angular distributions, the results of the simulation can only be used as a tool to understand the effects of broadening the angular distribution on film conformality To obtain information about a particular process more detailed information is required A more realistic distribution could be

obtained by physically measuring the distribution or simulating particle transport using a simulation package such as SPUTSIM.

3.5.7 Interpretation of More Complex Distributions

This section describes a method of obtaining bottom coverage and sidewall coverage data for more complex incident atom angular distribution functions using the relationships generated for uniform angular distribution functions.

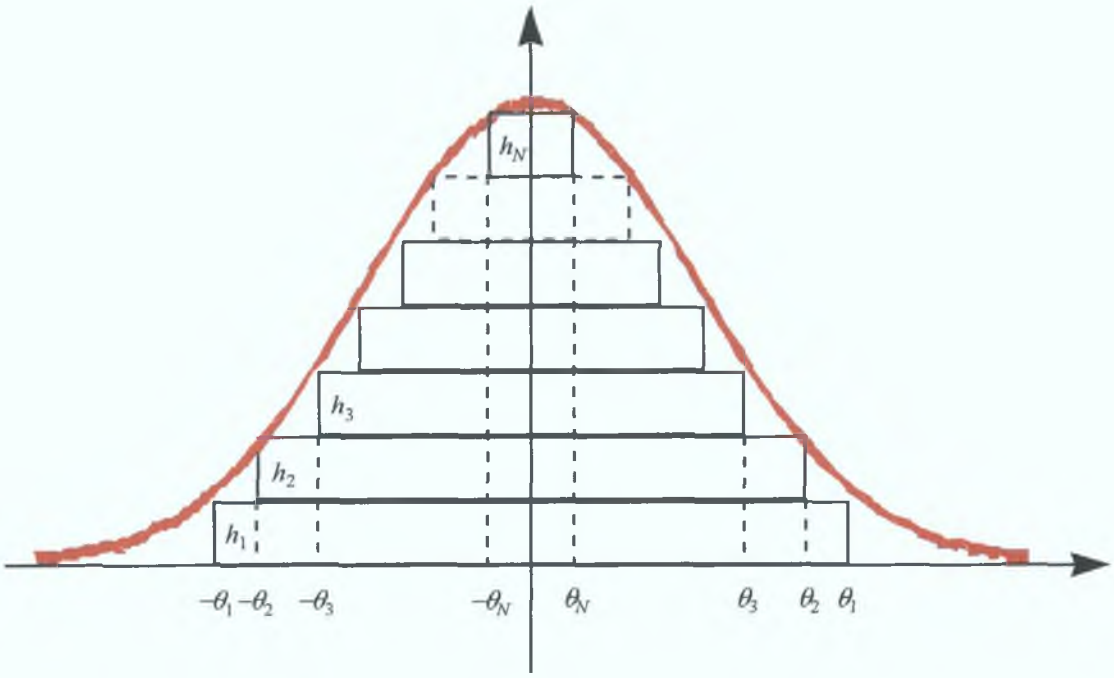

Figure 3.20 *Rectangular Area under Complex Distribution*

Take a curve describing the angular distribution function and divide it into a series of rectangles defined by a width θ_i and a height h_i. Let N be the number of rectangles fitted under the curve.

The area under the curve A_c, can now be approximated as the sum of the areas of all the rectangles under the curve

$$A_c = \sum_{i=1}^{N} 2\theta_i h_i$$

The fractional bottom coverage for a uniform angular distribution between +/-θ is given by the equation

$$BC = f(\theta)$$

So the bottom coverage associated with one of the rectangles is given by

$$BC = f(\theta_i) * 2\theta_i h_i / A_c$$

The total bottom coverage can then be given by

$$BC = \sum_{i=1}^{N} f(\theta_i) * \frac{2\theta_i h_i}{A_c}$$

An example calculation is given in appendix D

3 6 Process Extendibility

So far the relative conformality performance of the various PVD processes have been studied However, a key question remains to be answered *What are the aspect ratio limits of each of the processes ?* To answer this question, acceptance limits must be put on each of the critical conformality parameters The performance of each process must then be evaluated in turn Take film overhang and minimum film bottom coverage as critical film parameters that need to be met

From equation 1, the film overhang can be expressed as

$$O_v = Ax + B \quad (2)$$

where O_v is the overhang, A and B are constants and x is the width of the angular distribution This expression expresses the overhang as a fraction of the field thickness Note that it is independent of the feature aspect ratio

The expression for bottom coverage is more complicated as the bottom coverage depends not only on the angular distribution but also on the feature aspect ratio The equation for bottom coverage presented previously is only useful for a 3 1 aspect ratio feature In order to generate an expression independent of aspect ratio further simulations were run at different aspect ratios The bottom coverage results are presented in figure 3 21 The following equations were fitted to the data

1 1

$$y = 1\ 521x^{0\ 24} \quad (R^2 = 94\ 73\%) \qquad x>26\ 56^\circ$$

3 1

$$y = 5\ 17x^{-0\ 85} \quad (R^2 = 94\ 73\%) \qquad x>9\ 56^\circ$$

5 1

$$y = 28\ 69x^{1\ 6} \quad (R^2 = 94\ 73\%) \qquad x>5\ 71^\circ$$

7:1

$$y = 124.58x^{-2.42} \qquad (R^2 = 94.73\%) \qquad x>4.08^{\circ}$$

The R^2 values are a measure of the goodness of fit.

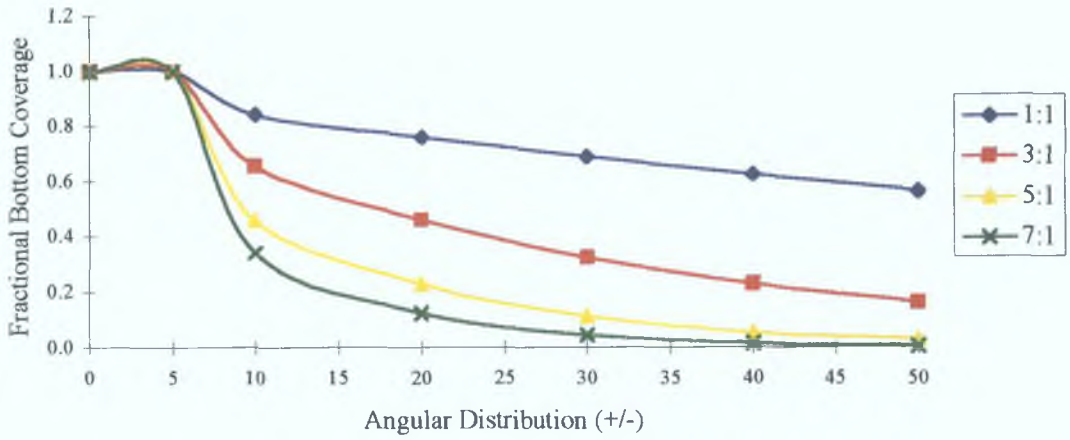

Figure 3.21 *Bottom Coverage versus Aspect Ratio*

From these results a generic expression for bottom coverage is

$$BC = Cx^{-a} \qquad x > \theta_c$$
$$BC = 1 \qquad x < \theta_c$$

where x is the angular distribution, a and C are functions of the aspect ratio and can be calculated from the data presented in figure 3.21. θ_c is the critical angle defined in section 3.5.2.

In this analysis the expressions generated for bottom coverage and overhang are un-coupled. In a real process the overhanging film tends to shield some of the material from reaching the bottom of the feature. As the field thickness of the film gets thicker the feature height gets higher and the opening of the feature decreases. Therefore the aspect ratio does not remain constant throughout the film growth. For very thin films it is reasonable to ignore the aspect ratio change, however when the thickness of the film

becomes a significant fraction of the height of the feature or the overhang blocks off a considerable fraction of the opening, then inaccuracies are introduced into the simulation

At a time t the aspect ratio (AR) of the feature is given by

$$AR = (L + h(t)) / (r - 2* d(t))$$

where L is the original feature height, r is the original feature diameter, $h(t)$ is the film field thickness at time t and $d(t)$ is the overhang at a time t

If this change in aspect ratio is such that it may significantly effect the simulation accuracy, the results need to be adjusted to take this effect into account The simulation could be run a number of times, breaking the film into a number of thinner films using the aspect ratio data from one simulation to determine the starting aspect ratio for the next simulation, averaging the results at the end Alternatively the equations already generated could be used to provide more accurate results The variable a in the expression for bottom coverage is a function of the aspect ratio and the angular distribution For a constant angular distribution, the variable a can be plotted against the aspect ratio and an expression relating a to the aspect ratio obtained For a given film thickness the bottom coverage can be calculated over a range of a and the average calculated

The data presented in the literature shows large variations in the reported values for bottom coverage as a function of aspect ratio One reason for this variation is that the reported values do not take into account the effects of changing aspect ratio during deposition For reported data to be meaningful the thickness of the film deposited on the field must also be quoted

3 7 Summary

A simple model has been implemented to examine the relationship film conformality and the angular distribution of incident atoms The simulations were run on a number of different aspect ratio features and the results obtained were as intuitively expected Equations relating bottom coverage and side wall coverage to the angular distributions were generated from the data Although the angular distributions used in the simulations bear a poor resemblance to the angular distributions of real PVD processes, it has been shown that it is possible to interpolate the results to gain information about more complex distribution functions

Actual deep-sub-micron 3 1 aspect ratio features were coated using standard, collimated, ionised and biased ionised PVD process and the relative conformality of each characterised The standard process is unlikely to provide adequate conformality for typical metallisation barrier and liner processes beyond 3 1 aspect ratio features The collimated process is much superior to the standard process, however the tendency for films to overhang at the mouth of features limits the maximum field thickness allowable with this process which in turn limits the film bottom thickness Higher aspect ratio collimators should provide better results due to the narrowing of the angular distribution but as the aspect ratio of the collimator increases the production worthiness of the process degrades The ionised process is a big improvement on the collimated process and has proven its production worthiness over the past two to three years However it also suffers from overhang at the mouth of the feature The biased ionised process provides excellent film conformality and does not suffer as much from the overhang effect due to the inherent 'rounding' or facetting of the feature due to etching by high energy ions

Chapter 4 Sub-Micron Feature Fill

4.1 Introduction

The current trend in via fill processing is away from high resistivity materials such as tungsten to lower resistivity materials such as aluminium and copper[66] W CVD for via fill applications is a well established production worthy technology that is still used widely throughout the microelectronics manufacturing industry The challenge is to replace this process with Al and Cu processes which are at least as production worthy

Typically, interconnect lines are made from Al and are deposited using a PVD process The natural trend therefore has been to employ this aluminium as a plug fill material, thus simplifying the manufacturing process considerably The difficulty however is that filling sub 0 5μm large aspect ratio features is extremely difficult with PVD style processes[75] Small features tend to fill from the top down leaving the potential for voids in the material One means of increasing the amount of aluminium reaching the bottom of a feature is to increase the surface mobility of aluminium adatoms[76]

In this chapter the process of filling deep sub-micron features with Al is examined in detail First a simulation package is used to identify process parameters which can be manipulated to assist the fill process The development of a fill process on an IPVD deposited liner is discussed and it is shown that it is possible to fill very small features from bottom to top without having to rely on the rather slow bulk and surface diffusion processes In section 4 6 a model is introduced to help explain the aspect ratio dependency of the fill process Finally some electrical results are presented firstly to demonstrate the repeatability of the fill process and secondly to highlight the advantages of Al-plugs over the more commonly used W-plugs

4.2 Surface Diffusion

The fundamental concept behind high temperature aluminium processing is to increase the amount of surface diffusion of surface adatoms and bulk diffusion of vacancies through the aluminium

Surface diffusion is the movement of atoms along the surface of the film or along the grain boundaries The initial topographical development of a surface feature due to sputter deposition is a function of the material fluxes to the surface and the surface diffusion of the film during the deposition process[77] When considering elevated temperature deposition of aluminium, surface diffusion plays a significant role in the film topography development over a surface feature

It is possible to describe this material surface transport process in terms of its driving force[78] The surface contour of the sub-micron feature provides the driving force that directs material flow ad-atoms incident on the substrate surface diffuse in order to minimise surface energy Atoms on a convex surface are not thermodynamically stable and tend to flow to a location where the chemical potential is low (i e a concave surface) The surface flux between two points on a 3D surface can be approximated as

$$J \approx \left(\frac{1}{r_2}+\frac{1}{r_1}\right)+\left(\frac{1}{R_2}-\frac{1}{R_1}\right)$$

which describes the flow of material on the surface due to surface diffusion

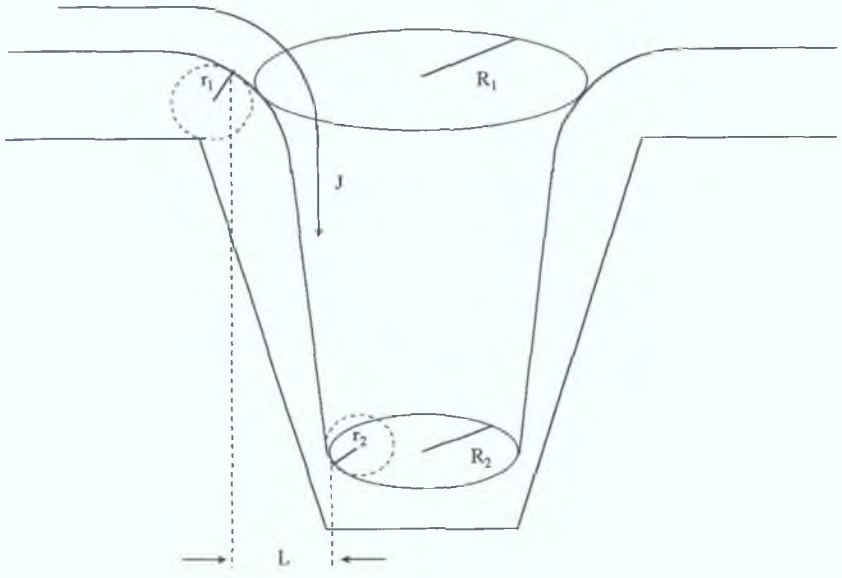

***Figure 4.1** Material Flux due to Surface Curvature*

R_1 and r_1 represent the in-plane and out-of-plane radii of curvature at the feature opening and R_2 and r_2 represent the in-plane and out-of-plane radii of curvature at the bottom of the feature.

The smaller R_2 is relative to R_1, the more intense the flux of material is to the bottom of the feature. Also, the smaller r_2 and R_2 the more intense the flux is to the bottom of the feature. For sloped contacts in which $R_2 < R_1$ the flux is driven to the bottom of the feature and 'bottom to top' fill of the feature. This is the fill mechanism typically observed for larger features. For small features however the film overhang at the top of the feature changes the situation. Due to the overhang the radius at the opening R_1 shrinks until it becomes smaller than R_2 or the radius at any point below the opening, resulting in reduced flux movement from top to bottom. This effect becomes more pronounced if the deposition rate is too high. In this case sputtered material at the overhang cannot be transported away sufficiently fast so that the feature opening eventually closes. This situation is know as bridging and is undesirable as it limits the means by which the feature can be filled to bulk diffusion, i.e. top to bottom fill. Figure 4.2 illustrates the principle of curvature induced surface diffusion for large and small contacts. Figure 4.2.i shows surface diffusion into a small feature, resulting in bottom to top fill. Figure 4.2.ii shows the situation for a relatively small feature where the

change of radius at the feature opening due to film overhang leads to bridging Figure 4 2 iii illustrates a situation where the surface diffusion is completely suppressed due to bridging

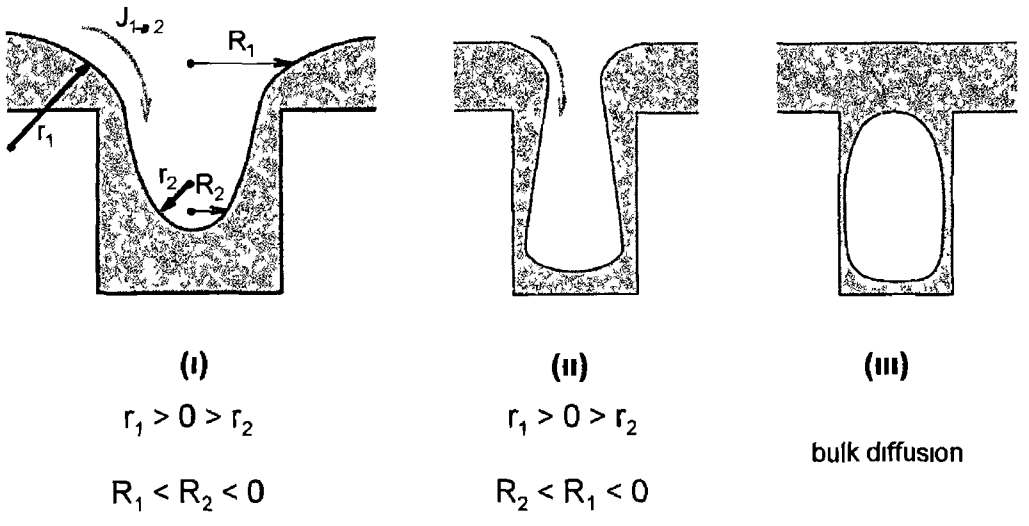

Figure 4 2 *Schematic of Fill Process*

Bulk diffusion is the movement of vacancies through the bulk material Like surface diffusion, matter tends to move from regions of high surface potential to regions of lower surface potential Surface diffusion takes place tangential to the film surface whereas bulk diffusion takes place perpendicular to the film surface Bulk diffusion therefore tends to be the redistribution of material from the top surface to the voids in the material[79]

4 3 Wettıng Angle

The wettıng angle of a film of materıal on a substrate ıs a measure of the tendency of the depositıng materıal to agglomerate or 'bead up' In the case of aluminium on SiO_2 the depositıng aluminium tends to bead up and prevent flow of aluminium ınto contact and vıa type features In practice an mterfacıal materıal (or wettıng layer) ıs used to cırcumvent thıs problem

Durıng ınıtıal depositıon the ısland formatıon on a substrate can be approxımated by a hemıspherıcal cap as ıllustrated ın figure 4 3

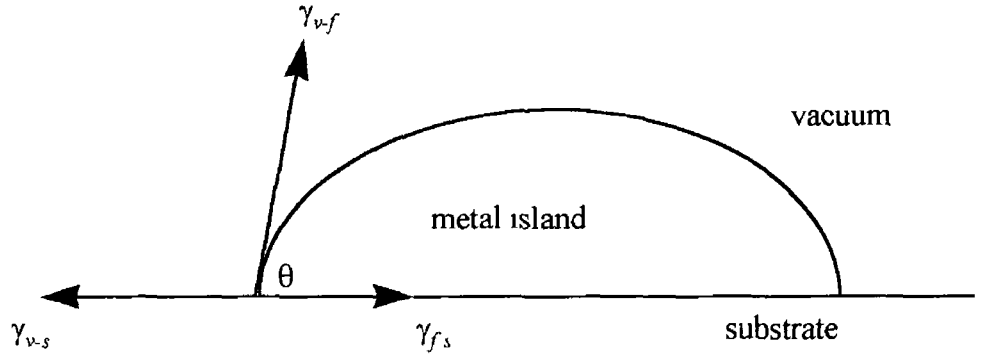

Figure 4 3 *Island Formatıon on a Substrate*

where

$\gamma_{v\text{-}s}$ = vacuum- surface ınterfacıal energy

γ_{fs} = metal - substrate ınterfacıal energy

γ_{vf} = vacuum - metal ınterfacıal energy

These surface and ınterfacıal energıes are related to the wettıng (or contact) angle by Young's equatıon[80][71]

$$\cos\theta = \frac{(\gamma_{v-s} - \gamma_{f-s})}{\gamma_{v-f}}$$

This relationship holds if there is no chemical reaction between the substrate and the depositing film It is known however that under the influence of interfacial chemical reactions the wetting angle is not stable and is time dependent The actual and final wetting angles obey the following empirical relationship

$$\theta_t - \theta_f \propto e^{-t/\tau}$$

where θ_t is the contact angle at time t, θ_f is the final stable contact angle and τ is a time constant characteristic of the liquid-solid reactivity[81] In the case of aluminium on titanium τ is typically in the range 5 - 15 seconds In order to investigate this phenomenon the contact angles of aluminium deposited on a Ti/TiN/TiN_x stack were measured using an AFM As the samples constitute a multi-phase system, the values of the contact angle show the non-equilibrium state of the wetting behaviour From the results presented in figure 4 4 the contact angles for this aluminium / substrate combination starts off at a reasonably low value As the thickness increases and presumably the wafer temperature increases (see appendix E), the contact angle gets even lower with a final contact angle of approximately 2 degrees This final contact angle is very low for this substrate compared to similar measurements on other substrates, Al on TiN 60°, Al on SiO2 60°, Al on Ti 15°[82]

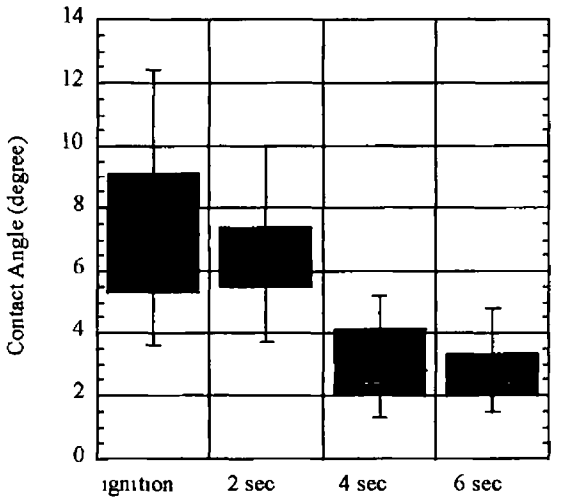

Figure 4 4 *Contact Angle vs Time*

4 4 Using a Thin Film Growth Simulation Package to Examine Al Via Fill Evolution

A thin film growth simulation package was used to examine the evolution of an Al via fill process The influences of adatom diffusion length and wettability of the wetting layer on the fill process are studied It is found that an adatom diffusion length in excess of 1μm is required to fill 0 35μm 3 1 aspect ratio vias if surface diffusion is the dominant diffusion process

In this study the commercially available SIMBAD simulation software is used to examine the influences of adatom surface mobility and wetting layer wettability on the via fill process

The SIMBAD model has already been discussed in detail in chapter 2 Here extensions to the model to allow for elevated temperature processing are discussed The SIMBAD model has been extended to model the high temperature sputtering of aluminium using a diffusion algorithm in which the driving force is a surface potential determined by the curvature of the surface[83][84]

4 4 1 Calculation of Diffusion Lengths

When an adatom impinges on a surface the adatom moves across the surface in a direction to reduce surface energy associated with areas associated with high curvature For a given metal and a given surface orientation the surface diffusion co-efficient (diffusivity) may be expressed by an Arrhenius type relationship

$$D = D_0 e^{Q/kT}$$

Where D_0 is the material constant known as the frequency factor, Q is the activation energy, k is Boltzmann's constant and T is the absolute temperature

The average diffusion length can then be expressed as

$$L = \sqrt{Dt}$$

where t is the average length of time an adatom is mobile on the film surface

The surface mobility of the adatoms on the surface is a function of substrate temperature, substrate contamination, substrate material and deposition rate Film grain size is a function of diffusion length By first measuring the average grain size for a given process and then simulating the process to achieve a comparable film, the average diffusion length of an adatom on a surface can be estimated

Dew et al[83] utilises the fact that the activation energy for surface diffusion can be empirically expressed by

$$Q_s = 5kT_m$$

Where T_m is the melting point of the material
From this, the expression for diffusion length becomes

$$L = \sqrt{D_0 \tau} \exp(-5T_m / 2T)$$

By comparing a sputtered film to a simulated film in terms of average grain size, it was estimated that a deposition temperature of 250°C corresponded to a diffusion length of 0 2μm

Let L = 0 2μm, T_m = 660°C, T = 250°C

$$-5T_m(K)/2T(K) = -4\ 45$$

$$e^{-4\ 45} = 0\ 01156$$

$$\sqrt{D_0 \tau} = 0\ 2/0\ 01156 = 17\ 30$$

So for T = 500°C (773°K)

$$L = 17\,30 * e^{\frac{-5.933}{2 * 773}} = \mathbf{0\ 84\mu m\ @500°C}$$

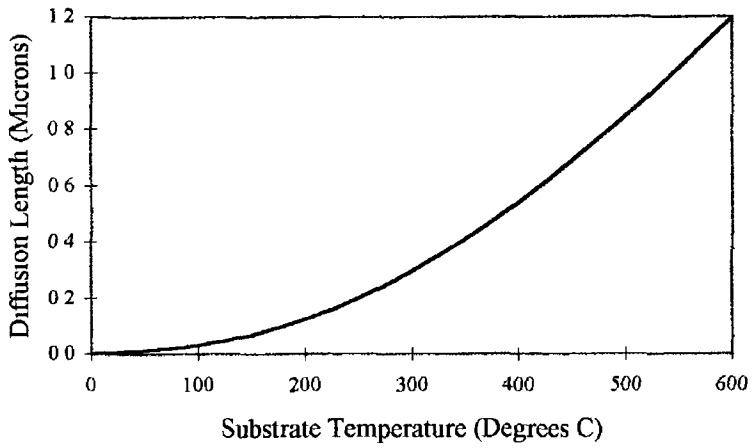

Figure 4 5 *Diffusion Length of Al*

Using SIMBAD to examine the relationship between diffusion length and grain size for the 0° wetting angle case, the following relationship exists between grain size and diffusion length

Average Diffusion Length (μm)	Average Grain Size (μm)
0 03	0 10
0 10	0 20
0 60	0 70

Table 4 1 *Diffusion Length vs Grain Size*

As expected the film grain size is a function of the diffusion length

On examination of aluminium films of similar thickness to the simulated films the following relationship was observed between measured substrate temperature and grain size

Substrate Temperature (°C)	Average Grain Size (μm)
50	0 25
500	0 60

Table 4 2 *Grain Size vs Substrate Temperature*

From this data it can be estimated that the 0 6μm diffusion length films correspond to an approximate measured substrate temperature of 500°C

4 4 2 2D Simulation of Via . Effects of Diffusion Length and Wetting Angle

The simulations were designed to evaluate the influences of diffusion length and wetting angle on the fill process It was assumed that bulk diffusion had no influence on the fill process The influences of bulk diffusion will be the subject of a further study

The feature size and shape are detailed in figure 4 6 This feature size and shape is typical of the size and shape of 0 3/0 35μm 3 1 aspect ratio vias The slope at the opening of the via is usually the result of a sputter etch prior to metal deposition

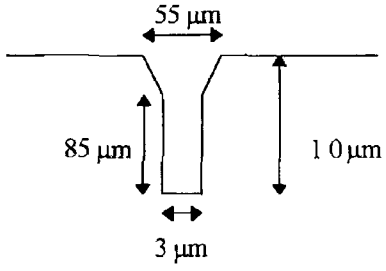

Figure 4 6 *Geometry of Simulated Via Structure*

The angular distribution of the incoming flux is given by [85]

$$f(\theta) = \begin{cases} \cos(6\theta / 5), |\theta| \leq 5\pi / 12 \\ 0, |\theta| > 5\pi / 12 \end{cases}$$

Where θ is the angle at which the particle was launched

The simulation was run for four different wetting angles 180°, 90°, 45° and 0° and three different diffusion lengths 0.03μm, 0.1μm and 0.6μm. The thickness of the simulated film was 0.3μm. The sticking coefficient was assumed to be 1. The simulation results are shown in figure 4.7.

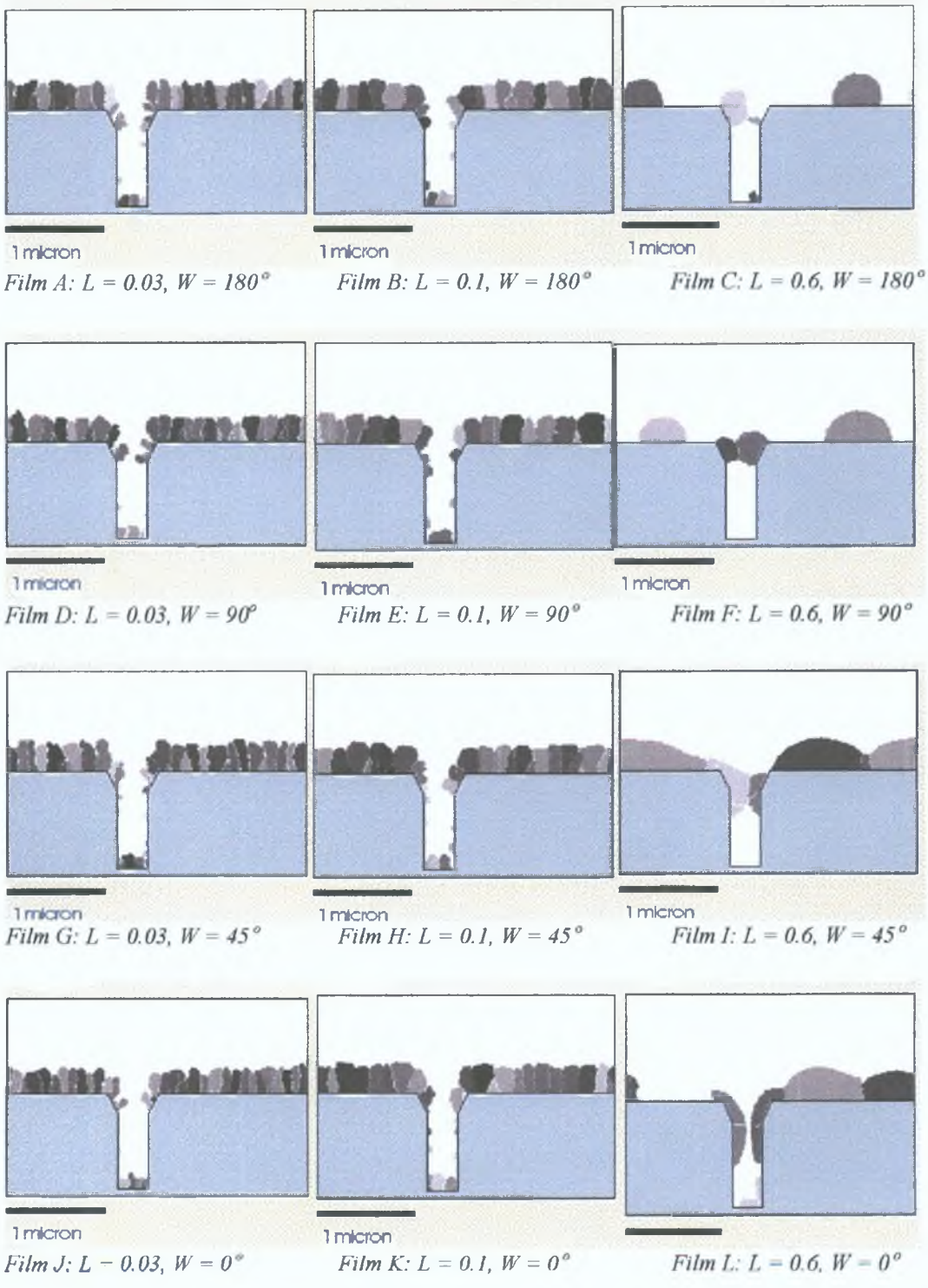

Figure 4.7 *SIMBAD Hot Al Simulation Results*

4.4.3 Analysis of Simulation Results

For the incoming flux angular distribution used it can be seen that the bottom and sidewall coverage for the lower diffusion length processes is reasonable but neither process is suitable to be used as a via fill process. The 0.6μm diffusion length process is a more promising via fill process. For the 180°, 90° and 45° wetting angle, 0.6μm diffusion length processes, bridging occurs at the top of the via. Once bridging occurs the only means of completing the fill of the via is through bulk diffusion of the material to the bottom of the feature. The 0°, 0.6μm diffusion length process achieves the best via fill but it is likely that a thicker film would lead to bridging and the consequent formation of a void.

Two further simulations were run with a diffusion length of 1μm and wetting angles of 45° and 0°. The results are shown in figures 4.8 and 4.9 respectively. In both cases the fill achieved is superior to the 0.6μm case. The 1μm, 45° film has a small void in the centre of the film but the 1μm, 0° film appears as though it may result in via fill with a thicker film.

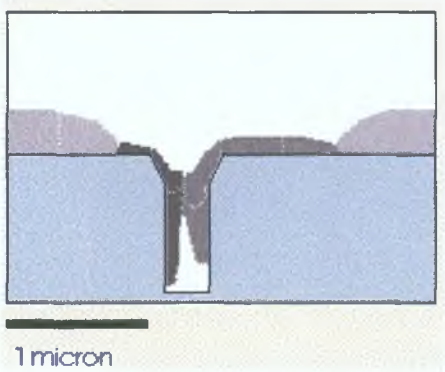

Figure 4.8 *1μm, 45° Film*

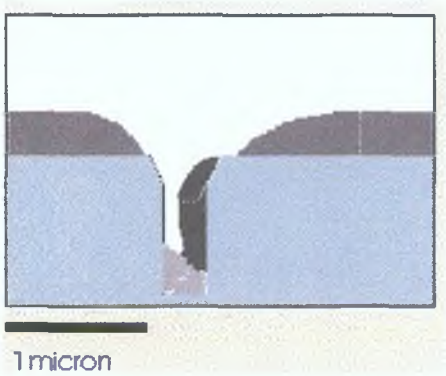

Figure 4.9 *1μm, 0° Film*

These results suggest that in order to fill 0 35μm 3 1 aspect ratio vias with aluminium assuming surface diffusion is the dominant process, a diffusion length of approximately 1μm and an excellent wetting angle is required The 0 3μm film is probably not thick enough to completely fill the via simulated over the diffusion lengths considered In a real PVD process bulk diffusion may in fact play a more significant role in the via fill process

4 5 Experimental Analysis of the Fill Mechanism

4 5 1 Introduction

The results of these simulations indicate that fill of deep-sub-micron features can be achieved by surface diffusion alone if the wetting angle between the deposited material and the substrate is small enough In a typical aluminium fill process material overhang at the top of the feature leads to bridging of the feature and a void in the aluminium is created This void can only be filled by bulk diffusion of vacancies through the bulk material which in turn relies on crystallographic defects[86]

Filling a feature using predominantly bulk diffusion is a slow process and is costly in terms of wafer throughput and wafer thermal budget The following list of conditions are believed to be the main parameters influencing the via fill mechanism

- Al - Ti Reaction (Chemical Reactions)
- Profile Of Feature (Wetting/Barrier Layer Deposition Process)
- Temperature (Diffusion Length, Wetting Angle)
- Wetting Layer Composition / Structure
- Roughness
- Al Deposition Conditions (Deposition Rates, Time at Temperature)

In the following study the influences of seed layer deposition temperature and liner type on the via fill mechanism are examined The object of the study is to find a process where surface diffusion of the aluminium is maximised in order to fill the features from bottom to top

The aluminium deposition process is normally carried out in three steps

1 'Cold' Seed Layer
2 Hot Low Power
3 Hot High Power

The seed layer is typically sputtered fast and cold in order to suppress the $TiAl_3$ reaction This seed layer needs to be continuous along the sidewall of the feature in order to allow subsequent material flow easily over it The low power high temperature step helps the fill process in two ways

a) At low deposition rates the average diffusion length of the adatoms is likely to be longer than at high deposition rates[88]
b) When the deposition rate is lower the wafer is at temperature for longer giving the material more time to diffuse into the feature by solid phase diffusion

An overview of the 3-step deposition process is given in table 4 3

Step	Purpose	Temperature	Deposition Rate	Typical Thickness
1	Continuous Film	30-150°C	High	100 - 400nm
2	Al Surface and Bulk Diffusion	400-550°C	Low	100 - 400nm
3	Increase Throughput, Tailor Reflectivity	400-550°C	High	Balance Al

Table 4 3 *3 Step Deposition Process*

4 5 2 Experimental

It was decided to experiment with three different liner processes which from previous experience were known to provide good feature fill The first two liners were IPVD $Ti/TiN/TiN_x$ triple layers and the other was a IPVD Ti layer The difference between the two triple layers was the deposition pressure of the TiN_x layer (low pressure vs high pressure) The TiN_x layer is known as a 'flash' layer After TiN deposition the nitrogen supply to the chamber is switched off and the nitrided target is sputtered in a pure argon plasma The result is a film with a nitrogen content gradient, with the

surface being pure titanium For each of the liners the seed layer deposition temperature was included as a split

The wafers used were patterned wafers with a 1000nm PECVD oxide layer on top of the metal 1 stack The deposition sequence of the wafers was as follows

1 Degas (500°C)
2 Sputter Etch
3 Liner Deposition
4 Wafer Cool (for some splits)
5 Aluminium Deposition
6 Wafer Cool

Note that all of the above, including the transfer of the wafers from the different deposition chambers were carried out in a high vacuum environment The wafers were de-gassed at a temperature of 50°C higher than that of the aluminium deposition process in order to prevent material out-gassing from the wafer during the aluminium deposition process The Ti/TiN/TiN_x stacks were deposited in the same chamber There was no active wafer temperature control during barrier deposition but previous measurements have shown that the wafer reaches a temperature in the 400-450°C region due to plasma induced wafer heating

4.5 3 Results and Discussion

For each of the process splits 'Focused Ion Beam' analysis was carried out after seed layer deposition and after 75nm of the low power warm layer The results are tabulated in table 4 4

Split	Liner	Seed Layer Temp	Seed Fill	Warm Fill
1	Low Pressure Ti/TiN/TiN_x	Low	↓	↓
2	Low Pressure Ti/TiN/TiN_x	High	↑	↑
3	High Pressure Ti/TiN/TiN_x	Low	↓	↓
4	High Pressure Ti/TiN/TiN_x	High	↓	↓
5	Ti Only	Low	↓	↓
6	Ti Only	High	↓	↓

↓ refers to Top to Bottom fill
↑ refers to Bottom to Top fill

Table 4 4 *Fill Mechanism Experimental Results*

In all cases, except for split 2, the via fill proceeds from the top to the bottom which is normal and is what is commonly seen for small contacts Before explaining why bottom to top fill has been achieved in split 2 it should be mentioned that the aluminium deposition process used is a standard deposition process From the work in chapter 3 it was seen that for the 3 1 aspect ratio features, a continuous film on the sidewalls is unlikely to be achieved

In split 2 no attempt was made to sputter the seed layer cold, in fact the likely deposition temperature is in the 300 - 350°C range

Figures 4 10 to 4 13 shows the evolution of the via fill in split 2 The first two photographs show the 0 25μm and 0 4μm features after seed layer deposition The aluminium has flowed to the bottom of the via as indicated by the arrows About 30% of the via has been filled The next two photographs show the feature fill after 70nm of aluminium deposition at 1kW deposition power No bridging has occurred and the fill has proceeded further from the bottom to the top In fact some of the 0 25μm features have been planarised in this remarkably short time The fill of the 0 4μm features lags behind but nevertheless fill has proceeded from bottom to top without any bridging

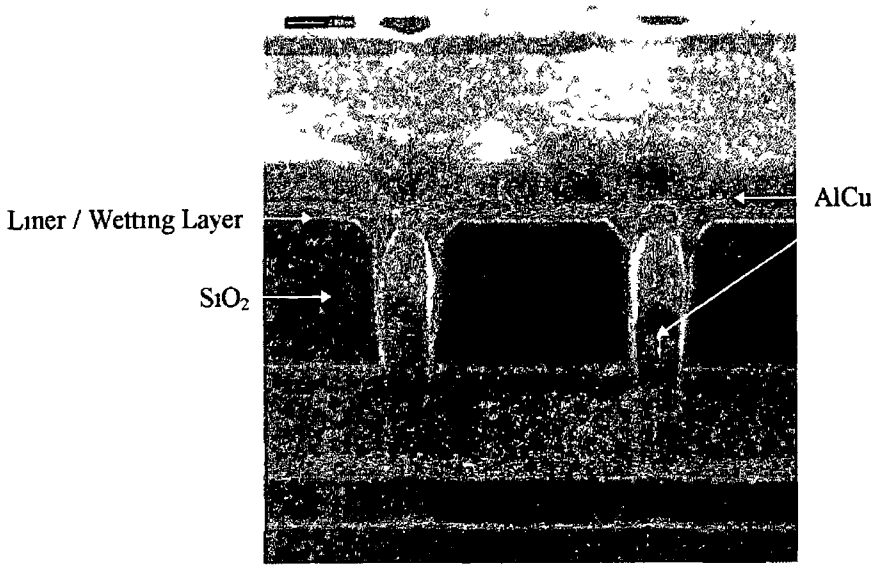

Figure 4 10 *Cross section of 0 25 μm vias (aspect ratio 4 1) after the deposition of the Al seed layer (Split 2)*

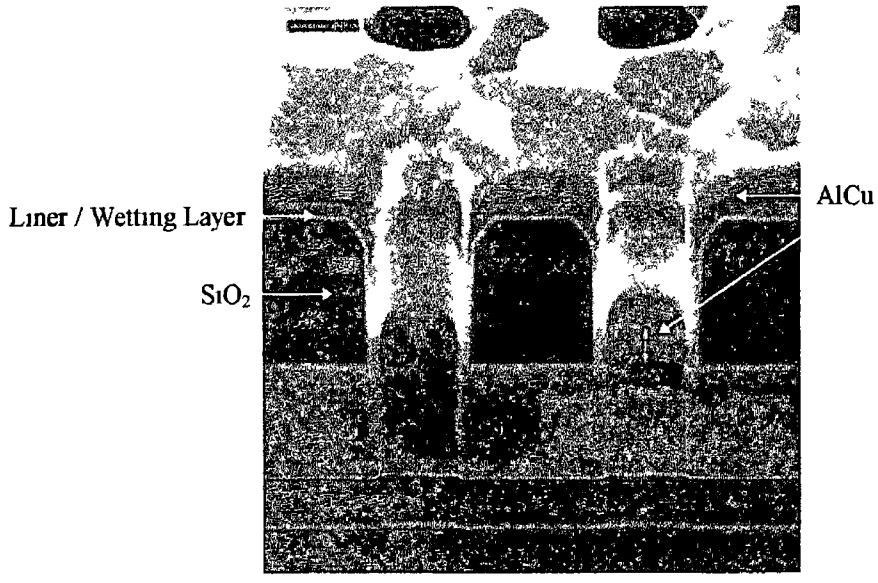

Figure 4 11 *Cross section of 0 4 μm vias (aspect ratio 2 5 1) after the deposition of the Al seed layer(Split 2)*

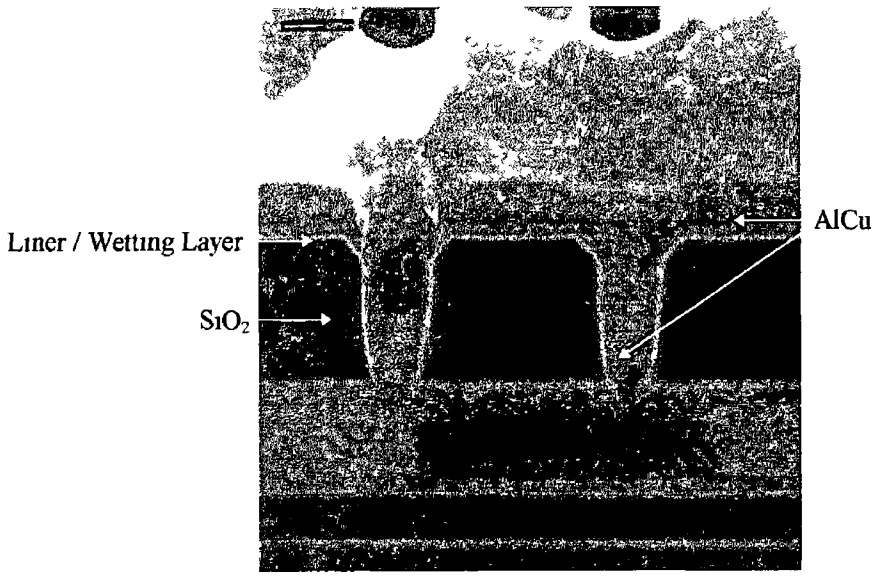

Figure 4 12 *Cross section of 0 25 μm vias after the sequential deposition of the Al seed layer and the 1 kW flow(Split 2)*

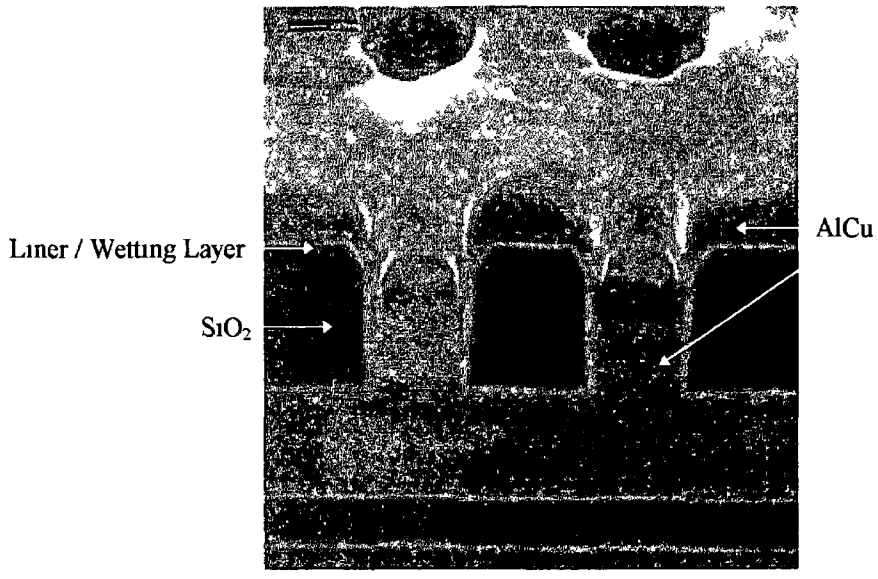

Figure 4 13 *Cross section of 0 4 μm vias after the sequential deposition of the Al seed layer and the 1 kW flow (Split 2)*

The feature fill evolves completely differently for each of the other splits Figures 4 14 to 4 17 show the evolution of fill for split 1, which is similar for splits 3 - 6 The first two photographs show the 0 25μm and 0 4μm features after seed layer deposition The overhang of sputtered material develops quickly at the opening of the features, especially in the case of the 0 25μm features The next two photographs show the evolution after 70nm of aluminium deposition at 1kW deposition power In all cases

the overhang has become more pronounced and some of the 0 25μm features have been completely closed The 0 4μm features are still open, however there is very little material at the bottom From experience and experiments performed in chapter 5 it is known that it will take approximately 180 seconds to fill features in which bridging has occurred

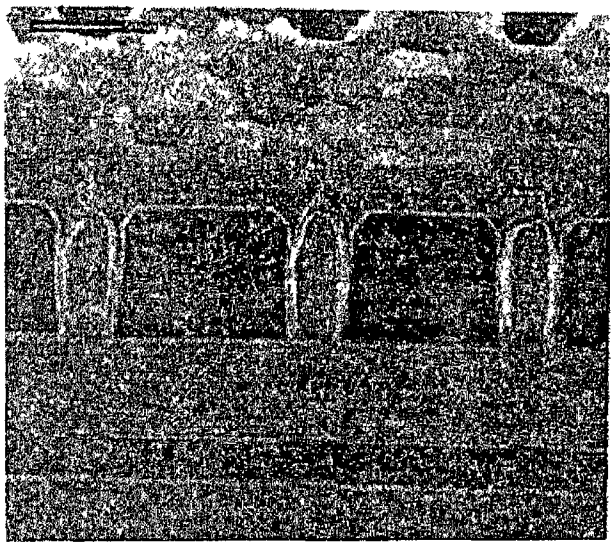

Figure 4 14 *Cross section of 0 25 μm vias (aspect ratio 4 1) after the deposition of the Al seed layer (Split 1)*

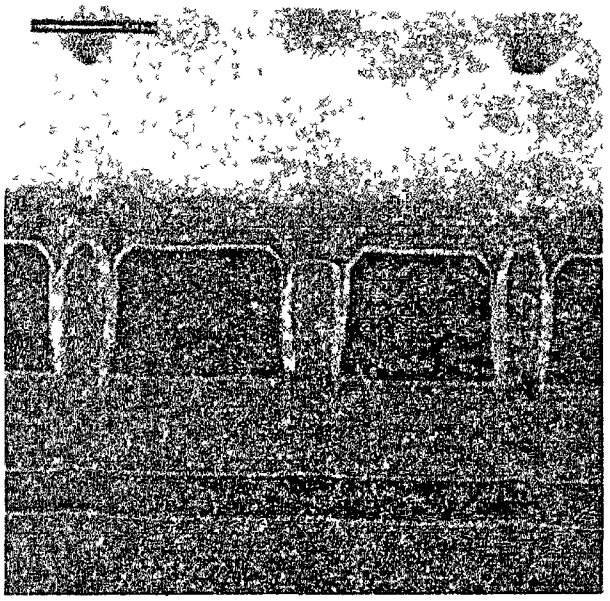

Figure 4 15 *Cross section of 0 4 μm vias (aspect ratio 2 5 1) after the deposition of the Al seed layer(Split 1)*

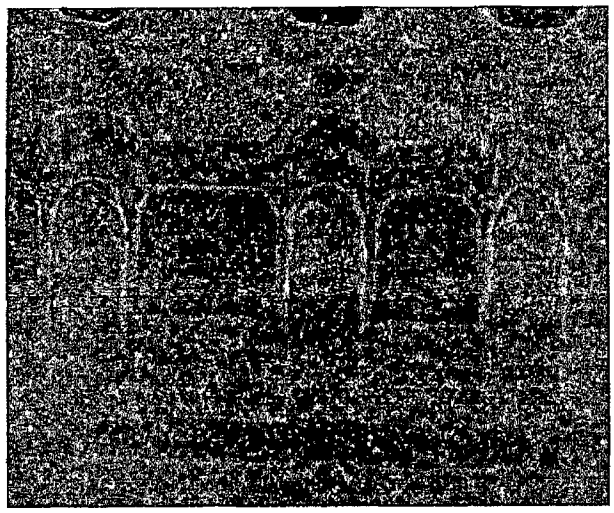

Figure 4 16 *Cross section of 0 25 μm vias after the sequential deposition of the Al seed layer and the 1 kW flow(Split 1)*

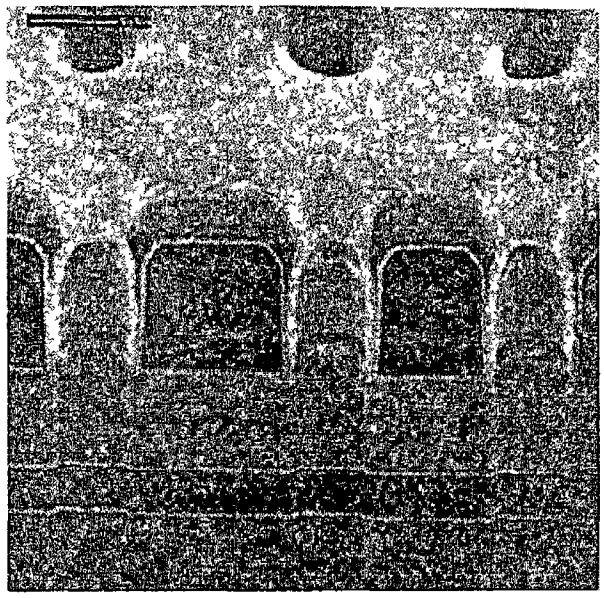

Figure 4 17 *Cross section of 0 4 μm vias after the sequential deposition of the Al seed layer and the 1 kW flow (Split 1)*

According to the simulations run earlier the only possible means of achieving bottom to top fill on small features is to have the diffusion length of the adatoms sufficiently long and the wetting angle sufficiently small For the diffusion length to be sufficiently long the seed layer must be continuous over the feature sidewalls Subsequent aluminium, if deposited on a good aluminium seed layer will have the potential to have long diffusion lengths and low wetting angles The deposition of a continuous seed layer using a conventional PVD process has been explained recently by Beyer et al[89] Other techniques have been employed to achieve continuous seed layers over high aspect ratio features For example CVD aluminium has recently attracted a lot of

attention and is used at a number of production sites throughout the world Excellent conformal low resistivity films can be deposited[90] however there are many disadvantages relative to a PVD based process, the most obvious being process complexity Long throw low pressure aluminium deposition processes are also gaining wider acceptance[91] The other advanced process currently in use is collimated aluminium sputtering[92]

It has been shown in chapter 3 that a continuous seed layer over high aspect ratio features is not achievable with the standard PVD process The continuous seed layer achieved in split 2 could only have been achieved by a phenomenon known as reaction induced wetting[89] Reaction induced wetting is a phenomenon that can be employed to form an aluminium containing seed layer over aspect ratios normally too aggressive for the standard aluminium process Reaction induced wetting utilises the spreading characteristics of the titanium-aluminium reaction The driving force of spreading (or wetting) of a liquid - solid interface is related to the amount of reduction in energy by the creation of the new liquid - solid interface Spreading will occur as long as there is a driving force i e as long as

$$\gamma_{v-s} - \gamma_{f-s} > \gamma_{v-f}$$

where $\gamma_{v-s}, \gamma_{f-s}, \gamma_{v-f}$ are as defined in chapter 4 page 5

When there is a chemical reaction (as is the case with hot aluminium on titanium), the free energy of the reaction (dG) enhances the driving force for wetting

$$\gamma_{v-s} - (\gamma_{f-s} + \frac{-dG}{dAdt})$$

The $TiAl_3$ reaction is exothermic and the additional source of localised heating helps the aluminium flow

To utilise the reaction induced wetting phenomenon the seed layer needs to be deposited hot in order to start the Ti-Al reaction and hence start to flow along the sidewall, as in split 2 of the above experiment

The continuous seed layer helped to promote the surface diffusion enough to allow bottom to top feature fill The continuous seed layer was achieved by starting the flow down the sidewall as soon as the sputtering starts utilising the reaction induced wetting phenomenon However, it should be noted that the surface diffusion competes with the formation of an overhang at the top of the feature and the $TiAl_3$ reaction at the sidewall It is reasonable to assume that the deposition rate of the aluminium film needs to match the diffusion of the aluminium into the feature If the former is too high with respect to the latter an overhang of deposited material will evolve at the opening of the via ultimately resulting in void formation in the film Similarly the Ti-Al reaction on the sidewall needs to be matched to the flow of aluminium down the sidewall in order to allow Al surface diffusion on an Al surface The flow of Al on the sidewall needs to exceed the T-Al reaction front so that every new Al atom is not consumed by the reaction front

From the results shown in figures 4 9 and 4 10 there appears to be an aspect ratio dependence on the time to fill the features This can be explained by a simple geometrical model of the fill process

4 6 Geometrical Model of the Fill Process

4 6 1 Model

Assume that the vast majority of material reaching the bottom of the via flows in over the edge This assumption is supported by the pictures in figure 4 14 where the surface diffusion is suppressed and there is very little material at the bottom as a result of line of sight sputtering It is further assumed that the surface curvature is the same for all conditions, hence the driving force will not change during the experiment The via fill process can now be explained in terms of the supply of the material relative to the demand (i e the volume to be filled), as illustrated in figure 4 18

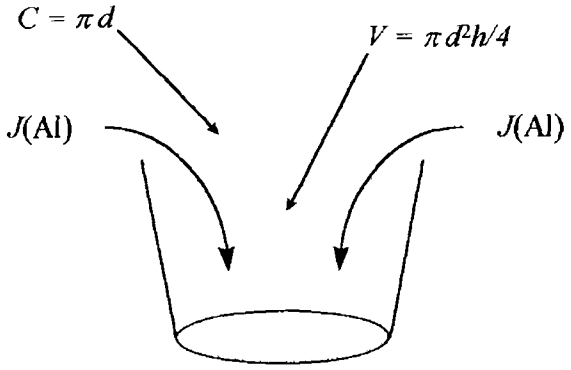

Figure 4 18 *Flow of Aluminium into a Circular Via*

Let Supply / Demand = Circumference C / Via Volume V

$$\frac{C}{V} = \frac{\pi * d}{\pi * d^2 / 4 * h}$$

$$\frac{C}{V} = 4 * \frac{1}{d * h}$$

where d is the via diameter and h is the height of the via

This shows that there is a $1/dh$ relationship between supply and demand which serves as a scaling factor to compare different aspect ratio vias This relationship indicates that the via fill process is strongly geometry dependent Whereas the circumference grows linearly with the diameter, the volume is proportional to the diameter by the power of 2 and to the height in a linear fashion

4 6 2 Experimental Verification of Geometrical Model of Via Fill Process

The validity of this geometrical model of via fill was tested in two experiments In the first experiment aluminium was sputtered onto patterned wafers with via diameters ranging from 0 25μm to 0 5μm The thickness of the patterned wafer oxide was 1μm Prior to aluminium deposition an IPVD Ti/TiN/TiN_x wetting layer (as described previously) was deposited on the wafer The aluminium was deposited at two different

deposition powers, 1kW and 12kW. The sputtered wafers were then cross sectioned and the aluminium fill versus via diameter was measured and tabulated. The results are presented in figure 4.19

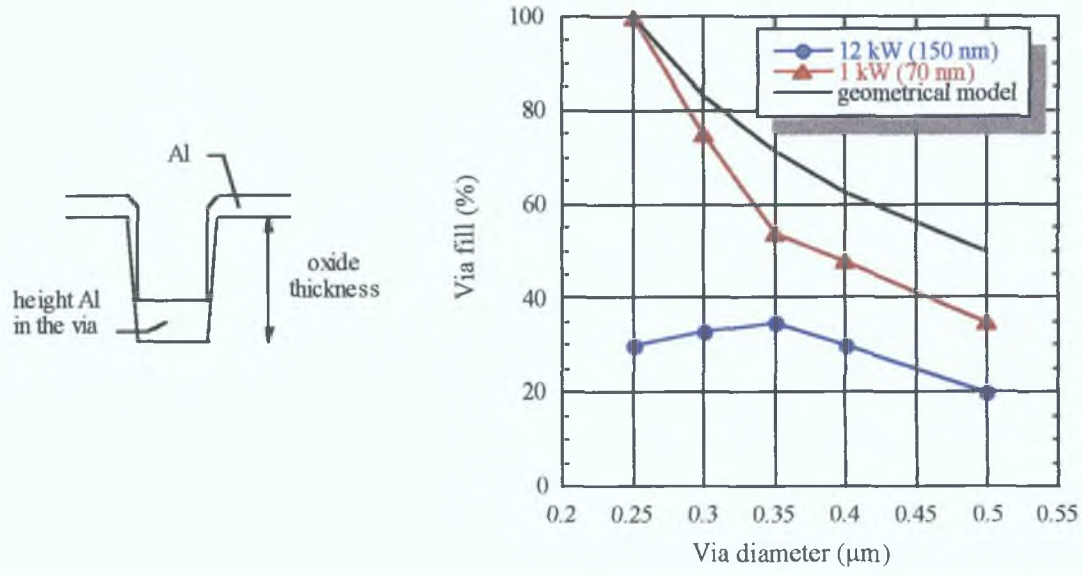

Figure 4.19 *Fill as a Function of Aluminium Deposition Power and Via Diameter*

The results show that the geometrical model does not accurately model the fill process in this case. The 1kW process fills the vias more slowly than expected, especially for the larger vias. One reason for this could be the presence of more titanium at the sidewalls of the larger vias. When the aluminium is sputtered slowly it has time to react with the titanium, forming $TiAl_3$. This intermetallic compound does not flow, thus delaying the fill process. The 12kW process appears to be too fast. Although the vias are filling from bottom to top a high degree of film overhang at the via openings can be observed in the cross sections. This appears to retard the fill considerably.

A second set of experiments were carried out except this time the aluminium was sputtered as a 12kW - 1kW stack, with the 12kW layer acting as a seed layer for the subsequent 1kW film. This means that the flow of sputtered aluminium at 1kW occurs on an aluminium surface which should maximise the degree of surface diffusion that takes place. Cross sections were prepared by FIB and the results are presented in figure 4.20. In this case the geometrical model describes the fill process with a high

degree of accuracy. As the aluminium now flows on aluminium, the Ti - Al reaction is minimal and hence does not retard the flow.

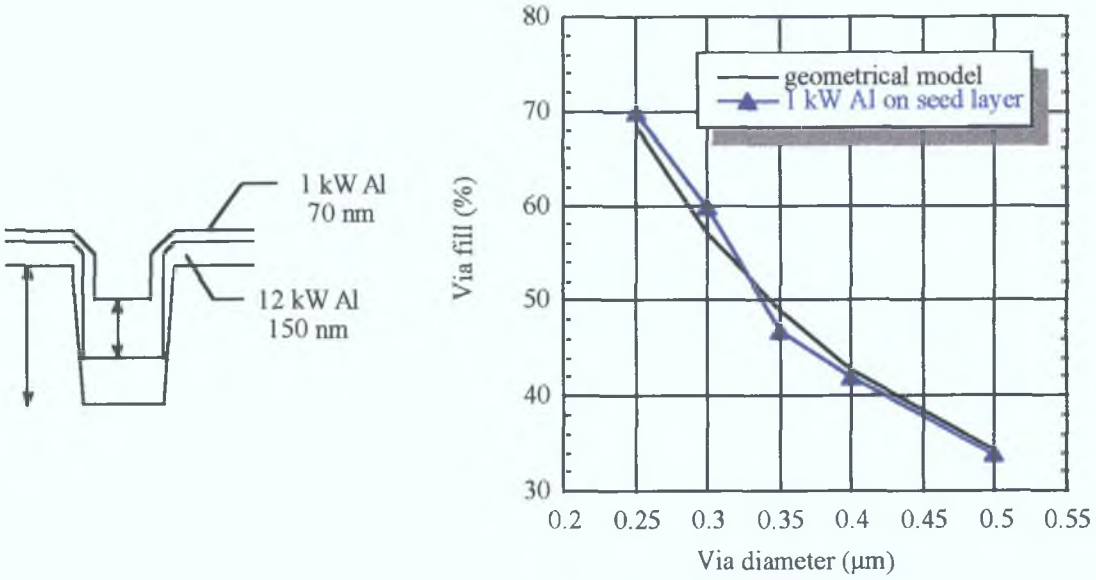

Figure 4.20 *Via Fill vs. Via Diameter for the Aluminium Flow at 1kW on the 12kW Aluminium Seed Layer*

4.7 Electrical Results

The Ti/TiN/TiN_x liner/wetting layer helps promote surface diffusion of the aluminium, however electrical results presented by other authors show that the via resistance of the Ti/TiN/TiN_x type liners is inferior to that obtained with Ti liner[66][86]. This may be due to the formation of high resistivity AlN due to the presence of N in the wetting layer[93][94][95].

Cross sections of features have indicated that the low pressure IPVD Ti/TiN/TiN_x barrier / cold - hot aluminium combination (Split 2) gives good fill characteristics. The true test of a via fill process' merit lies in the electrical results of a large number of vias. Reliable fill of a large number of vias is required before a process can be implemented in a real BEOL production process. The via yield on chains containing 10^6 vias with a diameter of 0.3 μm was measured. A cumulative plot of the resistance per via is given in figure 4.21. For the sake of comparison, yield data for a W-plug

process on an IPVD Ti/TiN liner is included in the graph. The excellent yield achieved with this novel aluminium via fill process is apparent. Not only is the yield better than the W-plug process but the via resistance is considerably lower. The striking thing about these results is the fact that the via resistance and yield achieved was achieved using a standard aluminium PVD process without a lengthy, high temperature re-flow step. The total aluminium deposition time was approximately 79 seconds whereas typical times reported by other authors to fill similar size features is approximately 3- 4 minutes.

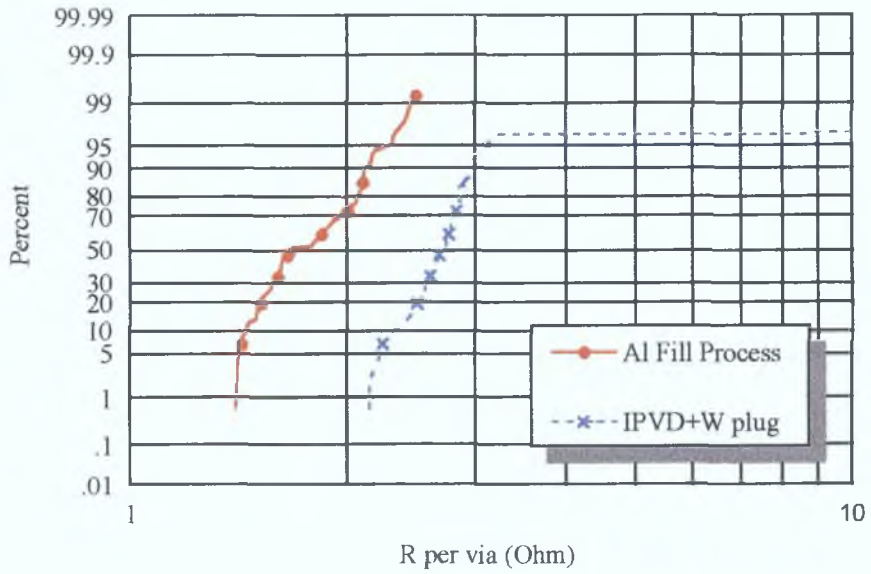

Figure 4.21 Al-Plug and W-Plug Electrical Data

At the beginning of this chapter the trend away from high resistivity materials to lower resistivity materials for contact and via fill applications was mentioned. This trend is necessary if the contribution of via resistance to the reduction in device speed is to stay minimal. As the diameter of a via shrinks the associated resistance increases. In order to keep this increased resistance controllable the resistivity of the material must be decreased. To understand this consider a via as a piece of metal wire.

The resistance of a piece of metal is given by the equation

$$R = \rho L/A \qquad (1)$$

where L is the length of the wire, ρ is the resistivity of the material and A is the cross sectional area. For a via

$$A = \pi r^2$$

$$R = \rho L / \pi r^2 \quad (2)$$

which shows that the via resistance is indirectly proportional to the square of the via radius. Typically when shrinking a process the via diameter decreases by a certain amount but the thickness of the dielectric (L in equation 2) needs to stay approximately constant due to interline capacitance considerations. Therefore the only term in the via resistance equation left to play with is the material resistivity.

The Kelvin via resistances for features with aspect ratios ranging from 2.0 to 4.0 were measured for a standard W plug process and for the aluminium process described above. The purpose of this experiment was to understand the contribution of material resistivity to via resistance. The results are presented in figure 4.22. The significant contribution of aluminium to lower via resistances especially at higher aspect ratios is obvious from the data.

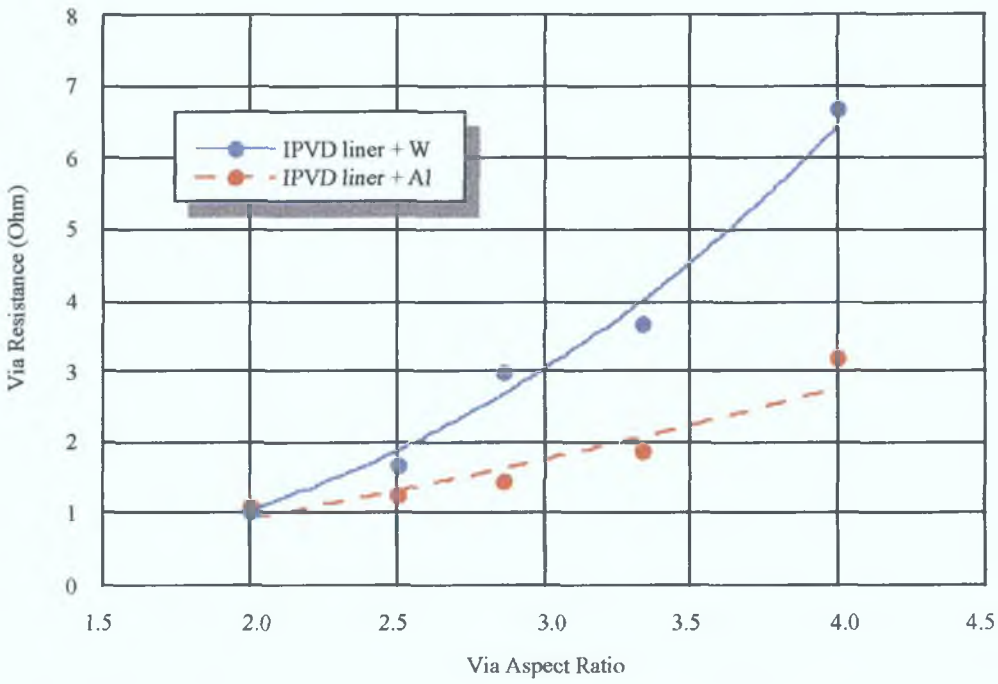

Figure 4.23 *Via Resistance Dependence on Aspect Ratio*

4 8 Summary

The filling of deep sub-micron features with aluminium has been examined both experimentally and by simulation Simulation results predict that typically, sub-micron features fill from top to bottom, relying on bulk diffusion of the aluminium to fill the feature However the simulations also suggest that by optimising the wetting angle and maximising the average adatom diffusion length, bottom to top fill can be achieved By experimentation an IPVD liner / wetting layer was found which facilitated bottom to top fill of 0 25μm vias This process has proven to be repeatable and production worthy, exhibiting excellent via resistances and yield This is the first time bottom to top fill has been achieved on 0 25μm features A model was introduced to explain the aspect ratio dependency of the fill process and was found to match closely the experimental results

Chapter 5 Development and Simulation of a Deep-Sub-Micron Feature Fill Process Using a Collimated Wetting Layer

5.1 Introduction

In the previous chapter the via fill mechanism was examined theoretically and experimentally. The wetting layer / barrier achieved with the IPVD process proved to be almost ideal. However, the IPVD process is still relatively new and expensive to purchase and install. The fact that it is an immature technology also raises questions about its production worthiness. On the other hand the standard and collimated PVD processes have been around for a long time and their production worthiness have been proven in the field. Also the cost of setting up a standard or collimated process is still only a fraction of that of the IPVD processes.

Coherent processing is an extension of the basic magnetron sputtering process where a collimator is placed between the target and substrate to filter out sputtered particles travelling at oblique angles to the substrate. In chapter 3, the effects of wide sputtered angular flux distributions were examined and the effects on bottom and sidewall coverage discussed. Coherent processing can be used to improve sidewall and bottom coverage by tightening the flux distribution width. The higher the aspect ratio of the collimator the more selective it becomes and the narrower the angular distribution able to pass through it.

Of course, material sputtered from the target deposits not only on the substrate but a certain percentage of it also deposits on the collimator. For example a 1.5:1 collimator typically collects up to 75% of the sputtered material. This is the major disadvantage of the collimated sputtering process. Deposition on the collimator gradually decreases the size of the holes which further reduces the transmission of the collimator. A rule of thumb used in the industry to determine the end of a collimator lifetime is that the collimator has reached the end of its life when the deposition rate reaches 50% of that at the beginning of collimator life. As the collimator aspect ratio increases the percentage of the material collected by the collimator also increases, hence reducing the effective lifetime of the collimator. For this reason, high aspect ratio collimator

processes (>2 1) tend not to be production worthy processes due to the required shield and collimator change frequency

The angular distribution of material sputtered from the target and arriving at the collimator also influences the collimator lifetime For example, aluminium which has a lower mass than titanium will tend to be scattered more by collisions with the sputtering gas, leading to a wider angular distribution and hence a shorter collimator lifetime The angular distributions of particles from the target can be tailored for a collimated process by controlling the crystalline orientation of the target[96]

Another concern with this process is the potential for particle contamination on the wafer The collimator is placed directly over the wafer surface and is subject to large changes in temperature There is a strong possibility of material delaminating or flaking from the collimator and falling on the wafer Careful hardware design and good preventative maintenance techniques are necessary to ensure the particle performance of a collimated process rival that of the conventional process Simulating the flux of material to a substrate in a collimated process is a relatively simple extension of a model of the standard sputtering process

In this study the ability of a PVD process to adequately fill 0 25μm features is examined A standard Ti wetting layer is contrasted with a collimated Ti wetting layer The influence of wetting layer thickness is also examined as is the type of Al process employed The role of the aluminium process time/deposition power and temperature were found to be very important as was the type of wetting layer used

5 2 Experimental

The experiment was performed on an Endura PVD system equipped with a standard Ti chamber, a collimated Ti chamber(1 1 aspect ratio), a cold (50°C) Al chamber and a hot (500°C) Al chamber The following parameters were varied and their effect fill properties studied

- Liner Type
- Liner Thickness
- Al Process Power
- Sputter Clean Time

The process conditions are detailed in table 5 1 and a summary of the split lot is given in table 5 2 The wafers used were 150mm diameter SMF (semi-major flat) wafers The feature's dimensions are shown in figure 5 1

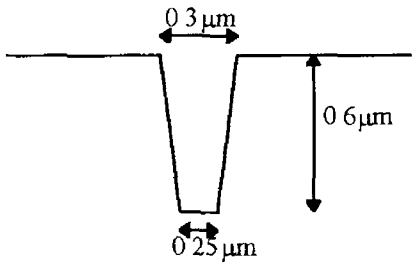

Figure 5 1 *Schematic of the Via*

There was no vacuum break between the layers as transfer of the wafers between the different process chambers was carried out in a high vacuum environment The sequence was designed to minimise the amount of time the wafer sits idle between the cold and hot aluminium steps The wafers were cooled after de-gas and prior to sputter etch to avoid possible contamination due to the wafer out-gassing at high temperatures

Process	Thickness	Power	Chuck Temp	Process Time
Degas	-	-	500°C	120s
Preclean	40nm / 80nm	125+300	-	60 6s / 121s
Liner	40nm Ti/ 40nm C-Ti/ 10nm C-Ti	3kW / 14kW / 14kW	200°C (Coherent)	14 8s / 18 4s / 4 6s
Cold Al	200nm	10 8kW	50°C	12 5s
Hot Al	600nm	1/ 2/ 10 8kW	500°C	375 2s/187s/34 7s

Table 5 1 *Summary of Process Conditions*

Wafers	Degas	Cool	40nmSE	80nmSE	40nm Ti	40nm C Ti	10nm C Ti	Cold Alu	Al 1Kw	Al 2Kw	Al 10.8Kw
1	y	y	y		y			y	y		
2	y	y	y		y			y	y		
3	y	y	y		y			y		y	
4	y	y	y		y			y		y	
5	y	y	y			y		y	y		
6	y	y	y			y		y	y		
7	y	y	y			y		y		y	
8	y	y	y			y		y		y	
9	y	y	y				y	y	y		
10	y	y	y				y	y	y		
11	y	y	y				y	y		y	
12	y	y		y	y			y	y		
13	y	y		y	y			y	y		
14	y	y		y	y			y		y	
15	y	y		y	y			y		y	
16	y	y		y		y		y	y		
17	y	y		y		y		y	y		
18	y	y		y		y		y		y	
19	y	y		y		y		y		y	
20	y	y		y			y	y	y		
21	y	y		y			y	y	y		
22	y	y		y			y	y		y	
23	y	y	y			y		y			y
24	y	y	y			y		y			y

Table 5 2 *Details of Process Split*

The purpose of the Ti wetting layer is to prevent deposited aluminium from de-wetting at high temperatures It is important that the Ti wetting layer is continuous and a minimum sidewall thickness of 50-70A is recommended A disadvantage of the presence of a Ti - Al interface is the $TiAl_3$ reaction which takes place at elevated temperatures This compound has a higher resistance than aluminium and therefore contributes significantly to via and line resistance The cold aluminium seed layer provides a path for aluminium atoms to diffuse at high temperatures Again it is important to get the thickness of this seed layer right as too thin a layer may lead to film discontinuities and too thick a layer will result in film overhang at the neck of the via making eventual filling more difficult

5 3 Experimental Results

SEM cross sections were made of a number of the wafers Photographs of the SEM cross sections are presented in figures 5 5 - 5 8

In order to identify the optimum process, the details of the experimental conditions and experimental results were examined using a data analysis tool The amount of material sputter etched, the wetting layer type, and the aluminium deposition power were

designated input factors and the degree of via filling and the amount of $TiAl_3$ formation were designated output responses. See figure 5.2 for an illustration.

Figure 5.2

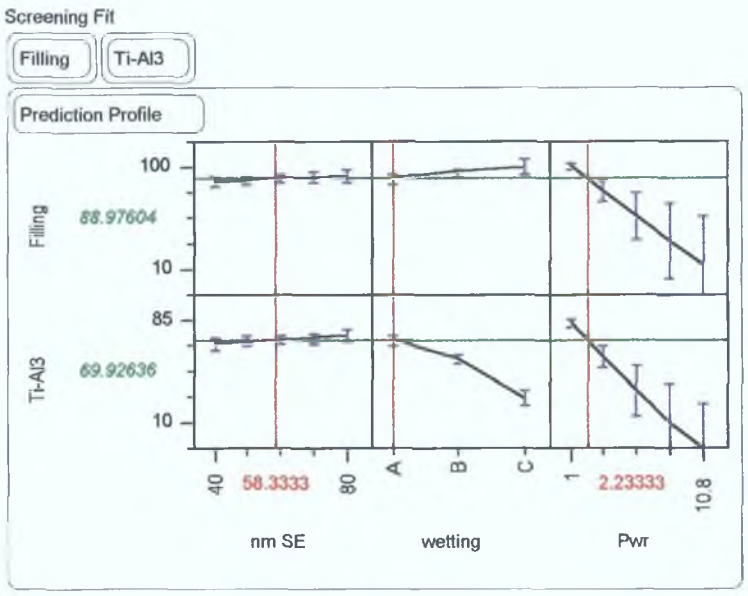

Figure 5.3 *Prediction Profiles for Process Split*

Prediction profiles of the responses as a function of the factors are presented in figure 5.3. From the graphs, the effects of the factors on the responses can be clearly seen. The degree of filling is a strong function of the deposition power but is not influenced to any great degree by the etch or the type of wetting layer used. The amount of $TiAl_3$ formation is a strong function of the deposition power and the type of wetting layer used.

5.3.1 Sputter Etch

The sputter etch was performed on the wafers prior to deposition of the Ti/Al/Al stack. Prior to sputter etch the features were straight-walled. The sputter etch had the expected effect of facetting of the edges of the feature at the top of the via (figures 5.5,

5.6). The extent of this facetting is physically determined by the dielectric material, the sputter etch wafer bias voltage, the feature shape and the amount of material etched.

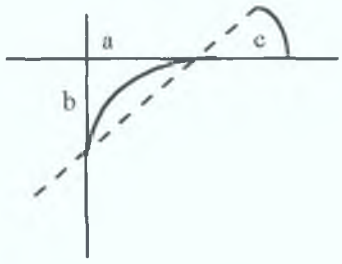

Figure 5.4 *Facetting of Corner due to Sputter Etch*

Figure 5.4 shown above identifies three quantities: a, b and the slope c. The values of these three parameters are compared in table 5.3.

Etch (nm)	a (nm)	b (nm)	c (degrees)
40	110	115	43.7
80	400	245	58.5

Table 5.3 *Facetting of Corner due to Sputter Etch*

The longer etch time opens up the via considerably. The convex sidewall shape of the 80nm via makes it relatively easy for aluminium to flow to the bottom of the via, however the extensive rounding of the via also increases the volume to be filled by aluminium. In this case there was not enough aluminium sputtered to fill the via.

The 80nm process is also likely to result in electrical isolation problems on device wafers due to the extended mouth size.

5.3.2 Aluminium Deposition Power

For all 1kW and 2kW processes via fill was achieved (see figures 5.5, 5.6 and 5.8). However the 10.8kW process resulted in large voids as shown in figure 5.7. There are two reasons why the 10.8kW fill process is inferior to the low power fill processes. Firstly, the average diffusion length of aluminium adatoms may be reduced at the higher deposition rates due to sputtered atoms being 'covered over' by other depositing atoms[88]. Secondly, the lower the deposition rate the longer the wafer is at temperature. A long time at temperature may be required to allow diffusion of the void

vacancy through the aluminium The 10 8kW process time is only 10 - 20% that of the lower power processes

5 3 3 Titanium Wetting Layer

The thin Ti layer is important to prevent de-wetting of the aluminium seed layer The titanium also acts as a getter for oxide and interfacial impurities It has the effect of reducing metal oxide formation and hence promoting good ohmic contacts between the metal vias Unfortunately at high temperatures there is an interaction between Ti and Al which results in the formation of $TiAl_3$ This compound has a high resistivity relative to the Al resistivity Excessive $TiAl_3$ formation can lead to high via and line resistances and poor yield

The extent of the $TiAl_3$ formation is a function of the temperature at which the Al was sputtered and the thickness of the Ti wetting layer The challenge is to minimise as much as possible the thickness of the Ti wetting layer without compromising the fill process

In the experiment, three different types of Ti wetting layer were deposited, 40nm of standard Ti ,10nm of coherent Ti and 40nm of coherent Ti Standard Ti should give a thicker sidewall film and coherent Ti should give better bottom coverage and thicker coverage at the bottom of the sidewall

For all three Ti processes, via fill was achieved when a low aluminium deposition power was used For the 40nm standard, it can be seen from the cross section that there is a significant amount of $TiAl_3$ formation To a lesser extent $TiAl_3$ formation is seen for the 40nm coherent Ti process The 10nm coherent process is relatively free of $TiAl_3$ formation

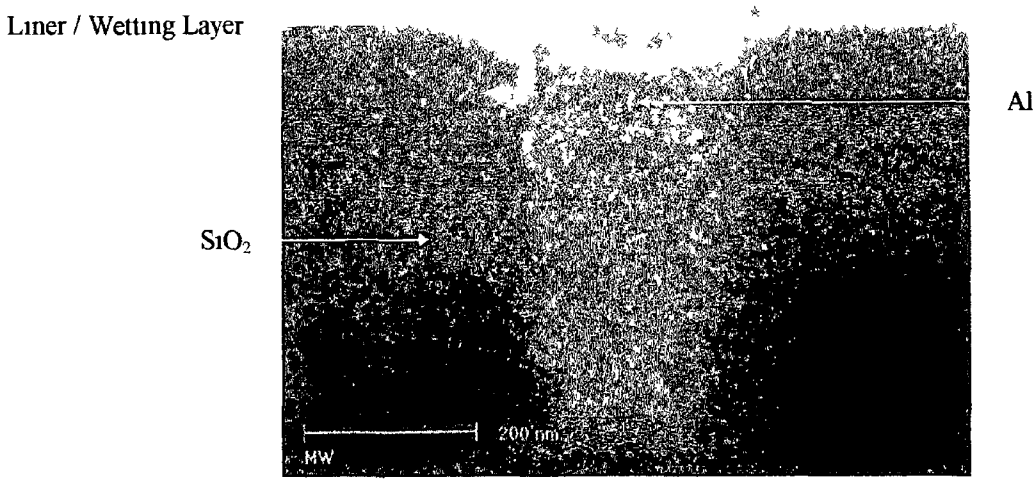

Figure 5 5 *40nm Sputter Etch, 10nm Coherent Ti, Al Power 1kW (Wafer 7)*

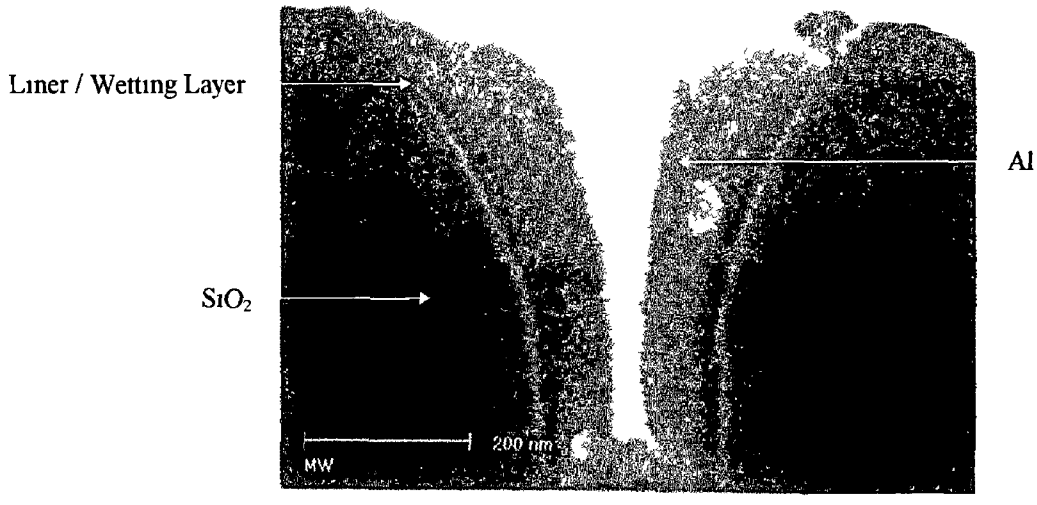

Figure 5 6 *80nm Sputter Etch, 10nm Coherent Ti, Al Power 1kW (Wafer 20)*

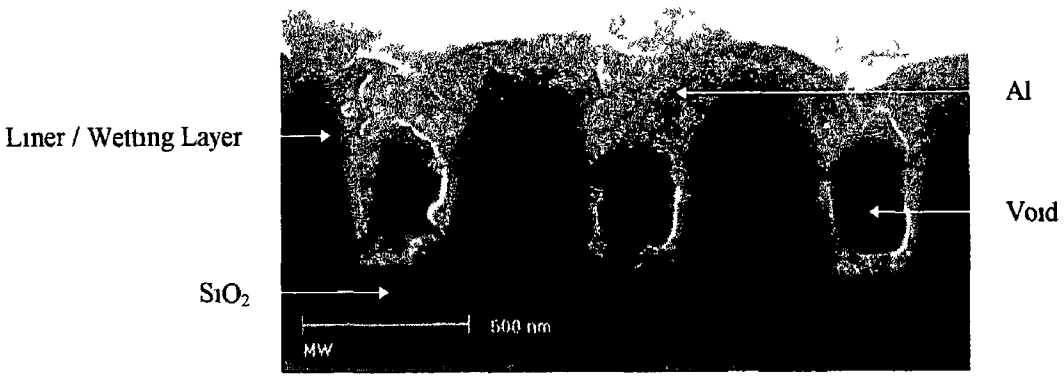

Figure 5 7 *40nm Sputter Etch, 40nm Coherent Ti, Al Power 10 8kW (Wafer 18)*

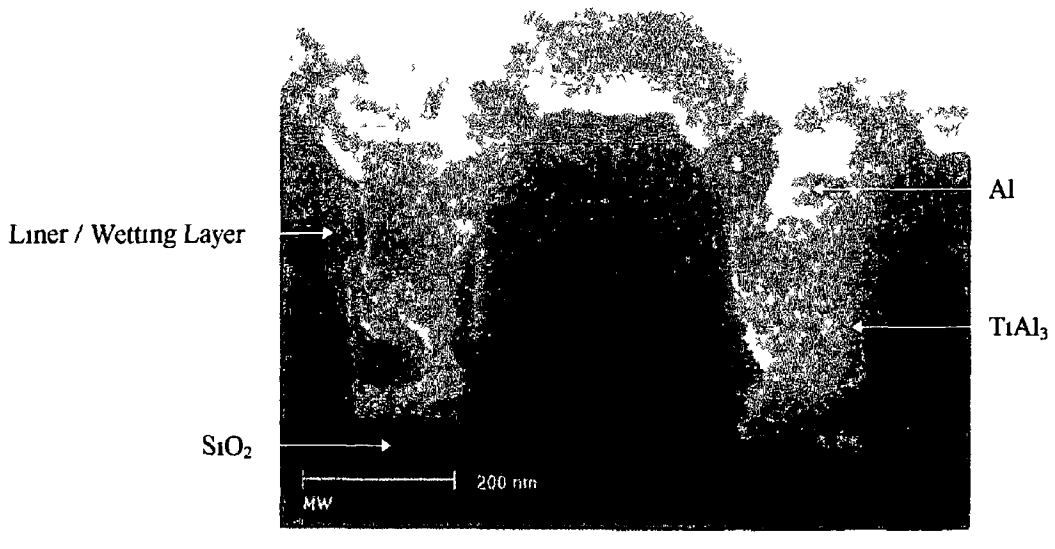

Figure 5 8 *40nm Sputter Etch, 40nm Standard Ti, Al Power 2kW (Wafer 4)*

5.4 Including the Effects of a Wetting Layer and a Cold Aluminium Seed Layer when Simulating the Aluminium Fill Process

In chapter 4 the SIMBAD simulations assumed that there was no reaction between the depositing aluminium and the substrate In practice however, the substrate on which the initial layer of aluminium is deposited is titanium Titanium is widely used as a wetting layer for aluminium to prevent de-wetting at high temperatures Titanium and aluminium react at elevated temperatures(>350°C) to form $TiAl_3$ This reaction is likely to retard the aluminium flow, especially if there is significant reaction at the mouth of the feature The nature of this reaction makes the simple SIMBAD model invalid for aluminium flow on titanium

Typically, modern PVD aluminium processes involve a two-step deposition of the aluminium film This two-step process involves the deposition of a thin cold 'seed' layer followed by a high temperature 'main' layer

The cold seed layer minimises the formation of the $TiAl_3$ compound and provides a path for the aluminium to diffuse at high temperature In order to model a 'real' Ti/Al/Al process the simulation would have to be performed in three steps

1 Simulation of Ti Deposition
2 Simulation of Cold Al Seed Layer Deposition
3 Simulation of Hot Aluminium Deposition

In the previous section, the angular distribution of the sputtered flux was the default distribution provided by the simulation software To accurately model the deposition process at small diffusion lengths a more precise knowledge of the flux distribution is required to predict the bottom and sidewall coverage In order to get a measure of the angular distribution of the sputtered flux the SIMBAD simulation is used

5.4.1 Using SIMSPUD to Obtain Angular Distributions at Wafer Surface

The SIMSPUD simulation requires process and hardware details to accurately carry out the simulation. The following are the parameters used for the aluminium and titanium simulations:

Parameter	Al	Ti	Units
Binding_E	3.39	4.85	eV
Collect_Size	1	1	cm
Collect_Stop	100,000	100,000	
Gen_Stop	500,000	500,000	
Max_Radius	4	4	cm
Particle_Mass	26.96	47.9	amu
Pressure	2mT	2.4mT	mT
Sigma	50	48	ang2
Sub_Distance	5	5.3	cm
Target_Voltage	400	550	V
Therm_Sigma	60	68	ang2
Thick_Bins	20	20	
Emission_File	altsg.emit	titsg.emit	file
Target_File	al.target	ti.target	file

Table 5.4 *SIMSPUD Simulation Parameters*

The altsge.emit and titsge.emit files contain data on emission angular distributions under ion bombardment. The al.target and ti.target files contain data on the target erosion profile. The resulting angular distributions are shown in figures 5.9 and 5.10.

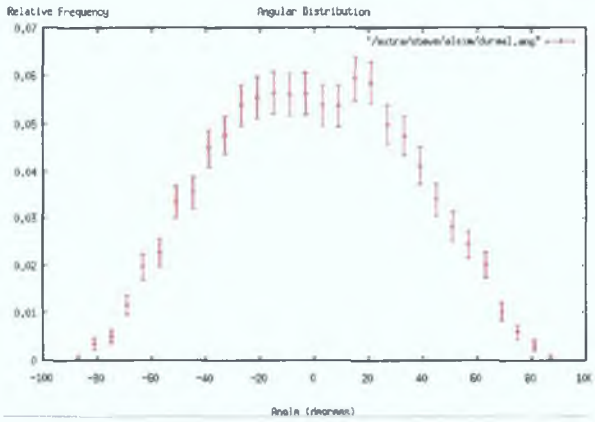

Figure 5.9 *Al Flux Angular Distribution*

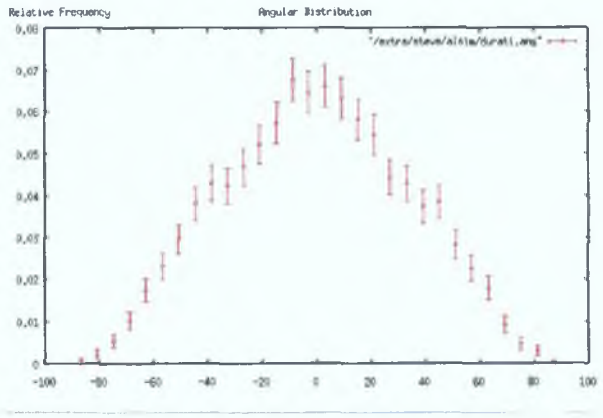

Figure 5.10 *Std Ti Flux Angular Distribution*

Two simulations were also run for the Ti process with a 1:1 collimator inserted between the target and substrate. The collimator parameters are given below and the resulting angular distributions for two different target to wafer spacings are shown in figures 5.11 and 5.12.

Collimate	H	H
Coll_dist	3.5	6
Coll_pitch	1	1
Coll_size	10	10
Coll_thick	1	1
Coll_wall	0.01	0.01
Sub_dist	5.3	8.6

Table 5.4

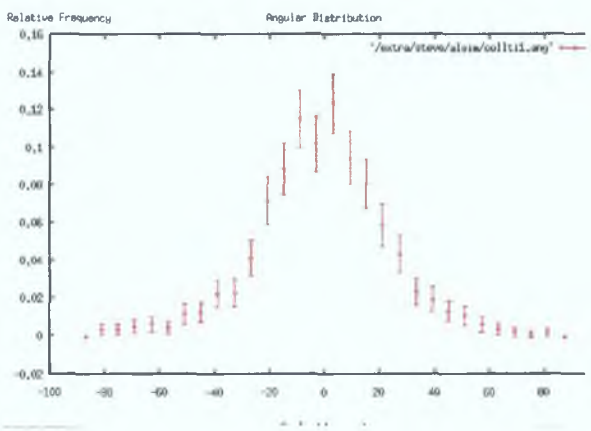

Figure 5.11 *Collimated Ti (1) Flux Angular Distribution*

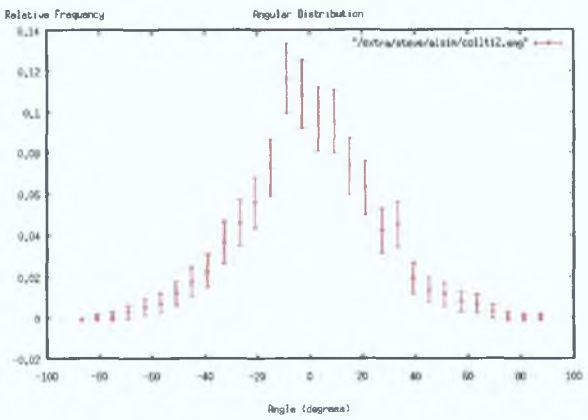

Figure 5.12 *Collimated Ti (2) Flux Angular Distribution*

5.4.2 Simulation of Wetting Layer, Seed Layer and Stack

These angular distributions were then used as inputs to the SIMBAD film growth simulation package and a multi-layer layer film built up. Using this technique of first simulating the wetting and seed layers and then simulating the hot aluminium, it was attempted to mimic the deposition of the Ti/Al/Al stack on a 0.35μm via structure similar to that shown in figure 5.7. The goal is to achieve a void of approximately the same size and shape as the one seen in the SEM cross section. The stack used on that particular wafer was 40nm coherent Ti, 200nm Aluminium at 50°C and 600nm Aluminium at 500°C.

Figures 5.13 and 5.14 show the step coverage for a 0.4μm and a 0.1μm thick standard titanium film. The shadowing at the top of the structure for the thick 0.4μm film affects the bottom and sidewall coverage due to self shadowing.

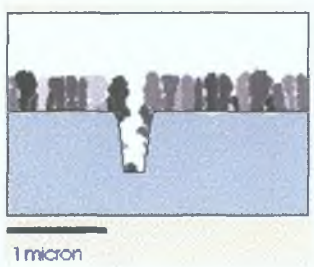

Figure 5.13 *0.4μm Std Ti Film*

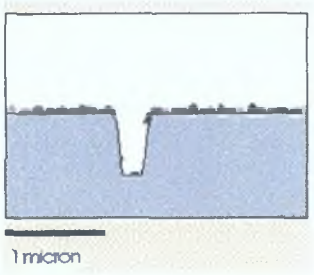

Figure 5.14 *0.1μm Std Ti Film*

Figures 5.15 and 5.16 show the step coverage for a 0.4μm and a 0.1μm collimated (Collimator 2) film(~10%). The effects of self shadowing as the film gets thicker is more severe for the collimated process than for the standard process. This agrees with what is generally observed[97].

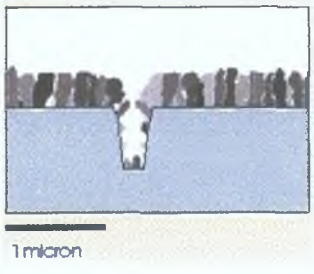

Figure 5.15 *0.4μm Collimated Ti Film*

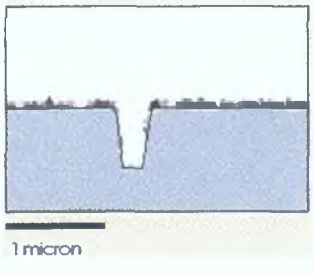

Figure 5.16 *0.1μm Collimated Ti Film*

Figure 5.17 is a picture of the 0.2μm cold aluminium film, again there is a considerable amount of overhang at the mouth of the structure. The resulting Coll-Ti 40nm / Cold Al 200nm stack is shown in figure 5.18. This stack will be the substrate for the hot aluminium deposition.

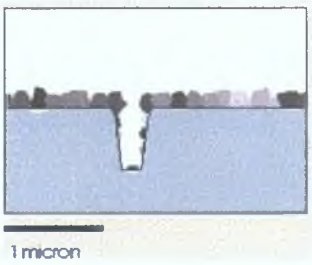

Figure 5.17 0.2μm Cold Aluminium Film

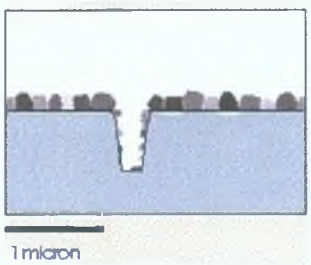

Figure 5.18 Coll-Ti 40nm / Cold Al 200nm Stack

Figure 5.19 is the result of a simulation of the hot aluminium on the collimated Ti/Cold Al stack discussed above. For the hot aluminium simulation the average adatom diffusion length was assumed to be 0.6μm and the angular distribution of the incoming flux of aluminium atoms was assumed to be the same as the cold aluminium flux. For the sake of comparison the simulation of the above aluminium on a bare substrate was also carried out and the results are shown in figure 5.20. The influence of the under-layer on grain size is apparent.

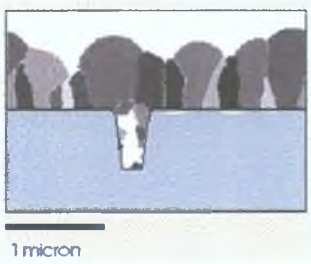

Figure 5.19 Hot Aluminium on Collimated Ti/Cold Al Stack

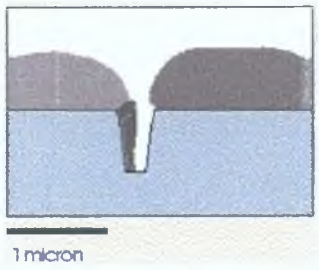

Figure 5.20 *Hot Aluminium on Bare Substrate*

Both the hot aluminium simulations ignored bulk diffusion of the aluminium. At 500°C bulk diffusion may play a significant role in the aluminium fill process. The specific hot aluminium process which is being simulated lasted 34.7 seconds. The hardware used had previously being characterised to look at the real wafer temperature as a function of time in process. After 34.7 seconds the wafer without plasma would not have reached the required 500°C, so for the majority of the deposition time the true wafer temperature is unknown but it is well below the 500°C set point (see appendix E). Nevertheless a certain amount of bulk diffusion is likely to have occurred. This will be the subject of a later study.

5.5 Summary

An aluminium via fill process can be achieved with a wetting layer deposited using a standard and a coherent Ti process. The thickness of the wetting layer has an influence on the extent of the formation of the $TiAl_3$ compound. A low aluminium deposition power / long deposition time is required to fill the via without void formation.

The sputter etch process causes 'rounding' of the top corners of the vias. The extent of this rounding is a function of the sputter etch time.

It can also be concluded from the results of the experiments and from the simulation results that the fill proceeds from top to the bottom when a standard or collimated wetting layer is used. This filling mechanism requires a 'long' time at temperature to allow diffusion of the vacancies to the surface. The simulation results indicate that the

average lateral diffusion length may be reduced due to the surface roughness of the underlayers

Chapter 6 The Ionised Metal PVD Process

6 1 Introduction

The Ionised Physical Vapour Deposition (IPVD) process has already been discussed in earlier chapters and in chapter 3 the film conformality achieved with this process over sub-micron via-type features was studied in detail In that chapter it was determined that the superior film bottom coverage achieved with the IPVD process relative to other PVD processes was due mainly to the tighter angular flux distribution of the flux of sputtered material to the substrate In this chapter the fluxes of materials arriving at the substrate during the IPVD process are studied in more detail It will be shown that predicting IPVD film profiles over sub-micron features is not simply a case of choosing a suitably accurate angular distribution of the sputtered flux, but rather the influences of three separate fluxes need to be taken into consideration, including the a flux of low energy sputtered atoms, high energy sputtered ions and high energy gas atoms Using both experiment and simulation the influences of the various fluxes on film bottom coverage profiles is evaluated

6.2 IPVD Background Discussion

Ionised magnetron sputtering is a variation of the standard magnetron sputtering process where plasma ionisation is increased by adding an inductively coupled rf (RFI) plasma in the region between the cathode and the substrate[98] This denser plasma causes significantly higher ionisation of the metal sputtered flux on transport from the target to the substrate The probability that a sputtered metal atom will be ionised is a function of the plasma density and the energy of the metal atom as it passes through the plasma Sputtered atoms typically have energies of the order of 1 - 10eV The process pressures used for the ionised sputtering process are usually higher than the standard sputtering process, ~30 10^{3} mbar is typical The electron temperatures at this pressure are usually quite low ~ 1 - 2eV The plasma density is of the order of $10^{11}/cm^{3}$ which corresponds to an ion/neutral ratio of ~ 0 1 - 1% A diagram showing the generic set-up is shown in figure 6 1

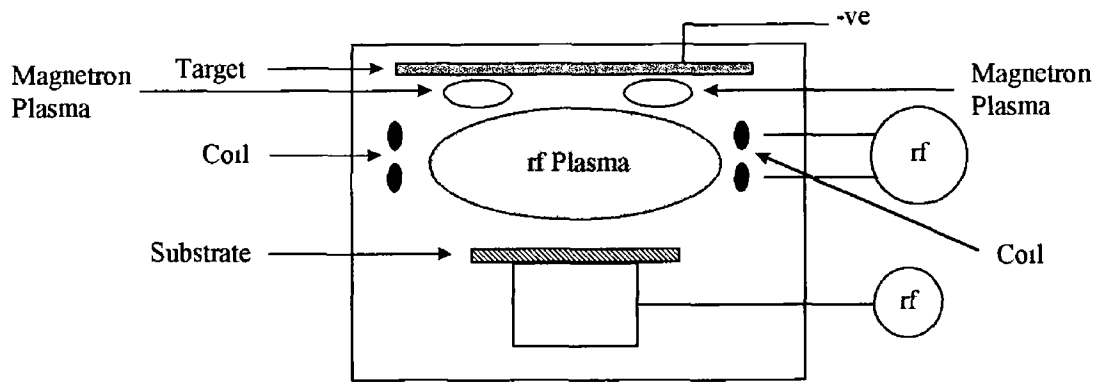

Figure 6 1 *Schematic of IPVD Deposition Chamber*

Power is supplied to the target and the coil and when the plasma is ignited sheaths develop at the target, the coil and on the floating substrate The substrate potential can also be controlled by the addition of a power supply (biased sputtering) The potential developed on the coil is usually enough to result in significant sputtering of the coil Hence the coil is a source of sputtered material to the substrate which influences film deposition rate and uniformity This phenomenon must be taken into account during the system design

The advantage of the ionised process over conventional sputtering is that the directionality of the metal particles can be better controlled which can lead to better step coverage and planarisation over high aspect ratio contacts and vias Secondly, it is easier to get large substrate bias currents with this process which may have benefits for mechanical films

Most of the ionisation events that occur in plasmas are due to electron impact ionisation This is also likely to be the case in the IPVD plasma Particles in plasmas are typically described by their energy distribution functions Figure 6 2 shows a typical energy distribution function for electrons in a discharge The ionisation potentials for argon and a number of metals are included on the graph From the graph it can be seen that the amount of electrons with energies high enough to ionise the metals is significantly larger than that available to ionise the argon This suggests that large

percentages of the sputtered metal flux can be ionised while the overall plasma ion/neutral ratio remains small (typically <1%).

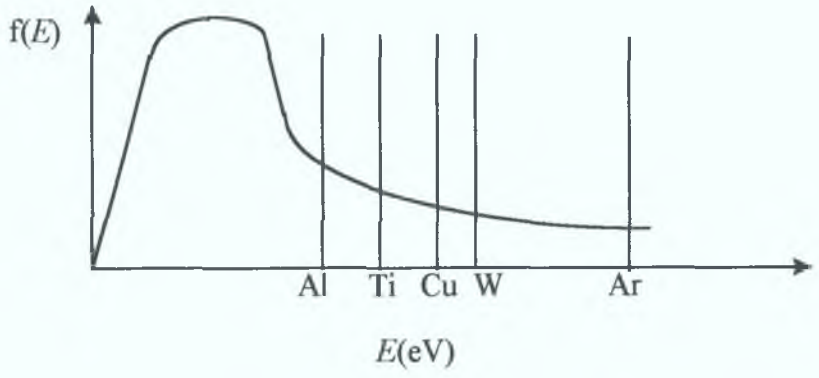

Figure 6.2 *Electron Energy Distribution Function*

Metal	Ionisation Potentials
Aluminium	6.0eV
Titanium	6.8eV
Copper	7.7eV
Tungsten	8.0eV

Table 6.1 *Ionisation Potentials for Commonly Used Metals*

Results presented by Rossnagel and Hopwood[98] show that for a 200W induction power in a 48 10^{-3} mbar argon plasma, up to 80% of the sputtered atoms reaching the substrate are ionised whereas with 0W induction power the percentage of sputtered atoms reaching the substrate ionised is less than 5%. Rossnagel found that the relative ionisation rate increased as a function of the process pressure, ranging from 40% at 13 10^{-3} mbar to 80% at 53 10^{-3} mbar.

It is expected that the probability that a metal atom will be ionised as is passes through a discharge will depend on the energy (speed) of the metal atom and the discharge density. This is true of the IPVD discharge. However, a saturation point exists where, for a given coil power and process pressure, as the density of sputtered material from the target increases the relative amount of ionised material saturates, i.e. the ability of the discharge to ionise the metal saturates when the density of the incoming metal exceeds a certain level. This can be explained by plasma cooling of the electron

temperature in the coil discharge due to the excessive amount of metal atoms in the plasma As the electrons in the plasma cool, the probability of ionisation decreases

From the above it is clear that there are three major particle fluxes bombarding the substrate during the IPVD process

- Sputtered Metal Ions
- Neutral Metal Ions
- Sputter Gas Ions

It is reasonable to assume that each of the above will play a significant role in determining the step coverage of a film deposited over a sub-micron via type feature

In chapter 1 it was shown that a floating substrate immersed in a discharge will acquire a negative potential with respect to the plasma potential, hence a sheath will develop at the substrate surface A sheath will also develop on a substrate immersed in a discharge with an external power supply attached to the substrate to induce a negative discharge Either of the above are typical of an IPVD process In fact, as the floating potential is a function of the plasma density, the potential developed on a substrate during the IPVD process is typically greater than that for any other PVD process with a comparable deposition rate

The presence of the sheath alters the energy and angular distribution of the ionised fluxes impinging on the surface Charged particles are accelerated in the direction of the target surface As the electric field is normal to the substrate surface the ions are accelerated perpendicularly to the surface The kinetic energy of the ions can be controlled by adjusting the relative potential between the plasma and the substrate

6.3 Experiment

The experiment was carried out in an Applied Materials IMP™ IPVD deposition chamber The chamber configuration is similar to that illustrated in figure 6 1 The

target to wafer spacing was set at 140mm and the process pressure was set at 20 10^{3} mbar The substrate bias was controlled via an external rf power supply The wafers used had 0 35μm 3 1 aspect ratio features etched into PECVD oxide

Two IPVD liner films were deposited on the above wafers using the above equipment Details are given in table 6 2

Process	Bias	Pressure	Deposition Rate
Proc1	-50V	15mT	0 5nm/s
Proc2	-100V	15mT	0 5nm/s

Table 6 2 *IPVD Process Details*

After deposition of the IPVD liner, the wafers were then placed in an aluminium deposition chamber and the features were filled with aluminium deposited at 450°C

6 4 Results

After deposition the wafers were cross sectioned and high resolution TEM analysis carried out Photographs of the cross sections are shown in figures 6 3 - 6 6

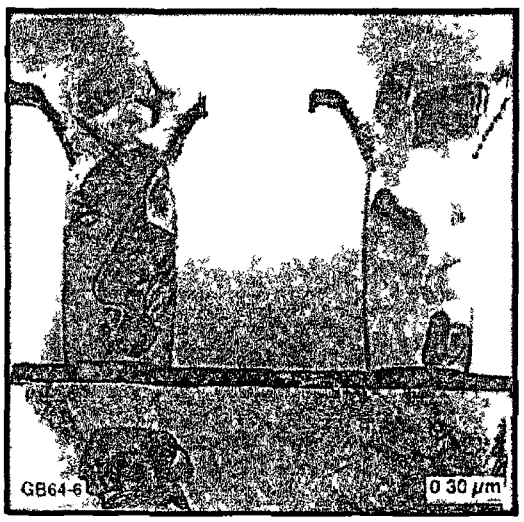

Figure 6 3 *Low Bias IPVD Film*

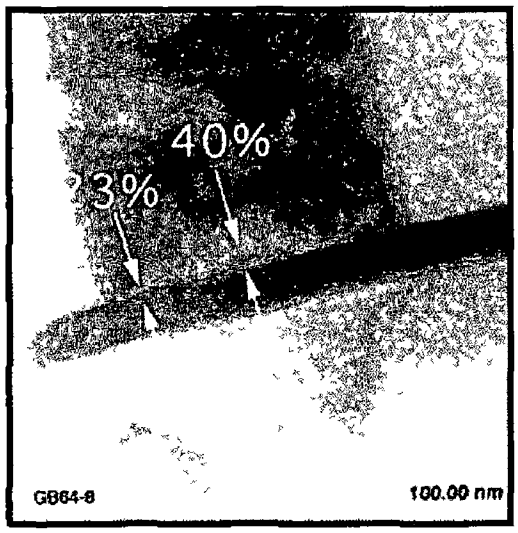

Figure 6 4 *Low Bias IPVD Film Bottom Profile*

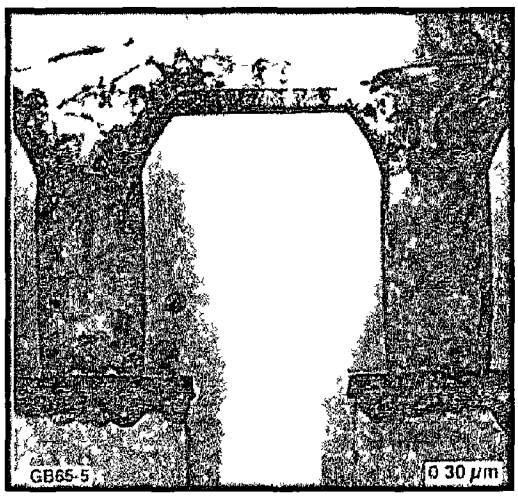

Figure 6 5 *High Bias IPVD Film*

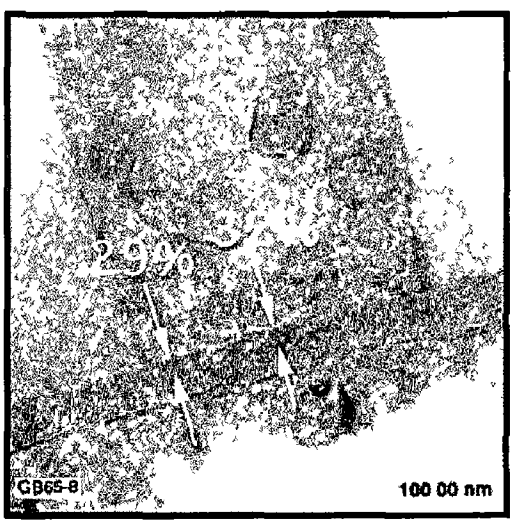

Figure 6 6 *High Bias IPVD Film Bottom Profile*

6 5 Analysis of Results

The results show that the film at the bottom of the feature deposited using the low bias process is non-uniform, with the film being thicker at the centre than at the edge The high bias process has a more uniform bottom coverage

The differences in the bottom coverage can be explained by two processes

a) The higher wafer bias forces the ionised metal atoms to be more normal to the surface than the lower bias

b) The higher bias induces more re-sputtering of the deposited film at the bottom of the feature

To determine an estimate of the effects of the electric field on the directionality of the ions the following analysis was carried out[99]

Consider a particle with velocity V_0 entering the sheath electric field In two dimensions the velocity can be separated into x and y components

$$V_x = V_0 \sin\theta \quad (1)$$

$$V_y = V_0 \cos\theta \quad (2)$$

Where θ is the angle at which the particle enters the sheath relative to the normal The sheath potential drop is along the y-axis so particles entering the sheath will have the V_y component of their velocity accelerated but the V_x component remains constant (assuming no collisions in the sheath)

The motion of the particle in the y-direction can be described by the equation for a uniformly accelerated body

$$y = y_0 + At + Bt^2 \qquad (3)$$

where y_0 is the initial position on the y-axis, and t is a measure of the time the particle has been in the sheath

$$A = V_0 \cos\theta \quad (4)$$

$$B = \frac{qE}{2my_0} \qquad (5)$$

where q is the particle charge (1 6*10 ^{19}C), m is the mass of the particle and E is the sheath potential The sheath thickness is given by y_0

At $t = 0$, the position of the particle is defined as $(0, y_0)$

Define the time it takes the particle to traverse the sheath as t_{fin} At $t = t_{fin}$ the particle position is $(x_{fin}, 0)$

From equation 3 at $t = t_{fin}$ and $y = 0$

$$0 = y_0 + At_{fin} + Bt_{fin}^2 \quad (6)$$

t_{fin} can then be found from

$$t_{fin} = \frac{-A - \sqrt{A^2 - 4By_0}}{2B} \qquad (7)$$

Knowing the relationship between t_{fin} and x_{fin},

$$x_{fin} = V_0(\sin\theta)t_{fin} \qquad (8)$$

It is now possible to calculate x_{fin} from t_{fin} Replacing t in equation 3 with x gives

$$y = y_0 + Dx + Cx^2 \qquad (9)$$

where

$$D = \cot\theta \qquad (10)$$

$$C = \frac{B}{V_0^2 \sin^2\theta} \qquad (11)$$

Differentiating equation 9 at x_{fin} gives the slope of the line at that point

$$\frac{dy}{dx} = D + 2Cx_{fin} \qquad (12)$$

the derivative is the tan of the impact angle, hence the impact angle γ can be found

To calculate the trajectory of a particle the particle charge q, mass m, energy E and initial angle θ need to be known Also the sheath voltage and sheath thickness need to be known Normally for a given process the sheath voltage can be measured but the sheath thickness needs to be calculated If the plasma debye length is known the sheath thickness is approximately ten times the debye length[100] The debye length is given by the equation

$$\lambda_D = \sqrt{\frac{\varepsilon_0 kT_e}{n_0 e^2}} \approx 743\sqrt{\frac{T_e(Volts)}{n_e(cm^{-3})}}$$

For the IPVD plasma with a typical plasma density of $10^{11}/cm^3$ and an electron temperature of the order of 2-5eV, the debye length is of the order of 100 - 160μm which indicates a sheath thickness of the order of 1 to 2 mm

The above equations were used to calculate the impact angle as a function of substrate bias. For a sheath thickness of 1.5mm and a particle energy of 0.1eV, the impact angle for an argon ion was calculated for various bias voltages. The results are tabulated in table 6.3 and presented in figure 6.7.

Sheath Voltage	Impact Angle (degrees)
50V	87.441
100V	88.190
150V	88.522
103V	89.427
105V	89.943

Table 6.3 *Impact Angle vs. Sheath Voltage*

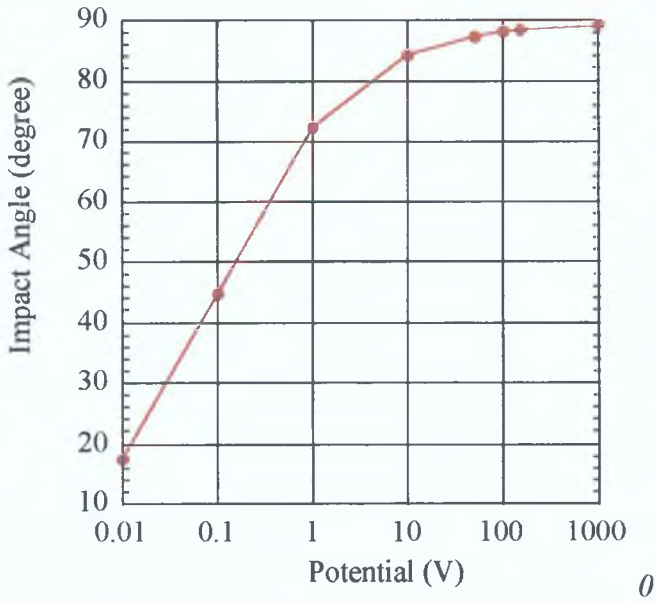

Figure 6.7 *Impact Angle of Argon Ion*

From the results of the motion of a particle in an electric field analysis it can be concluded that all of the charged particles that enter sheath are directed to an angle +/- 3° from the surface normal. For argon ions the difference between a sheath voltage of -50V and -100V translates to an angle difference of only 0.75°. From this it can be concluded that different bottom coverage profiles between the low bias and high bias processes is not likely to be due to increased directionality of the metal ions.

The only other possible explanation is re-sputtering of the material at the bottom of the feature during deposition due to ion bombardment. Re-sputtering can occur due to the bombardment by both metal and gas ions, however as the gas density is likely to be greater than the metal ion density, most of the re-sputtering is likely to be due to gas ion bombardment. The greater the potential drop across the sheath, the greater the energy of the ions when they reach the substrate surface. It was shown in chapter 1 that the sputter yield is a strong function of bombarding particle energy, therefore more re-sputtering during the high bias process is expected.

To investigate the influences or the relative flux concentrations to the substrate the SIMBAD film growth simulation was used. SIMBAD has recently been extended to account for the effects of an ion flux bombarding the film during growth[101]. This extension involved the addition of ion disks, each representing a statistical average of a large number of physical ions. These disks are launched at a specified rate and with a defined angular distribution just above the film surface. These disks may:

a) Reflect
b) Cause film re-sputtering
c) Cause local surface diffusion

The likelihood of any of the above occurring depends on the reflection probability, the angle of incidence and the energy deposited per ion. Ion reflection was based on calculations by Hou[102] using MARLOWE[103] to estimate the reflection probabilities of argon ions from copper. The probability that a re-sputtering event will occur is determined by the sputter yield which is a function of the material being bombarded, the incident ion, the ion energy and the angle of incidence[104]. The sputter yield as a function of impact angle needs to be inputted by the user to the simulation software. The angular distribution of the re-sputtered flux was calculated by approximating experimental data for argon sputtering of several metals [105][106].

As explained earlier there are two separate fluxes of sputtered material impinging on the substrate during the IPVD process; the low-energy neutral flux which has undergone collisions with the background gas and the high energy, highly directional

ionised flux which is accelerated by the sheath electric field towards the substrate surface. To model this situation using SIMBAD it is necessary to treat these fluxes as separate entities. The SIMBAD simulation allows the inclusion of a second depositing flux which is normally used for modelling co-sputtering processes[107]. For each flux an angular distribution needs to be defined and the relative intensities of each need to be set. The angular distribution of the neutral flux was easily calculated using the SIMSPUD simulation package and the ionised flux angular distribution was assumed to vary by +/- 3° from the normal. The flux distributions are shown in figures 6.8 and 6.9.

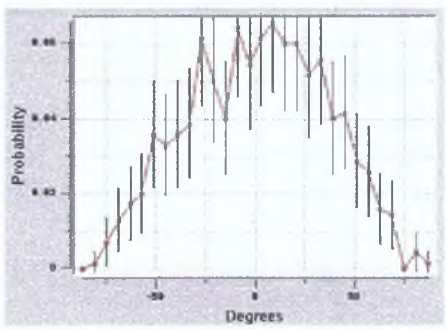

Figure 6.8 *Angular Distribution of 20 10^{-3} mbar Neutral Flux*

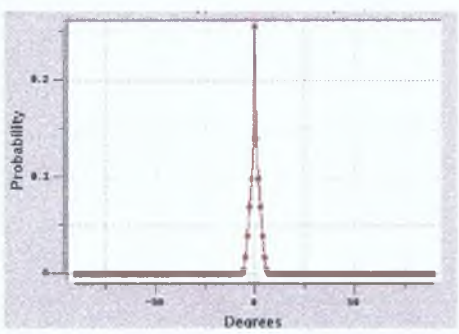

Figure 6.9 *Angular Distribution of Ionised Flux*

The relative intensities of the ionised and neutral fluxes is an unknown. Calculating this ratio is difficult as an accurate description of the plasma is not available. For this reason three separate simulations were run with varying ionised flux - neutral flux ratios. The results are shown in figures 6.10 - 6.12. From the work carried out in chapter 3 it is known that the bottom coverage of the ionised PVD process for a 3:1 aspect ratio feature is approximately 50%. The film shown in figure 6.10, which has

the 1:1 flux ratio also has a bottom coverage of 50% so it can be assumed that the ratio of ionised material to neutral is approximately 1:1.

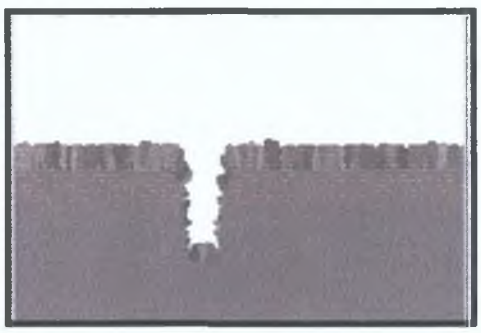

Figure 6.10 *(Flux 1) /(Flux 2) = 1:1*

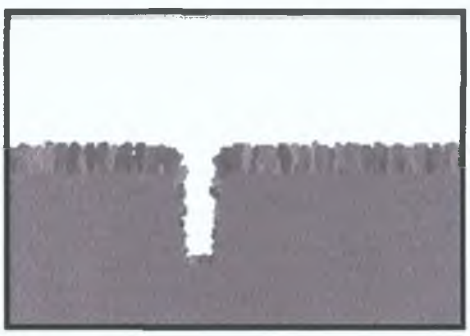

Figure 6.11 *(Flux 1)/(Flux 2) = 9:1*

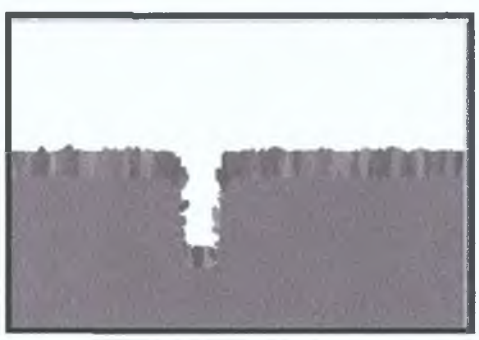

Figure 6.12 *(Flux 1)/(Flux 2) = 1:9*

As well as the two depositing fluxes the SIMBAD simulation also allows the inclusion of a separate ion flux. The ion flux was assumed to approach the substrate at an angle +/- 1° from the normal. The yield as a function of incident angle is shown in figure 6.13. This data is for a 600eV beam of argon ions on titanium so this sputter yield is likely to be higher than the true sputter yield by a factor of approximately 4. This needs

to be taken into account when interpreting the results as a function of the flux ratios As the film shown in figure 6 10 most accurately represents the profile of the unbiased IPVD process, the process conditions simulated for that film were used for the biased IPVD simulations The relative amount of ion bombardment was varied as shown in figures 6 14 - 6 16 The simulation results clearly show the effects of re-deposition from the bottom to the sidewall

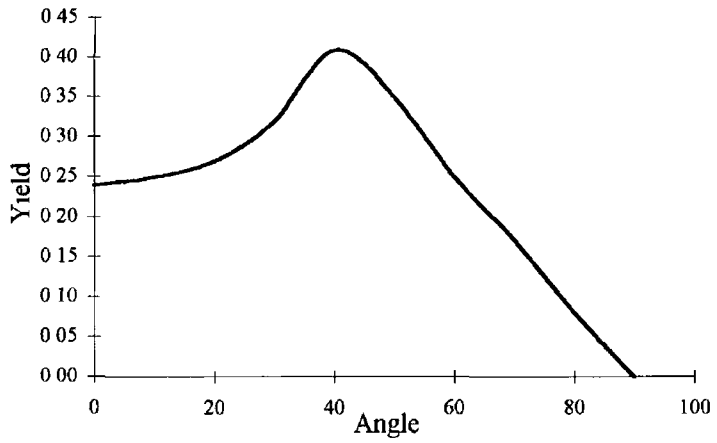

Figure 6 13 *Angular Dependence of Substrate Sputter Yield*

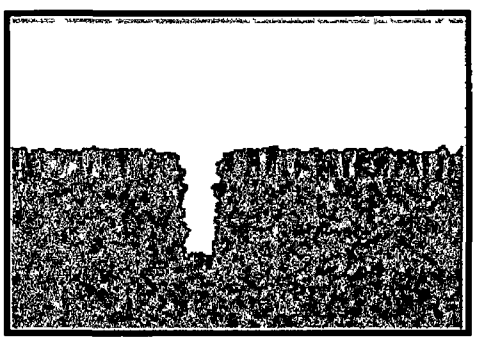

Figure 6 14 *(Flux 1)/(Flux 2) = 0 5 0 5 (1 1) Ion Flux 0 1*

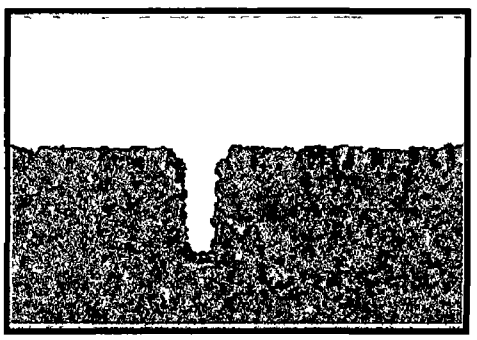

Figure 6 15 *(Flux 1)/(Flux 2) = 0 5 0 5 (1 1) Ion Flux 0 5*

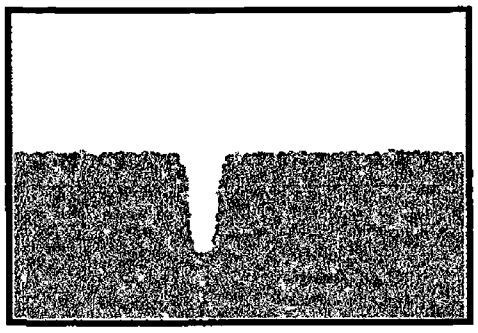

Figure 6 16 (Flux 1)/(Flux 2) = 0 5 0 5 (1 1) Ion Flux 0 9

6 6 Summary

From the above experiments and simulations two conclusions can be drawn

a) Higher bias does not significantly better align the ionised flux once the bias is above a certain threshold (~50V)

b) The higher the substrate bias the greater the amount of re-sputtering at the bottom of the feature This re-sputtering redistributes the material at the bottom of the feature onto the lower sidewalls and the edges of the bottom surface

Chapter 7 Conclusions

This work has examined the PVD-sputtering process and a number of its extensions in detail The work is primarily concerned with the sputtering process in the context of the semiconductor fabrication industry where sputter processes are used to coat and fill sub-micron size high aspect ratio features with metals and metal compounds

The first conclusion that can be drawn from this work is that process simulations can greatly assist in equipment design, process design and process optimisation The SPUTSIM simulation package developed at DCU was simple, fast, easy to use and it provided accurate descriptions of particle fluxes to surfaces during the sputter process Simulation packages such as SPUTSIM can easily be applied to macroscopic as well as microscopic situations For example in chapter 2 SPUTSIM was used to examine thin film uniformity over a substrate with dimensions of the order of centimetres whereas in chapter 3 it was used to examine film conformality over sub-micron features

However, SPUTSIM is only useful in predicting film conformality when events happening at the film surface are such that self shadowing of the growing film and diffusion effects can be neglected When surface-adatom interactions or activity are significant, simply predicting particle fluxes will not yield much information, particularly when dealing with features of the order of a micron

Commercial simulation packages such as SIMBAD tend to divide the modelling task into two parts the process scale model and the feature scale model (the film growth model) The SPUTSIM simulation is based on a process scale model When modelling and simulating complex processes such as the hot aluminium deposition process, where surface and bulk diffusion processes take place to a significant degree, or when modelling the bias sputtering process where ion bombardment of the growing film induces significant re-sputtering and re-deposition of the growing film, the SIMBAD thin film growth simulation package was used SIMBAD, when properly calibrated, agreed with experimental results up to the point where chemical reactions between the growing film and the substrate became significant It was shown in chapters 4 and 5 that in the case of hot aluminium deposition on a titanium wetting layer the reaction

between the titanium and the aluminium rendered the simulation results invalid. The SIMBAD simulation was found to be of enormous benefit in predicting fill evolution on an ideal surface, where surface diffusion of the adatoms and the film contact angle dominated the feature fill process. From the simulation results it can be concluded that it is possible to fill deep sub-micron features from bottom to top by maximising the diffusion length of the sputtered adatoms and minimising the film-substrate contact angle. This fact was utilised in designing a fill process for 0.25μm 3:1 aspect ratio features which fills the features from bottom to top. This is the first time such a feat has been reported for features of this size using a standard PVD-sputtering process. The combination of wetting layer, seed layer, barrier-isolation layer and aluminium deposition rate influences the fill mechanism and needs to be taken into consideration when designing a fill process. From the results presented in chapters 4 and 5 it can also be concluded that the presence of a TiN isolation layer is beneficial for the fill process. Presumably the TiN isolates the wetting layer from the oxide which may outgas impurities, thus preserving the good wetting characteristics of the titanium wetting layer.

Electrical results comparing the traditional W-plug approach to feature fill to the new Al-Plug approach showed the much superior via resistances of the Al-plugs. The fact that the electrical measurements were carried out on chains of 10^6 vias demonstrate the repeatability of the process.

In this work the fill process simulations ignored the effects of bulk diffusion of the deposited material. This is due to the fact that the bulk diffusion process is poorly modelled by SIMBAD and no other suitable simulation package currently exists. A more through study of the bulk diffusion mechanism would complement the work undertaken in this present study.

Over the next few years aluminium based metallisation schemes will be replaced by copper metallisation schemes. For this reason it would be interesting and important to extend this work to examine copper fill processes of high as aspect ratio features. The evolution of copper fill using PVD, CVD and electroplating techniques is an area of

study that will gain increasing importance over the coming years. Of immediate importance is the evolution of electroplated copper films on various seed-layer / barrier combinations.

The suitability of PVD based processes for depositing diffusion layers, wetting layers, seed layers and W-plug liners etc. was addressed in chapter 3. Through a series of simulations and experiments it was concluded that for modern deep-sub-micron feature sizes the standard magnetron sputtering process is not adequate. The limitations of standard sputtering is due to the poor sidewall and bottom coverage at high (>2.5:1) aspect ratio features. The film overhang at feature openings tends also to be excessive for the standard process.

From the experimental and theoretical results comparing standard, collimated and ionised sputtering it can be concluded that the ionised sputtering process will be the process of choice for the future in semiconductor manufacturing. The ionised sputtering process can be manipulated to achieve the required bottom and sidewall coverage while maintaining acceptable levels of film overhang. Semiconductor fabrication technology is currently undergoing a transition from aluminium based metallisation schemes to copper based metallisation schemes for 0.25μm, 0.18μm, 0.15μm technologies and beyond. At time of writing ionised sputtering is the technology of choice for the vast majority of semiconductor manufacturers for depositing diffusion barriers (Ta/TaN) and Cu seed layers for their metallisation processes.

Chapter 6 studies the ionised sputtering process in detail and examines the effects of the various fluxes bombarding the substrate during film growth. The results of theoretical calculations show that the effects of wafer bias on ion bombardment is not so much an increased directionality of the ions but rather an increased level of re-sputtering of the growing film. This ability of ionised sputtering to re-sputter material deposited at the bottom of high aspect ratio features onto the lower sidewalls is a major advantage of this process over other directional processes such as collimated sputtering. Normally the lower sidewalls is a weak point where barrier integrity is most

vulnerable By re-depositing material on the lower sidewall, the film thickness and consequent barrier strength is increased

In this study the analysis of the ionised sputtering process relied on certain assumptions such as the plasma density, sheath thickness etc It would be better to get such parameters from an accurate process scale model of the process However, modelling the ionised sputtering process is a significant challenge The major difficulty is the lack of collision cross section data especially for aluminium and titanium However the knowledge base for copper is quite well characterised on account of past interest in copper vapour lasers[110][111] Therefore it may be possible to model the ionised copper sputtering process with an acceptable degree of accuracy With copper metallisation gaining more interest and the ionised copper sputtering process the current process of choice for depositing seed layers for electroplating over high aspect ratio features, it would be interesting to extend the work in chapters 2, 3 and 6 to develop a model and simulation of the ionised copper sputtering process

Appendix A The Reactive Sputtering Process

Reactive sputter deposition is used to deposit compound films such as nitrides or oxides A metal, alloy or compound target is sputtered in a plasma consisting of an inert gas such as argon and a reactive gas such as nitrogen The reactive gas particles react with the sputtered atoms to form the compound film on any surface exposed to the flux of sputtered particles and the reactive gas, including the target Using this process a wide variety of films and film properties can be synthesised As in any deposition process, the film properties will be a function of the process parameters Film stoichiometry is a measure of the ratio of the major film components to one another Film stoichiometry is a function of numerous process parameters, including target-substrate separation, the ratio of reactive gas to inert gas in the plasma, process pressure, substrate temperature, system / substrate geometry, discharge power and target material / sputtering gas interaction

The reactive sputter process has two modes of operation, the metallic mode and the poisoned mode Depending on the reactive gas pressure and the deposition power, the target surface can either be a ' clean ' metal surface or it can be covered in the compound material being deposited This 'clean' metal surface is called the metallic mode of operation and the covered target surface is called the poisoned mode of operation In general the metallic mode yields higher deposition rates than the poisoned mode due to the fact that the compound film typically has a lower sputter yield than the target metal For a fixed ion flux to the target, as the reactive gas partial pressure is varied (i e reactive gas flux to the target is varied), there is a transition from the metallic to the poisoned mode Similarly, for a poisoned target as the reactive gas partial pressure is reduced there is a transition from the poisoned to the metallic mode of operation However, this transition exhibits hysteresis as the transition flux for increasing the flux to pass from metallic to the poisoned mode is higher than the transition flux from the poisoned to the metallic This hysteresis effect is illustrated in figure A 1 The hysteresis curve in this example is for TiN

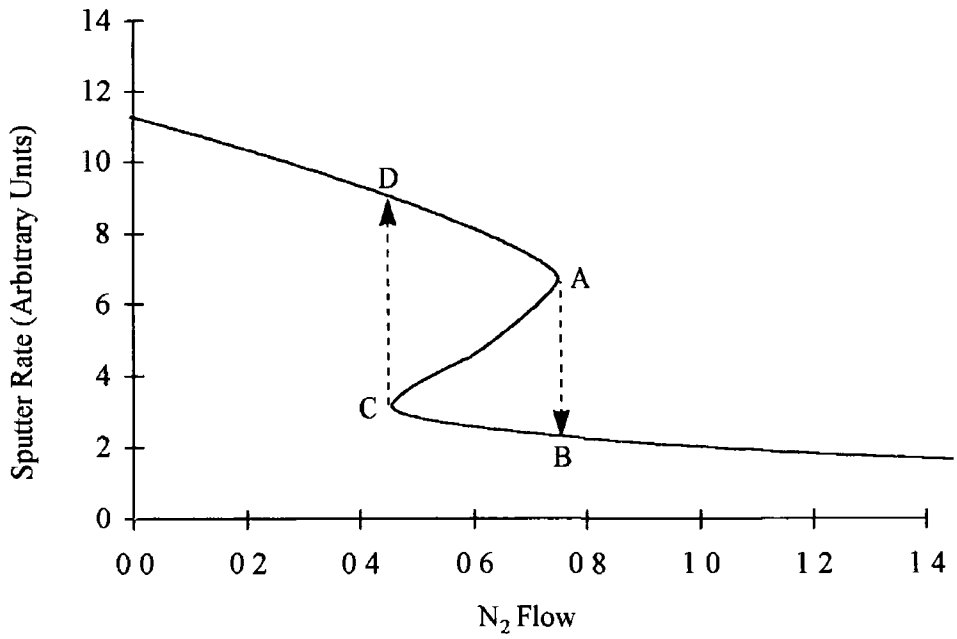

Figure A 1

The hysteresis effect can also be seen from the target voltage, current and process pressure

This hysteresis effect has been explained in a model presented by Berg et al[107][108][109]

Let A_t and A_s be the target and substrate surface areas, θ_t and θ_s be the fractions of the target and substrate areas covered by the compound film and s_m and s_c be the sputter yields of the metal and compound from the target In steady state conditions the rate of formation of the compound on the target must equal the sputtering rate of the compound from the target Define R_i and R_r as the incident ion and reactive gas molecule fluxes and let k_r be the sticking coefficient of a reactive gas molecule to the target The rate of change of target poisoning is then given by

$$n_t d\theta_t/dt = iR_r k_r(1-\theta_t) - R_i s_c \theta_t = 0 \qquad (1)$$

i is the number of atoms in the reactive gas molecule

θ_s has already been defined as the fraction of the substrate surface area covered by the compound film This fraction can be increased as

a) Reactive gas molecules are incident on the metallic parts of the target and substrate $(1-\theta_s)$

b) A fraction of the flux $(1-\theta_s)$ sputtered from the target is deposited on the metallic part of the substrate

The fraction θ_s is decreased because a fraction of the metal-atom flux θ_s from the target is deposited on the compound part of the substrate

From these relationships the rate of change of substrate compound coverage can be described by the equation

$$n_s d\theta_s/dt = iR_r s_r(1-\theta_s) + R_i k_c \theta_t (A_t/A_s)(1-\theta_s) - R_i k_m (1-\theta_t)(A_t/A_s)\theta_s = 0 \quad (2)$$

The total number of reactive gas molecules per second that are consumed to form the compound deposited on the substrate is given by the equation

$$dN_r/dt = R_{rsr}[(1-\theta_t)A_t + (1-\theta_s)A_s] \qquad (3)$$

The flux of material sputtered from the target can be expressed by the equation

$$R_{sput} = R_i[k_m(1-\theta_t) + k_c\theta_t] \qquad (4)$$

Equations 1 and 2 can be simultaneously solved to determine the compound coverages θ_t and θ_s on the target and substrate as a function of the fluxes, rate constants, and areas

The number of gas molecules consumed and the sputtering flux can then be evaluated to exhibit the hysteresis behaviour of the system

Appendix B Initial Sputter Flux Energy Generation

```
#include <stdio.h>
#include <math.h>
#include <graphics.h>
float rng( void ),

/*****************************************************************
*                                                                *
*       This program generates a file of random data with a      *
*       distribution based on the Thompson distribution function *
*       It uses a random variate generation method based on      *
*       rejection                                                *
*       output files  sputen.dat, sgrf.dat                       *
*                                                                *
*****************************************************************/


int colour, driver, mode,
int col, bkcol,
float Eb, E, X, Y,
/*float array[10000], */
FILE *fp, *fd, *fp2,
float temp,

main()
{
int i, j,
int npart1, datarr[50],
double total = 0,
double average = 0,
        fp = fopen("sputen.dat","w+"),
        fp2 = fopen("sgrf.dat","w+"),
        Eb = 4.85,                              /* Titanium */
        npart1 = 0,
        for (i=0,i<40,i++)
        {
                datarr[i] = 0,
        }

        /************** Rejection Algorithm ******************/

        while (npart1<30000)
        {
                E = 40*rng(),
                if ( E <= Eb ) { X = E/Eb, }
                if ( E > Eb ) { X = pow(E,-3/2), }
                Y = rng(),
                if ( Y < X )
                {
                        /* accept */
                        fprintf(fp, "%f\n",E),
                        total = total+E,
                        npart1++,
                        for(j=0,j<40,j++)
                        {
                        if ( ( E > j)&&( E <j+1) )
```

```
                    {
                        datarr[j] = datarr[j]+1,
                    }
                    }

                }
        }


         for (i=0,i<40,i++)
         {
        printf(" %i ", datarr[i]),
        fprintf(fp2,"%i\n",datarr[ i],
         }
         printf("\n"),

         average = total/npart1,
         printf("\n average energy = %f \n",average),
         getche(),

}
float rng()
                {
                float register random,
                static unsigned long x = 1, y = 1, z = 1,
                        x = (171*x)%30269,
                        y = (172*y)%30307,
                        z = (170*z)%30323,
                        random = x/30269 0 + y/30307 0 + z/30323 0,
                        /* Discard value (max=2) to left of decimal point */
                        while (random > 1 0)
                                random -= 1 0,
                        return random,
                }
```

Appendix C Derivation of Mean Free Path (mfp)

Assume that a molecule is moving with a constant speed v and that all other molecules are at rest

Assume the molecules are spheres of diameter d A collision will take place if the molecules come within a distance d of each other

For ease of computation, consider the molecule to have a diameter d and all other molecules to be points

As the molecule moves through space it sweeps out a cylinder with cross-sectional area πd^2

In a time interval Δt, the molecule moves a distance $v\Delta t$ The volume of space swept by the particle in a time Δt is given by

$$(\pi d^2)\ (v\Delta t)$$

Let N be the number of molecules / unit volume The number of collisions that occur in time Δt is then given by

$$N\ (\pi d^2)\ (v\Delta t)$$

So the mfp λ, is equal to the length of the path divided by the number of collisions

Assuming the other particles are stationary,

$$\lambda = \frac{1}{\pi N d^2}$$

$$N = \frac{nN_A}{V}$$

where

N_A = Avogadro's constant

V = volume occupied by one mole

n = number of molecules in a mole

But from the Ideal Gas Law

$$V = \frac{nRT}{P}$$

$$N = \frac{nN_A}{\left(\frac{nRT}{P}\right)} = \frac{N_A P}{RT}$$

where R = gas constant

So,

$$\lambda = \frac{RT}{\pi d^2 N_A P} = \frac{KT}{\pi P d^2}$$

where K is Boltzmann's Constant

$$K = \frac{R}{N_A}$$

$$\lambda = \frac{KT}{P}\frac{1}{\sigma}$$

where σ is the collision cross section (πd^2)

Appendix D Bottom Coverage Calculation

The following is an example where the bottom coverage associated with a complex angular distribution is interpreted from the uniform distribution results presented in chapter 3.

The angular distribution of the sputtered material to a substrate surface for a sputter process with a 1:1 aspect ratio collimator was obtained by simulating the process. The resulting angular distribution is shown in figure D-1.

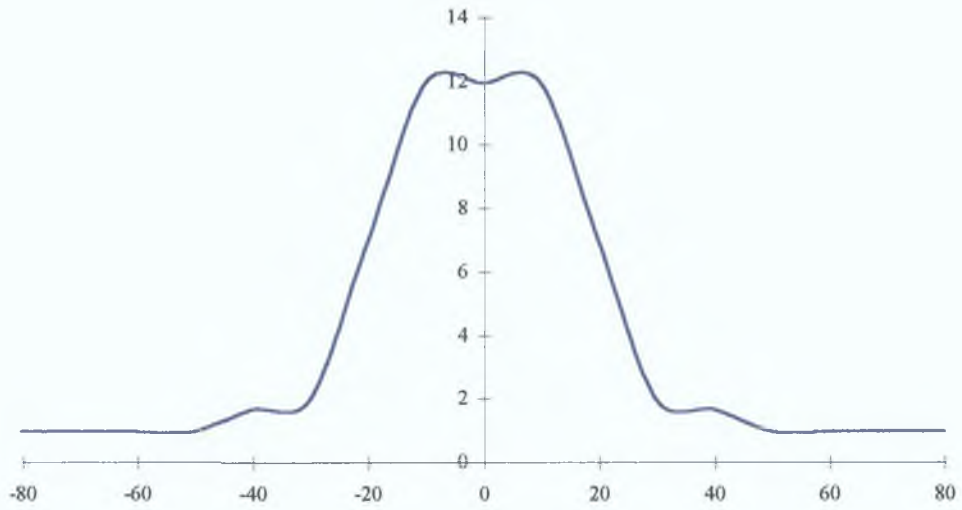

Figure D-1 *Angular Distribution of 1:1 Collimated Process*

From chapter 3 the equation for bottom coverage is

$$BC = \sum_{i=1}^{N} f(\theta_i) * \frac{2\theta_i h_i}{A_c}$$

Where, $A_c = \sum_{i=1}^{N} 2\theta_i h_i$, N, θ_i, h_i are as defined in chapter 3.

Fit four rectangles to the curve at $\theta = 10°$, $20°$, $40°$ and $60°$.

For a 3:1 aspect ratio feature the bottom coverage is given by the equation

Average Bottom Coverage, $ABC = 5\ 36\ \theta^{0\ 86}$ where $\theta > 9\ 46^{o}$

$ABC = 1$ where $\theta <= 9\ 46^{o}$

The data is summarised in table D-1

i	*q*	*h*	*f(q)* (Average Bottom Coverage)
1	10	4	0 73
2	20	6	0 40
3	40	1	0 22
4	60	1	0 15

Table D-1

Entering this data into the equation for bottom coverage yields a bottom coverage of 0 38 (i e 38%) This result is very comparable to the measured collimated bottom coverage of 30% 7

Appendix E True Wafer Temperature During Deposition

During deposition of the aluminium films in the experiments detailed in this work, the wafer was clamped to a heated surface The temperature of the heater surface is kept at a specified temperature by measuring the temperature using a thermometer and continuously adjusting the input power to the resistive heater to keep the temperature constant (a feedback control loop) In order to thermally couple the wafer to the heater a portion of the process gas was directed between the wafer and the heater

The pressure behind the wafer is in the regime where argon has high thermal conductivity (4- 8torr) Good thermal coupling is necessary to keep the wafer temperature constant during deposition External heat sources including the heat of condensation, kinetic energy of neutrals, secondary electron bombardment and bombardment of energetic ions tend to heat up the wafer beyond its set-point if thermal coupling is not adequate

Figure E-1 plots the true wafer temperature as a function of time From the graph two important points should be noted

a) It takes the wafer approximately 15 seconds to reach temperature from the time the backside gas is turned on

b) Even when well thermally coupled, the true wafer temperature exceeds the set-point due to the various heat sources associated with the sputter process

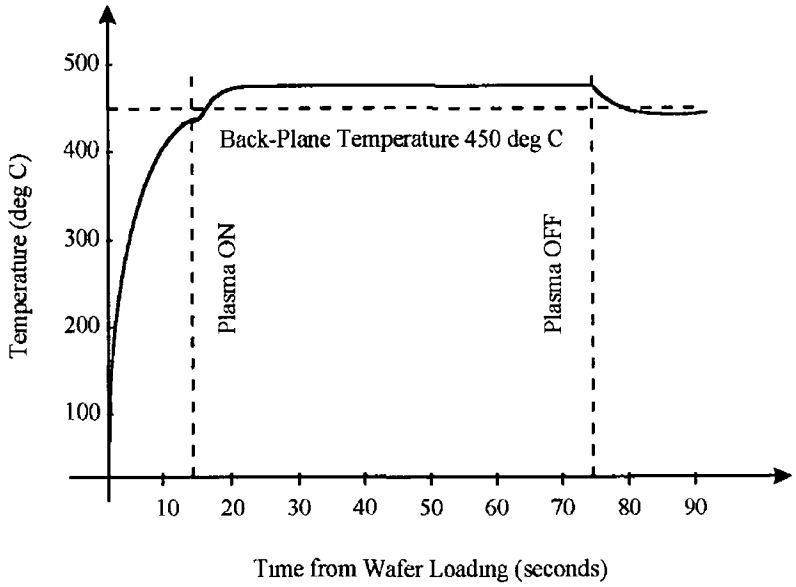

Figure E 1 *Wafer Temperature During Deposition Cycle Eclipse System*

References

1. S. M. Rossnagel, D. Mikalsen, H. Kinoshita, J. J. Cuomo, J. Vac. Sci. Technol. A 9, 261 (1991)
2. S. M. Rossnagel, J. Hopwood, J. Vac. Sci. Technol. B 12(1), 1994
3. H. C. Cheng in ULSI Technology, McGraw-Hill, New York, 1996 ed C.Y. Chang, S. M. Sze, pp 240 - 247
4. European Semiconductor, Feb 1998 pg 11-12
5. P. Van Zant in 'Microchip Fabrication', McGraw-Hill New York 1990, pp340-344
6. R. Glang in 'Handbook of of Thin Film Technology', L. Maissel and R. Glang ed., McGraw-Hill, New York 1970, pp 1-3 to 1-130
7. P. Van Zant in 'Microchip Fabrication', McGraw-Hill New York 1990, pp340; pp320-322
8. Z. Luo, W. Wu, Q. Hou, J.Appl.Phys., 75(8), pp 3789 - 3797 (1994)
9. H.D. Hogstrom in Ínelastic Ion Surface Collisions', ed. N.H. Tolk, J. C. Tully, W. Heiland, C. W. White, Academic Press New York 1977
10. E.W.McDaniel, Çollision Phenomena in Ionised Gases', Wiley, New York, 1964 pp 630 - 635
11. E.V. Kornelsen, Can. J. Phys. 42 364 (1964)
12. P. Blank, K. Wittmaack, J. Appl. Phys, 50, 1519, (1979)
13. S. Wolf, R. N. Tauber in 'Silicon Processing for the VLSI ERA', Vol 1, Lattice Press (1986), pp 342-343
14. P. Sigmund, Phys. Rev. 184, 383 (1969)
15. H. Fetz, Zeits .f. Phys. 119, 590, (1942)
16. G. Carter, J. S. Colligon, Ion Bombardment of Solids, Heinemann Educational Books, 1968 pp 318-319
17. M. A. Lieberman, A. J. Lichtenberg, Principles of Plasma Discharges and Materials Processing, Wiley, New York pg 523
18. H. F. Winters, J. W. Coburn , Surface Sci. Rep. 14, 161, 1992
19. K. Wasa, S. Hayakawa, Handbook of Sputter Deposition Technology, Noyes New Jersey (1995), pg. 68

20 G K Werner, J App Phys 26 1056 (1955)

21 E Wickersham, J Vac Sci Technol A 5 (4) 1987

22 I Shah in 'Handbook of Thin Film Process Technology', 1995 I O P Publishing Ltd, pp A3 0 4

23 B Chapman, Glow Discharge Processes, Wiley, New York, 1980 pp 65 - 70

24 F Chen, 'Plasma Diagnostic Techniques', R H Huddlestone, S L Leonard eds, Academic Press, New York 1965 pp 113

25 H R Koenig, L I Maissel, IBM J Res Devel 14, 168, (1970)

26 S M Rossnagel, J Vac Sci Technol A 6(2) Mar/Apr 1988

27 B Window, N Savvides, J Vac Sci Techn A 4 (3), May/Jun 1986

28 N Broughton, M J Brett, S K Dew, G Este, IEEE Trans Semi Manuf Vol 9, No 1, Feb 1996

29 A Belkind, Z Orban, J Vac Sci Technol A 11(3) May/Jun 1993, pp 642-646

30 B A Movchan, S V Demchishin, Fiz Met Metalloved 28, 653 (1969)

31 J A Thornton, Annual Rev Mater Sci 7, 239 (1977)

32 T Guo, L Chen, M Naik, Applied Materials HP PVD Update, April 1997 Vol 4, No 1 pg 6

33 B Zhao, S Q Wang, S Anderson, R Lam, M Fiebig, P K Vasudev, T E Seidel in Proc MRS Vol 427 (1997), ed K N Tu, J W Mager, J M Poate, L J Chen, pp 415-425

34 G K Wehner, G S Anderson in 'Handbook of Thin Film Technology, Mc Graw-Hill, New York (1970), ed L Maissel, R Glang, pp3-1

35 B Zega, Surface and Coatings Technology, 39/40 (1989) 507-520

36 J Musil, S Kadlec, J Vyskocil, V Poulek, Surf and Coatings Techn 39/40 (1989) 301-314

37 T Smy, K L Westra, M J Brett, IEEE Trans Electron Dev , Vol 37, No 3, March 1990

38 DEPICT, Technology Modeling Associates

39 M R, Witty, Semiconductor Research Corporation Newsletter, Dec 1992 Vol 10 No 12, pp2-3

40 J P McVittie, D S Bang, J S Han, K Hsiau, J Li, J Zheng, K C Saraswat, SPEEDIE 3 0 Manual 1995, Stanford University

41. S. K. Dew, T. Smy, M. Brett, Jpn. J. Appl. Phys. 33, 1140 (1994)
42. M. J. Goeckner, J. A. Goree, T. E. Sheridan, IEEE Trans. Plasma Sci., vol. 19, no.2 Apr 1991
43. R. Somekh, J.Vac. Sci. Technol. A Jul 1984
44. W.D. Westwood, , J. Vac. Sci. Technol. A 15(1) Jan/Feb 1978
45. M.W. Thompson, Philos. Mag. 18, 377 1968
46. A. M. Myers, J. R. Doyle, D. N. Ruzic, J.Appl.Phys. 72 (7), Oct 1992, pp 3064-3071
47. A. M. Myers, J. R. Doyle, J. R. Abelson, D. N. Ruzic, J. Vac. Sci. Technol. A 9 (3), May/Jun 1991
48. J.P. Biersack, L.G. Haagmark, Nucl. Instrum. Methods 174, 257 (1980)
49. J. A. Thornton in Deposition Technologies for Films and Coatings, Noyes Publications, New Jersey (1982), pp 188
50. T. Motohiro, J. Vac. Sci. Technol. A Mar/Apr 1986
51. M. Turner, I. S. Falconer, B. W. James, D. R. McKenzie, J. Appl. Phys. 65 (9) May 1989
52. M. Turner, I. S. Falconer, B. W. James, D. R. McKenzie, J. Vac. Sci. Technol. A 10 (3), May/Jun 1992
53. J. M. E. Harper, J. J. Coumo, R. J. Gambino, H. R. Kaufman, R. S. Robinson, J. Vac. Sci. Technol. 15, 1597 (1978)
54. R. S. Robinson, J. Vac. Sci. Technol., 16(2), Mar/Apr 1979
55. T. Motohiro, Y. Taga, Thin Solid Films, 112, 161 (1984)
56. S. Dushman in Scientific Foundation of Vacuum Technique, Wiley, New York, 1949; pp 32
57. S. Dushman in Scientific Foundation of Vacuum Technique, Wiley, New York, 1949; pp 41-43
58. J. B. Hasted, London Butterworths 1964 page 342.
59. Yamamura, Ishida J. Vac. Sci. Technol. A 13(1), Jan/Feb 1995
60. L.D. Landau, E. M. Lifshitz, Mechanics, Pergamom, London 1976 pp 48
61. R. A. M. Wolters, Proc Semicon 1997
62. J. Baliga, Semiconductor International March 1997 pg 76 - 80
63. P. Burggraaf, Semiconductor International December 1990 pg 28 - 31

64 F H Baumann, R Liu, C B Case, W Y C Lai, Proc VMIC 1993 pp 412 - 417

65 R Liu in 'ULSI Technology', McGraw-Hill Singapore1996, ed C Y Chang, S M Sze, pp 407-410

66 H J Barth, Mat Res Soc Symp Proc Vol 427

67 H Joswig, W Palmer, Thin Solid Films, 221 (1992) 228-232

68 G P Beyer, K Maex, S Daniels, N Maity, to be published in MRS

69 C S Chang, K A Monnig, M Melliar-Smith, Proc IITC 1998, pp 3-6

70 T Chiang, B Sun, P Ding, I Hashim, V Pavate, S Iyer, B Chin, Z Xu, M Narasimhan, Applied Materials HPPVD Update 1998, Vol 5 No 2 2

71 H H Manko in 'Mechanism of Wetting During Solder Joint Formation', (STP 319, (1963)

72 H J Bart, J Bierner, H Helneder, W Robl, K Schober, M Schneegans, Proceedings SPIE Vol 3214 pg 2 - 12

73 J N Broughton, M J Brett, S K Dew, G Este, IEEE Trans Semi Manuf, Vol 9 No1, Feb 1996

74 J E J Schmitz in 'Chemical Vapour Deposition of Tungsten and Tungsten Silicides for VLSI/ULSI Applications', Noyes Publications, New York, (1992), pp 21-40

75 D Pramanik, A N Saxena, Solid State Technology March 1990 pg 73 - 79

76 G Yao, S Chen, H Khurana, Z Xu, M Taoka, M Aruga, European Semiconductor, February 1996 pp 15-23

77 G Carter, Journal Materials Science 11 (1976) 1091 - 1098

78 J M Blakely in 'Surface Diffusion', Pergamon Press New York 1963

79 S S Winterton, T Smy, S K Dew, M J Brett, J App Phys 78 (6) 1995 pp 3572-3579

80 R W Berry, P M Hall, M T Harris in Thin Film Technology, D Van Nostrand, Canada (1968), pp 569-570

81 D A Weirauch, W M Balaba, A J Perotta, J Mat Res 1995, Vol 10, No 3 pp640

82 H Li, J Proost, Private Communication

83 S K Dew, T Smy, M J Brett, IEEE Transactions on Electron Devices, Vol 39, No 7, July 1992

84 T J Smy, S K Dew in 'SIMBAD v1 4 User's Manual', Feb 12, 1996

85 I A Blech, H A Vander Plas, J Appl Phys 54(6), June 1983, pp3489 - 3496

86 M N Webster, A G Dirks, Microelectronic Engineering 37/38 (1997) 313-318

87 A Aronson, I Wagner, M G Ward, Proc MRC 1991 Thin Film School

88 G P Beyer, Private Communication

89 G P Beyer, K Maex, S Daniels, S Lee, H Bender, M Judelewicz, N Maity, to be published in Materials Science in Semiconductor Processing

90 I A Saadat, E Beyer, S Sekigaham, B J Daniels, A Borba, M E Thomas, Proc VMIC 1996 pp455 - 460

91 B Zhao, M A Biberger, V Hoffman, S-Q Wang, P K Vasudev, T E Seidel, Electr Letters Jan 1997 vol 33 No 3 pp 247 - 248

92 D Restaino, C Szwejkowski, H Gilboa, Proc VMIC 1993 pp 502 - 504

93 L M Gignac, 'Thin Film Interactions between Ti, TiN, and Al during High Temperature Al Reflow for 1Gb DRAM Interconnects', to be published in MRS

94 Shi-Qing Wang, L H Allen, J Appl Phys , 79, 5 (1996)

95 Y Inoue, S Tanimoto, K Tsujimura, T Yamashita, I Ibara, Y Yamasita, K Yoneda, J Electrochem Soc , Vol 141, No4 April 1994

96 R S Bailey, N C Hill, Proc SPIE October 1995

97 A Classen, S Daniesl, R A M Wolters, Unpublished

98 S M Rossnagel, J Vac Sci Technol B 16(5), 1998, pp 2585-2608

99 D Bassanini, Private Communication

100 T Mantei, Basic concepts of plasmas and plasma damage, short course at the 3rd $P^{2}ID$ symposium, Honolulu, 1998

101 S K Dew, T Smy, M J Brett, J Vac Sci Technol A 9(3), 1991, pp 519

102 M Hou, M T Robinson, Applied Physics, Vol 17, 1978, pp371

103 O S Oen, M T Robinson, J Appl Phys, 35, 2515 (1964)

104 B Chapman in 'Glow Discharge Processes', Wiley, New York, 1980, pp 181

105 A Wucher, W Reuter, J Vac Sci Technol A 6(4) 1988, pp2316

106 H Tsuge, S Esho, J Appl Phys Vol 70, No 8 1991, pp 4295

107 S Berg, H-O Blom, T Larsson, C Nender, J Vac Sci Technol A 5 (2) Mar /Apr 1987 pp 202-207

108 S Berg, T Larsson, C Nender, H-O Blom, J Appl Phys 63 (3) Feb 1988 pp 887-891

109 S Berg, H-O Blom, M Moradi, C Nender, T Larsson J Vac Sci Technol A 7 (3) May/Jun 1989 pp 1225-1229

110 R J Carmen, D J W Brown, J A Piper, IEEE J Quantum Electron , 30, 1876 (1994)

111 M J Kushner, B E, Warner, J Appl Phys , 54, 2970, (1983)

112 T Heberlein, G Krautheim, W Wutte, Vacuum, 42, 47 (1991)

113 S Daniels, D C Cameron, Proceedings of the International Conference of Advances in Materials and Processing Technologies 1995, pp 953-958

114 S Daniels, D C Cameron, J Phys III France 6 (1996) pp 1213 - 1218